

Design of Deployable Solar Arrays for PocketQubes

AE5051: Master Thesis Aerospace Engineering
Divyam Agrawal



Delft University of Technology

Design of Deployable Solar Arrays for PocketQubes

by

Divyam Agrawal

to obtain the degree of Master of Science at the Delft University of Technology,
to be defended publicly on February 19, 2025 at 13:00

Student Name	Student Number
Divyam Agrawal	5810353

Thesis Committee: M.S. Uludag

P.P. Sundaramoorthy

Dr. A. Cervone

Faculty:

Aerospace Engineering, TU Delft

Supervisor

External Examiner

Committee Chair

Abstract

Research in miniaturization of satellite technology has enabled the development of a new class of satellites - PocketQubes. The extremely small form factor greatly limits power generation capabilities, with body-mounted arrays expected to generate around 1W average orbital power for the 3P size. Deployable solar arrays present an ideal solution for small satellites, enabling more demanding payloads onboard. Numerous designs for CubeSats have already been developed commercially and in academia.

This research focuses on adapting solar array designs available in literature to 3P PocketQubes, addressing their unique size, power and deployment constraints imposed by the deployer. A 4-panel array design in a wing configuration was designed, facilitating a peak power of 19.7 W. This was supported by a burn-wire mechanism and a torsion spring hinge. Structural analysis was conducted using LS-DYNA and ANSYS Mechanical to simulate deployment impact and launch vibrations, respectively. The analysis evaluated the design's response to dynamic launch loads and mechanical impacts during deployment. The final assembly weight was 204.8g, contributing to a specific power of 96.2 W/kg, comparable to many COTS deployable solutions for CubeSats. The procurement cost was found to be €1480 (excluding solar cell assemblies), and can be greatly lowered with higher order quantities for formation flying/distributed missions with multiple PocketQubes.

Additionally, this research examined the impact of solar array deployment configurations on power generation and orbital lifetime. Power generation was assessed using a simplified Python model, later verified through AGI STK simulations. Results indicated that the β angle significantly influences power output across different configurations. Moreover, for peak β angles representing noon-midnight and dusk-dawn orbits, seasonal variations were studied. This yielded an approximate 30% reduction during summer solstice for dusk-dawn orbits, but no visible change for noon-midnight orbits. For velocity-aligned PocketQubes, configurations with panels mounted on the 5×5 cm face at a 135° deployment angle were found to be optimal. In contrast, for PocketQubes with pointing capabilities and high peak power requirements, the previously designed wing configuration was recommended.

The study of orbital lifetimes was facilitated by ESA's DRAMA software and CROC was used to identify the minimum, average (random tumbling scenario), and maximum cross sections, contributing to a wide range of expected orbital lifetimes. In the velocity-aligned case, configurations featuring panels attached on the long edges (parallel to the drag force) yielded lifetimes suitable for long Earth observation missions. The latter configurations were found to be suited for shorter, technology demonstration missions. The launch date significantly impacted the results of the study, especially for configurations with higher ballistic coefficients. The results from this study however are highly idealistic, as the PocketQube angle of attack is expected to vary, largely influencing the drag area experienced. Assumptions regarding the drag coefficient and the use of NRLMSISE-00 drag model within DRAMA also limit the accuracy of the results, as seen when comparing the simulation and real observations from Delfi-PQ.

Acknowledgments

This thesis marks the conclusion of my two-and-a-half-year journey at Delft University of Technology. I vividly remember my first Space BBQ outside the Aerospace faculty—an evening filled with new cultures, a new continent, and an anxious excitement for the road ahead. Looking back, I could have never imagined how these years would shape me, both personally and professionally. I am deeply grateful for the opportunities this incredible campus has provided and for the people who made this journey unforgettable.

I would especially like to thank my supervisor, Mehmet Sevket Uludag, for his unwavering support and guidance throughout my thesis. His dedication, has been invaluable—always willing to put in extra time to steer me in the right direction whenever I felt lost. I am also grateful to Stefano Speretta for his insightful feedback during our meetings, which greatly enhanced the quality of my work. A special thanks to Simao Martins for his patience and long hours dedicated to strengthening my understanding of structural analysis.

Beyond academia, I am incredibly thankful for the amazing friends I have met along the way. They have given me a second home in Europe, and the memories we have created together will stay with me throughout my life. I also owe my deepest gratitude to my family for their unwavering support throughout my master's journey. Their encouragement, belief in me, and willingness to support my new life in Europe have meant the world. Whether helping me navigate challenges or celebrating successes, they have always been there. I will forever cherish their visits to Delft and look forward to making them proud in the years ahead.

*Divyam Agrawal
Delft, February 2025*

Contents

Abstract	i
Acknowledgments	ii
1 Introduction	1
1.1 PocketQube Specification and Standards	2
1.2 Delfi Space Program	4
1.2.1 Delfi-PQ	4
1.2.2 Delfi Twin	5
1.3 Research Framework and Goals	6
1.3.1 Research Objective and Questions	6
1.3.2 Thesis Outline	6
2 Literature Review	7
2.1 Power Generation	7
2.2 Existing PocketQubes and Deployment Configurations	8
2.2.1 Deployed Configurations	10
2.3 Deployment Mechanisms Overview	11
2.4 Hold Down and Release Mechanism	15
2.4.1 Custom Burn Wire Mechanisms	16
2.4.2 COTS HDRMs	19
2.4.3 Summary	21
2.5 Deployment Guide	22
2.5.1 Rigid Hinges	23
2.5.2 Flexible Hinges	24
2.5.3 Spin-Stabilized Deployment	27
2.6 Summary of All Options	27
2.7 Structural Analysis Theory	28
2.7.1 Static Analysis	28
2.7.2 Vibration Theory	28
2.7.3 Explicit Analysis	30
3 Design of Deployable Solar Arrays	32
3.1 Requirements	32
3.2 Design Process Overview	34
3.3 Deployment Mechanism and Subsystem Concept Trade-Offs	34
3.3.1 Deployment Mechanism Overview and Trade-Off	35
3.3.2 Hold Down & Release Mechanism Concept Selection	37
3.3.3 Deployment Guide Selection	44
3.4 PCB Assembly Design	46
3.4.1 Material Selection	47
3.4.2 PCB Layout	51
3.4.3 PCB Thickness and Spacing Analysis	53
3.5 Hinge Design	59
3.5.1 Torsion Spring Selection	59
3.5.2 Hinge Assembly	63
3.5.3 Hinge Impact Structural Analysis	68
3.6 Final Design and BOM	71
3.6.1 Structural Analysis of Array Assembly	73
3.6.2 Failure Modes and Mitigation Strategies	76
4 Evaluating Deployment Configurations and Their Impact on a 3P PocketQube Mission	79
4.1 Power Generation	79

4.1.1	Preliminary Power Generation Model	80
4.1.2	Python Model Results	83
4.1.3	Verification with Ansys STK	85
4.1.4	Comparison of STK and Python Data	86
4.1.5	Seasonal Variations in Power Generation	88
4.2	Mission Duration	90
4.2.1	Cross Section of Complex Bodies (CROC)	90
4.2.2	OSCAR Lifetime Evaluation	92
4.3	Results	94
5	Conclusion and Recommendations	96
5.1	Conclusion	96
5.2	Recommendation for Future Work	98
A	Appendix	105
A.1	Azur 3G3CA Assembly	105
A.2	PCB Design	106
A.2.1	PCB Thickness and Spacing Analysis Mode Shapes	107
A.3	DRAMA Code	108
A.4	Power Generation Model	110
A.4.1	Power Generation Spin Stabilized	110
A.4.2	Power Generation Plots, Single Orbit	114
A.4.3	RAAN Precession Rate Inclination & Altitude Combination	115
A.5	STK Power Generation	115
A.5.1	Tumbling and Sun-Pointing Settings in STK	116
A.5.2	Settings for Spin Stabilized Tumbling and Sun-pointing	116
A.5.3	STK Power Plots	117
A.6	Tape Spring Calculation	117
A.7	GEVS Profile	119
A.8	Hinge	119
A.8.1	Hinge Material	119
A.9	Final COTS Parts	120

Acronyms

- ACS** Attitude Control System. 79, 90, 94
- ADCS** Attitude Determination & Control System. 4, 45
- COTS** Commercial Off the Shelf. 1, 2, 12, 23, 34, 36, 39, 62, 77, 78, 97, 98
- CROC** Cross Section of Complex Bodies. iv, 90, 93, 94
- CTE** Coefficient of Thermal Expansion. 50, 51
- DRAMA** Debris Risk Assessment and Mitigation Analysis. 90
- DSSW** Deployment Status Switch. 18
- EO** Earth Observation. 95
- ESA** European Space Agency. 95
- EU** European Union. 7
- EXA** Ecuadorian Space Agency. 2
- FCC** Federal Communications Commission. 90, 92, 93
- FOS** Factor Of Safety. 58
- FOSA** Fold Out Solar Arrays. 13
- GaAs** Gallium Arsenide. 7
- GAUSS** Group of Astrodynamics for the Use of Space Systems. 2
- GEVS** General Environment Verification Standard. 29, 34, 49, 57, 75
- HDRM** Hold Down and Release Mechanism. vii, x, 2, 6, 12, 15, 20–22, 36, 37
- ICD** Interface Control Document. 3, 32, 33
- LEO** Low Earth Orbit. 1, 2, 5, 50, 67, 90
- MASTER** Meteoroid and Space Debris Terrestrial Environment Reference. 90
- MOS** Margin Of Safety. 58, 75
- MPPT** Maximum Power Point Tracking. 98
- NASA** National Aeronautics and Space Administration. 29
- NMD** Nano-Morphodynamic Muscle Strand Technology. 16
- PCB** Printed Circuit Board. 6, 58
- PSD** Power Spectral Densities. 29, 57, 75
- PV** Photo Voltaic. 1, 7
- RMS** Root Mean Square. 29
- SMA** Shape Memory Alloy. 16, 19, 26
- SMD** Surface Mount Device. 38

SMP Shape Memory Polymer. 25, 26

SMPC Shape Memory Polymer Composite. 26

SSO Sun-Synchronous Orbit. viii, 80, 81, 86, 88, 89, 94

TC Thermal Conductivity. 50

T_g Glass Transition Temperature. 50, 51

List of Figures

1.1	CubeSat to PocketQube	1
1.2	PocketQube Orientation [8]	3
1.3	PocketQube Dimensions [8]	3
1.4	AlbaPod Envelope [9]	3
1.5	AlbaOrbital’s AlbaPod [10]	3
1.6	Delfi PQ	4
1.7	Delfi-PQ Antenna Deployment Mechanism	5
1.8	Differential Drag Maneuvering	5
2.1	Power vs Incidence Angle [16]	7
2.2	Nanosatellite Database -Types of Small Satellites Launched [5]	8
2.3	Adam Thurn’s Burn Wire Mechanism [22]	12
2.4	Inflatable and Coilable Boom 1 [24]	13
2.5	Inflatable and Coilable Boom 2	13
2.6	Solar Array Drive Assembly [25]	14
2.7	Electric Motor Deployment and Folded Panel Infeasibility	14
2.8	Coilable Masts	14
2.9	Adam Thurn’s Burn Wire Mechanism [22]	17
2.10	Nichrome Burn Wire Electrical Setup [22]	17
2.11	Resistor-Based Burn Wire Electrical Schematic and Tie-down Knot [32]	18
2.12	Pogo Pin [33]	18
2.13	Pogo Pin Based Release Mechanism [35]	19
2.14	Pogo Pin Knot	19
2.15	DCUBED Nano Release Nuts [37]	19
2.16	Gecko Hold Down and Release Mechanism (HDRM) [38]	20
2.17	EXA NMD HDRM [39]	20
2.18	Helical Torsion Spring Hinges	23
2.19	Helical Torsion Spring Torque & Angular Deflection Relationship [43]	24
2.20	Dimensional parameters of the tape spring [44]	24
2.21	Equal and Opposite Sense Bending	25
2.22	Tape Spring Moment-Rotation Relationship [44]	25
2.23	SMP Programming	25
2.24	SMP Hinge 90 and 180 [45]	26
2.25	NASA Glenn’s SMA CubeSat Hinge [46]	26
2.26	Notable missions featuring solar array/sail deployment by spinning or centrifugal force	27
2.27	GEVS Vibration Qualification Profile	30
2.28	Explicit Dynamics Solution Process	30
3.1	Design Process Overview	34
3.2	Spring Loaded Mechanism Breakdown	36
3.3	Functional Overview of Spring-Loaded Deployment Mechanism	37
3.4	HDRM Electrical Setup	43
3.5	Electrical Schematics for Burn Wire Mechanism	43
3.6	PCB Dimension Variables	47
3.7	PCB Assembly Design Process	47
3.8	Natural Frequency of Simply Supported Rectangular Plate	49
3.9	Mode Shapes 1, 2, 3	50
3.10	PCB Layout 1	52
3.11	PCB layout 2	53
3.12	PCB Stowed Assembly Schematic	54
3.13	Würth Elektronik WA-SMSI SMT-M1.6 [72]	54

3.14	3D Model for Structural Analysis	56
3.15	Modal Analysis of Panel Assembly	56
3.16	Panel assembly deformation	57
3.17	Panel assembly Von-mises stresses	57
3.18	Solar Panel Envelope	59
3.19	Minimum and Maximum Spring Diameter	59
3.20	Spring Locations	62
3.21	Spring Free Positions	62
3.22	Spring Position Concept	63
3.23	Dimension Limitations	63
3.24	HP2P: Hinge Panel To Panel	64
3.25	HP2PQ1: Hinge Panel To PQ 1	65
3.26	HP2PQ2: Hinge Panel To PQ 2	65
3.27	Hinge Body Separation t_b	67
3.28	Thermal Deformation Observed on Female Hinge Body	67
3.29	Thermal Deformation Observed on Male Hinge Body	68
3.30	Minimum and Maximum Moment of Inertia Conditions	69
3.31	Stress Concentrations During Simulation - AL7075 Hinge	70
3.32	Stress Plot AL7075 Hinge	70
3.33	Render of Deployable Arrays - Deployed	71
3.34	Render of Deployable Arrays - Deploying	71
3.35	Render of HP2PQ and HP2P in Stowed Configuration	71
3.36	Render of Panel to Panel Hinge	71
3.37	Render of Deployable Arrays - Stowed	72
3.38	PocketQube Within AlbaPOD V1	72
3.39	Boundary Conditions for Structural Analysis	73
3.40	Final Array Mode 1	74
3.41	Final Array Mode 2	74
3.42	Final Array Mode 9	74
3.43	Final Array Mode 11	74
3.44	Final Array Mode 12	74
3.45	Final Array Mode 21	74
3.46	Random Vibration Deformation x-axis 2σ	75
3.47	Random Vibration Deformation y-axis 2σ	75
3.48	Random Vibration Deformation z-axis 2σ	76
3.49	Random Vibration Equivalent Stresses 2σ	76
4.1	Panel Deployment Configurations	79
4.2	Python Model Space	80
4.3	Maximum Eclipse Diagram [86]	81
4.4	Solar Beta Angle	81
4.5	Visualising Rotation Matrices	82
4.6	Power Generation Parameters	82
4.7	Average Power Generated for $\beta = 0$	84
4.8	Average Power Generated for $\beta = 90$	84
4.9	Average Power Generated While Varying β angle	85
4.10	Orbital Parameters	86
4.11	Sun-Synchronous Orbit (SSO) Orbit Visualized in STK	86
4.12	Power Verification for Configurations 1-135 and 1-90	87
4.13	Power Verification for Configurations 2 and 3	87
4.14	Noon-Midnight SSO	88
4.15	Dusk-Dawn SSO	88
4.16	Noon-Midnight Yearly Average Power	88
4.17	Dusk-Dawn Yearly Average Power	89
4.18	RAAN Change Config 1-90 Min Area	89
4.19	RAAN Change Config 1-90 Ave Area	89
4.20	Velocity Aligned Attitude Mode Applicable Cross Sections	91
4.21	Nadir Pointing Attitude Mode Applicable Cross Sections	91

4.22	Sensitivity analysis with launch date	92
4.23	Orbital Lifetime Chart Legend	93
4.24	Configuration 1-90 OSCAR Results	93
4.25	Configuration 1-135 OSCAR Results	93
4.26	Configuration 2 OSCAR Results	93
4.27	Configuration 3 OSCAR Results	93
5.1	Render of Deployable Arrays - Deployed	97
5.2	Render of Deployable Arrays - Stowed	97
A.1	Azur Space 3G30C	105
A.2	Cell Dimensions	105
A.3	Mode Shape 1	107
A.4	Mode Shape 2	107
A.5	Mode Shape 3	108
A.6	Mode Shape 4	108
A.7	Mode Shape 5	108
A.8	Config 1 135 Power Generation Python, Single Orbit	114
A.9	Config 1 90 Power Generation Python, Single Orbit	114
A.10	Config 2 Power Generation Python, Single Orbit	114
A.11	Config 3 Power Generation Python, Single Orbit	115
A.12	Altitude & Inclination for advised RAAN Precession	115
A.13	STK Environment for Tumbling	116
A.14	STK Environment for Sun-Pointing	116
A.15	Config1 (45°) Sun-Pointing	117
A.16	Config1 (45°) Tumbling	117
A.17	Config1 (90°) Sun-Pointing	117
A.18	Config1 (90°) Tumbling	117
A.19	Configuration 1 (45°) & Configuration 1 (90°)	117
A.20	Config2 Sun-Pointing	117
A.21	Config2 Tumbling	117
A.22	Config3 Sun-Pointing	117
A.23	Config3 Tumbling	117
A.24	Configurations 2 & 3	117
A.25	Tape Spring Bend Length	118
A.26	Tape Spring Bend Parameters	118

List of Tables

1.1	Specifications of PocketQube Units [8]	2
2.1	Overview of Satellite Missions and Deployed Configurations [5]	9
2.2	Overview of Various Mini-Cube Missions	10
2.3	Different Deployed Configurations	11
2.4	Deployment Mechanisms Overview	15
2.5	Comparison of different HDRMs	22
2.6	Overview of Sub-Mechanisms and Solution Options	27
2.7	GEVS Qualification PSD	30
3.3	Comparison of Deployment Mechanisms for Small Satellites. Ratings are color-coded as follows: Green meets requirements confidently, Yellow requires additional considerations to meet requirements, and Red is not expected to meet requirements.	35
3.4	Release Mechanism Attributes	38
3.5	Evaluation of Hold-Down Mechanisms	41
3.6	Hold-Down Concept Trade Off. Ratings are color-coded as follows: Green indicates optimal performance, Yellow represents suboptimal performance, and Red signifies unacceptable performance.	42
3.7	Tie-Down Cable Options	44
3.8	Hinge Comparison. Green represents desirable performance, Yellow represents acceptable performance	45
3.9	Solar Array PCB Suppliers [61][62][63][64]	46
3.10	Comparison of Rigid and Flexible Solar Panels for Spacecraft	48
3.11	Natural Frequency and Deformation Under Random Vibration Loads	50
3.12	Folded Deployable Panel Configurations	52
3.13	WA-SMSI SMT-M1.6 Specification [72]	54
3.14	Price (€) for 7 Day Lead Time [68]	55
3.15	PCB Specifications	55
3.16	Sample of Thickness and Spacing Combinations Analysed in ANSYS	55
3.17	Comparison of Panel Configurations with Deformation and Stress Metrics	58
3.18	Summary of Von Mises Stresses, Factor of Safety, Yield Strength, and Margin of Safety for each Option.	58
3.19	Table of Parameters and Values	59
3.20	Comparison of Properties for Music Wire and AISI 304 [74]	60
3.21	Spring free positions and deflections	62
3.22	LTR012A Specifications	63
3.23	Hinge Design Constraints	64
3.24	Parts Used in Hinge Assemblies [5]	65
3.24	Parts Used in Hinge and Bracket Assemblies	66
3.25	Spring Impact Velocity. S_t1 , S_t2 , S_t3 and S_t4 represent the torsion springs, starting with the one attached to PQ Bracket.	69
3.26	Explicit Dynamics Simulation Parameters	69
3.27	MOS Hinge Impact Analysis	70
3.28	Additional Parts Used in Deployable Solar Array Assembly [5]	72
3.29	Modal analysis results for final array assembly	74
3.30	MOS Hinge Impact Analysis	75
3.31	Failure Classification Levels [60]	76
3.32	Failure Modes and Mitigation Methods	77
3.33	Mass Budget	78
3.34	Cost Breakdown of Components	78

4.1	Average Power Generated in Orbit	84
4.2	Comparison of Python and STK Averages with Error	87
4.3	Solar Panel Parameters	91
4.4	CROC Cross Section Calculations	91
4.5	OSCAR: Orbital Parameters	92
4.6	Configurations for Different Orbit Conditions	94
4.7	Expected Orbital Lifetimes For Velocity Aligned PocketQubes with Suitable Mission Types	95
A.1	Thermal Conductivity and Coefficient of Thermal Expansion of Substrate Materials	106
A.2	Elastic Properties	106
A.3	Natural Frequency of Simply Supported Rectangular Plate	107
A.4	Random Vibration Profile	119
A.5	Comparison of Material Properties	119
A.6	COTS Parts and Suppliers	120

Introduction

Small satellites have been at the forefront of space research and development in the past decade with over 2800 being launched in 2023 alone [1]. This is due to the large scientific capability they can provide at a much smaller launch cost and mass. They have become the primary source of access to space for commercial, government, private and academic institutions. Standardized platforms for small satellites, such as CubeSats, have significantly improved access to space. This is driven by the increased availability of Commercial Off the Shelf (COTS) components, more frequent and economic launch opportunities enabled by standardized deployers from companies like EXOLAUNCH and ISISPACE, and consistent verification, testing, and validation practices.

While CubeSats have been a majority standard for small satellites being launched, increased development in miniature structures have led to an even smaller standard being developed in the form of PocketQubes. TU Delft is developing a formation flying mission in Low Earth Orbit (LEO) which will be demonstrated by two PocketQubes that are manufactured in-house by the students and researchers at the institute. A detailed mechanical overview of PocketQubes and relevant requirements are given in Chapter (2). This switch from the CubeSat form factor to the PocketQube form factor is visualized in figure 1.1.

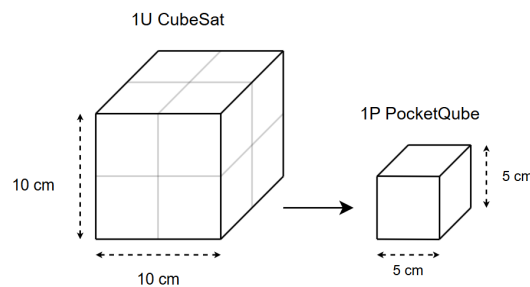


Figure 1.1: CubeSat to PocketQube

A significant challenge for small satellites, especially PocketQubes, is power generation. Primarily, satellites are powered by solar cells or Photo Voltaic (PV) cells and the power generated is directly proportional to the cell area on-board. However, with compact form factors like PocketQubes, the space for incorporating solar cells is severely limited. This limitation impacts the power supply, which in turn constrains the communication, instrumentation and overall mission capabilities of these satellites [2]. The maximum power obtained using body mounted solar panels and advanced triple junction solar cells (Azur Space 3G30C) on a 3P PocketQube is typically limited to around 2.5 W. Therefore, deployable structures for small satellites have been the subject of active research and development by academic and commercial institutions. Deployment mechanisms for solar arrays enable the stowage of larger panels than body-mounted options, increasing the total cell area exposed to sunlight and enhancing overall power generation. Another capability of deployable solar panels is to provide a surface that can be used for differential drag as a means of formation flying [3]. This can be vital in picosatellites where conventional propulsion modules are difficult to integrate due to their mass, volume and power requirements.

Reviewing the "NASA Space Mechanisms Handbook" [4] and many existing deployable structures on small satellites, it is evident that they tend to have four major stages.

1. Initial Blocking (Hold Down, Constraint)
2. Motion Release
3. Deployment Guide
4. Final Blocking (Deployed position lock)

Initial blocking refers to how the panels are held down in their stowed/launch configuration. Motion release refers to the setups that facilitates the panels' release from their hold down position. Both the initial blocking and motion release are facilitated by the HDRM for which both COTS and custom options are available and provided in 2.4. Deployment guide refers to the exact mechanism that facilitates the linear/rotational movement of the panels from their stowed position to their final deployed configuration and these are provided in 2.5. Once in their deployed position, the solar arrays need to be constrained and held in place. This is done with the final blocking mechanism.

PocketQubes are becoming more popular, with a growing number and frequency of launches every year due to brokers like Alba Orbital [5]. Consequently, the need for deployable solar array designs that can be adapted and developed by universities is growing as well. CubeSats have numerous COTS options for deployable solar arrays provided by suppliers such as EnduroSat, ExoLaunch, NanoAvionics, and Ecuadorian Space Agency (EXA). However, without such commercially available options for PocketQubes, a design for deployable arrays needs to be developed that is both modular, maximizes the solar cell area coverage, and fits numerous mission profiles.

The final deployed configuration of the deployable solar arrays also has an impact on various mission parameters, particularly the power generation capabilities and orbital lifetimes. There are many such options of deployed panels as seen in Chapter 2 with 3 main configurations. Every configuration fits a certain mission profile, and finding the suitable configuration is essential in Phase 0/A of PocketQube development.

For these purposes, the goal of this thesis will be to initially develop a design for deployable solar arrays that features a certain deployed configuration that is desired for future PocketQube missions within the Delfi Space Program. Consequently, the impact of the deployed configurations on 3P PocketQube missions will be evaluated, focusing intently on the power generation characteristics and orbital lifetime.

1.1. PocketQube Specification and Standards

PocketQubes were first proposed by Professor Bob Twiggs and a collaboration between Morehead State University and Kentucky Space helped establish initial specifications [6]. A standard has since been developed by a collaboration between AlbaOrbital, TU Delft, Group of Astrodynamics for the Use of Space Systems (GAUSS) Srl [7]. Establishing a standard helps facilitate uniformity in the space community with regards to design and development of such satellites. With uniformity come deployers that are able to accommodate multiple missions, COTS components, qualification standards, etc. Since the standards establishment, a number of PocketQubes have been launched and have completed successful missions in LEO. Similarly to CubeSats, PocketQubes can be categorized as presented in table 1.1.

Table 1.1: Specifications of PocketQube Units [8]

Number of Units (P)	External dimensions without backplate (mm)	Sliding backplate dimension (mm)
1P	50 x 50 x 50	58 x 64 x 1.6
2P	50 x 50 x 114	58 x 128 x 1.6
3P	50 x 50 x 178	58 x 192 x 1.6

The overall dimensions of the PocketQubes are presented in figure 1.3 and the axes used throughout the thesis are displayed in figure 1.2.

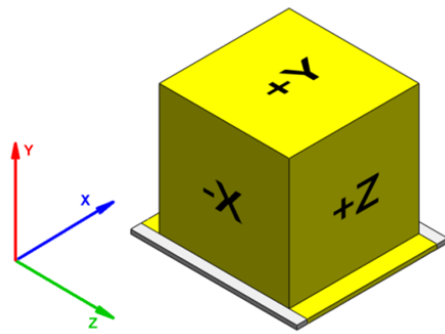


Figure 1.2: PocketQube Orientation [8]

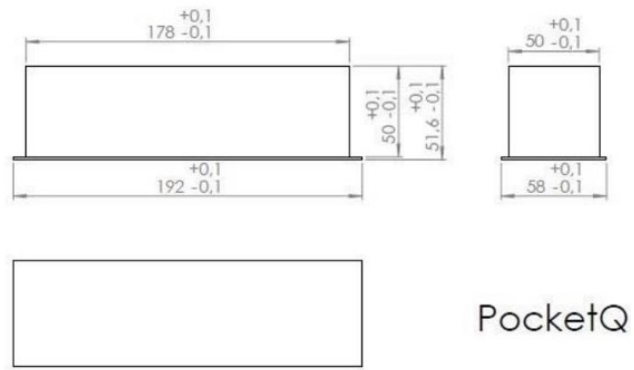


Figure 1.3: PocketQube Dimensions [8]

Within deployers like the AlbaPod, certain maximum appendage envelop limits have been provided [9]. This space is crucial in the development of deployable solar arrays as it will allow for multiple panels to be stowed and stacked (if multiple panels are required due to higher power requirements). The Interface Control Document (ICD) for AlbaPod gives these envelopes and requirements. AlbaPod will be the deployer of choice for this thesis since the Delfi Program has picked them for their upcoming mission.

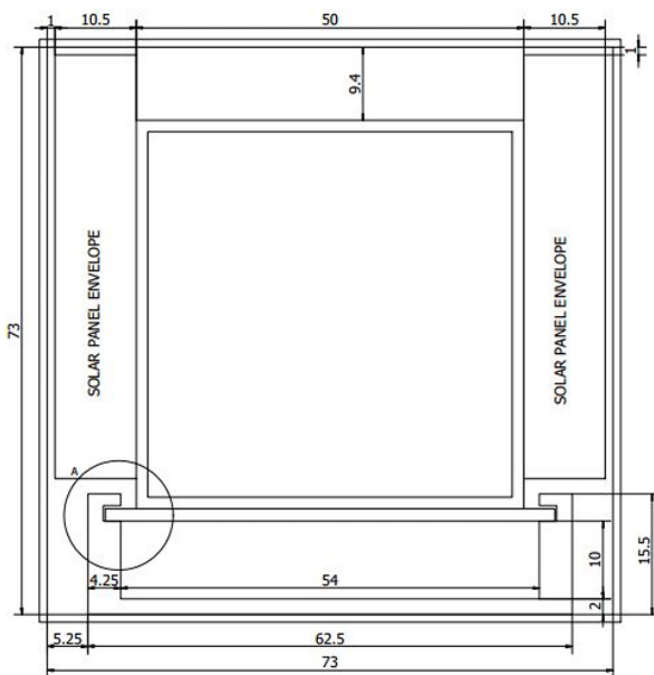


Figure 1.4: AlbaPod Envelope [9]



Figure 1.5: AlbaOrbital's AlbaPod [10]

As can be seen in Figure 1.4, with the maximum cross-section dimensions of 50mm of the PocketQube body, there is an additional 10.5mm width to accommodate solar arrays on either side ($\pm x$) of the PocketQube and 9.4mm width on the top. While this is the maximum separation available, the panels cannot make contact with the Alba Pod walls and should not be held down or constrained by them. On either side of the long edge ($\pm z$), there is an additional 7mm of spacing to accommodate additional structures. Additionally, the backplate also limits the volume envelope available as the deployer structure wraps around the backplate to constrain it.

1.2. Delfi Space Program

The Delfi program at Delft University of Technology, first established in 2004, is focused on space technology miniaturization and offering MSc students to work with real hardware and software development for space missions. The program aims to enable novel applications of very small satellites by building on state-of-the-art technology. The program has already overseen the launch of 3 missions:

1. Delfi-C3: Launched in 2008, Delfi-C3 is a 3 unit CubeSat and is the first nanosatellite from the Netherlands [11]. It demonstrated thin film solar cells, autonomous wireless sun sensors, and a radio with a linear transponder for radio amateurs.
2. Delfi-n3Xt: Launched in 2013 and a successor to Delfi-C3 [12], Delfi-n3Xt demonstrated the functioning and performance of a cold gas micropropulsion system, a CubeSat transceiver, and amorphous silicon solar cells.
3. Delfi-PQ: Launched in 2022, Delfi-PQ aimed to demonstrate an even smaller PocketQube platform in comparison to CubeSats [13]. It is further elaborated on in the following subsection.

1.2.1. Delfi-PQ

The Delfi-PQ (Figure 1.6), developed by Delft University of Technology's Faculty of Aerospace Engineering, represents the next class of miniaturized satellites. Building on its role in defining the PocketQube standard, this platform focuses on advancing research in system and component miniaturization [14].

It is a 3P PocketQube with a mass of approximately 545 g, with the core bus occupying 1P of the total volume. The second 1P is allocated for advanced subsystems such as Attitude Determination & Control System (ADCS) components, while the third 1P houses the scientific payload.

Technology Demonstration

1. Micropropulsion payload with a dual thruster system based on VML (Vaporizing Liquid Micro-resistojet) and LPM (Low-Pressure Micro-resistojet).
2. GPS payload.
3. Thermal payload by external partner demonstrating innovative thermal components.
4. Radio experiments.
5. Optical reflector.
6. Radar calibration experiment.

Deployables on Delfi-PQ

This PocketQube incorporates a deployment mechanism for the antenna with deployment switches as shown in Figure 1.7. The deployment mechanism features an RF connector that allows the antenna to rotate and a secondary fixture that limits the rotation and movement around one axis. The release is facilitated by a burn wire mechanism involving a tie-down cable and resistor circuit, and the deployment is guided by a small spring that is pre-tensioned by the tie-down cable in stowed configuration. This is similar to a rigid hinge assembly for solar arrays that will be shown in later chapters of the literature review. The total deployment system consists of six components that are all manufactured and assembled in house.



Figure 1.6: Delfi PQ

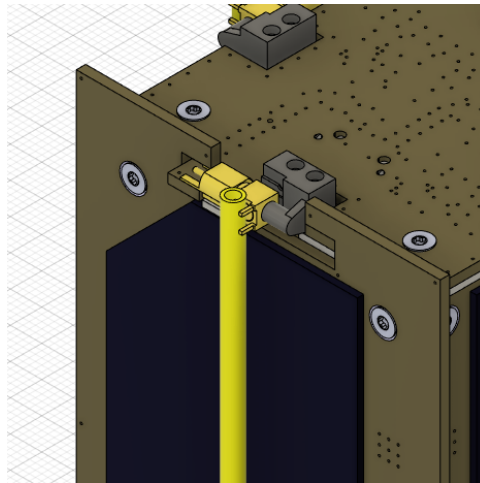


Figure 1.7: Delfi-PQ Antenna Deployment Mechanism

1.2.2. Delfi Twin

The TU Delft satellite group is also working on developing a new mission to demonstrate formation flying with PocketQubes over a lifetime of 6 months in LEO. This mission is not the primary focus for the design of deployable solar arrays in this thesis. However, it is important to examine it for its innovative formation-flying technique using differential drag, which could be a promising approach to enabling constellations of picosatellites in orbit. In this formation flying mission, the increase of drag area and the decrease of drag area are representative of retrograde and prograde burns respectively. This is because while increasing the drag area of the chaser satellite momentarily increases the distance between itself and the leading satellite, it causes the chaser to increase its acceleration due to a drop in altitude. This drop in altitude will cause the chaser to end up in an elliptical orbit where it is approaching its perigee. Manipulation of drag areas can therefore cause both PocketQubes to pursue a number of maneuvers of rendezvous and separation. A simple version of this can be visualized in figure 1.8.

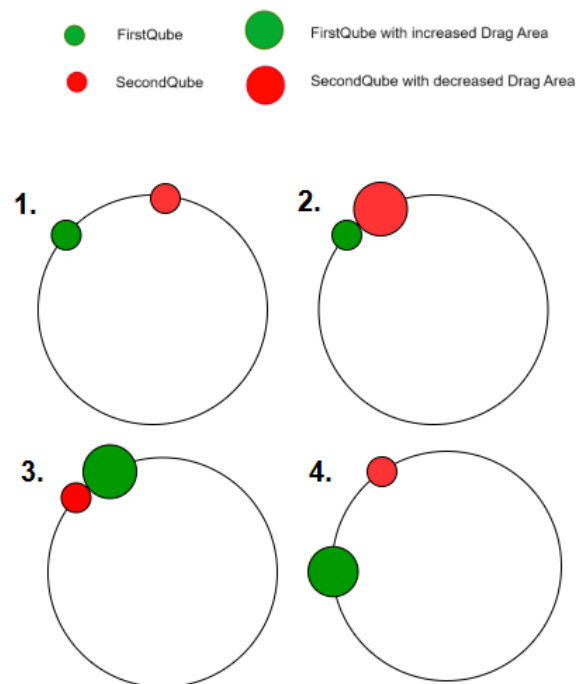


Figure 1.8: Differential Drag Maneuvering

1.3. Research Framework and Goals

1.3.1. Research Objective and Questions

With advancements in deployable appendages for spacecraft, particularly in their application to CubeSats and other small satellites with strict volume and mass constraints, it is equally important to explore such solutions for PocketQubes. PocketQubes are emerging as a popular standard in academic and research settings, with many already launched or having completed their missions. While advances in miniaturized electronics enable the development of even smaller and more compact satellites like PocketQubes, these satellites often remain power-intensive. As a result, deployable solar arrays are a popular option for small satellites to enable larger surfaces with incorporation of PV cells [15]. The overall research objective of the thesis is as following:

To design deployable solar arrays for 3P PocketQubes and assess how deployed configurations affect the mission parameters.

This research objective can be broken down further into research questions.

How does the deployment configuration impact the power generation and orbital lifetime of 3P PocketQubes with deployable solar arrays?

This question aims to see how the different configurations identified in the literature review impact the mission design. Insight into this question will allow researchers to choose a preliminary configuration for their deployable solar panels on PocketQubes. This will be done by analyzing the impact of the configuration on two main factors:

1. Power Generation
2. Orbital Lifetime

How can proven deployable solar array designs from small satellites be adapted to address the unique size, power, and deployment constraints of PocketQubes?

This research question aims to conduct a literature study of the design of deployable appendages on CubeSats and other small satellites and consequently provide a design that supports deployed panels in a wing configuration, suitable for peak power and pointing capabilities. Analysis will be done to study the material, dimensions and layout of PCBs that can withstand vibrational loads in orbit and a conceptual design and sizing estimates for a hinge will be provided that fit the panel assembly.

1.3.2. Thesis Outline

The thesis is structured as follows - **Chapter 2** offers a literature review, an in-depth analysis of deployable solar arrays in existing literature and heritage related to small satellites. It explores past missions and academic studies to identify various design options for deployment mechanisms, such as HDRMs and deployment guides, while evaluating their respective strengths and limitations. This review establishes the basis for defining requirements, identifying constraints, and performing trade-off analyses to support the design process. Based on the literature review, a design of deployable solar arrays is developed in **Chapter 3**, that focused on a specific deployed configuration discussed at the start of the thesis. It delves into trade-offs for types of deployment mechanisms, HDRMs, deployment guides, and consequently develops a conceptual design that supports these design choices. Structural analysis is also conducted to determine dimensional parameters for the Printed Circuit Board (PCB) and hinge assembly, and a final CAD and assembly specification is provided for the complete design. To assess the feasibility during launch and deployment, vibrational analysis is done on the final stowed assembly, and explicit analysis is done on the hinges to see whether they could withstand the impact at the end of deployment.

Proceeding the design, an evaluation is done to consider the impact of the deployment configurations on 3P PocketQube missions in **Chapter 4**. This particularly focuses on the power generation and orbital lifetime as the surface areas provided by the deployed panels and their orientation directly impacts these two parameters. This chapter also provides tools and steps to evaluate these parameters that can be used by students and researchers. Proceeding this and using the knowledge gained from Chapter 2, 3 and 4, **Chapter 5** will provide a conclusion of the research and outline key recommendations for future work.

2

Literature Review

This chapter will investigate existing PocketQubes that have been launched, and study their deployment mechanisms, deployed configurations, and key features. It will then explore the various types of deployment mechanisms identified, providing a detailed description of the HDRMs and deployment guides that constitute them using examples from previously flown small satellite missions and academic papers. Finally, a summary of all options for deployable solar array structures will be provided.

2.1. Power Generation

Solar cells, or PV cells, have been used to generate on-board power on satellites since the start of the space age. As of 2021, 85% of all nanosatellites are equipped solar panels and rechargeable batteries as the primary power modules [17]. The power generated by a solar cell can be calculated using the following equation:

$$P = \eta AS \cos(\theta) \quad (2.1)$$

Where:

- P = Power generated by the solar cell [W]
- η = Efficiency of the solar cell [dimensionless]
- A = Area of the solar cell [m^2]
- S = Solar flux (irradiance) [W/m^2]
- θ = Angle of incidence between the solar rays and the normal to the solar cell surface [radians]

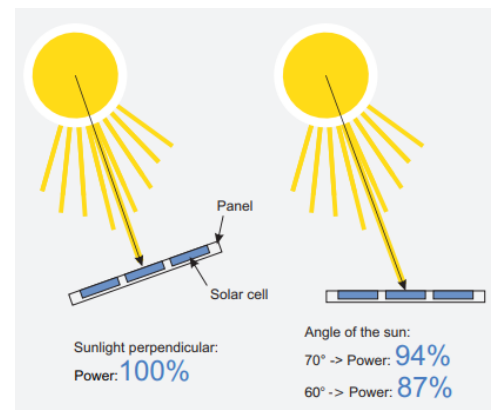


Figure 2.1: Power vs Incidence Angle [16]

Throughout the years, the efficiency of these cells has largely increased, with former amorphous silicon cells generating anywhere between 10% to 13%, and current GaAs cells with performance efficiencies ranging between 29% to 32%. This is largely due to multi-junction solar cells, made from multiple layers of light-absorbing materials that convert different wavelength regions of the solar spectrum into energy [17]. Solar flux is a quantity which is defined as the amount of solar energy per unit area at a certain distance from the sun. The solar flux received in low earth orbit (normally at an altitude less than 1000km) is approximately $1361 W/m^2$ [18]. While it isn't constant due to the elliptical orbit of Earth around the Sun, the value is widely used for most analysis and mission planning purposes.

A common supplier for Gallium Arsenide (GaAs) cells in the European Union (EU) is Azur space, also supplying cells for the Delfi Satellite program. Power generation for solar cells aboard PocketQubes can be estimated by using a product from Azur Space's catalogue [19]. This is a 30% Triple Junction GaAs Solar Cells (3G30C), shown in Figure A.1. The dimensions are also provided in A.1. Considering

BOL (Beginning Of Life) Voltage and current at max power of 2409mV and 502.9 mA respectively, peak power generation (when the incidence angle of solar irradiance is 90 degrees) from one cell is limited to 1.21 W. Generally, 1 solar cell this size can fit on the larger surface of a 1.5P PocketQube due to packing limitations. Similarly 2 cells can be incorporated on 3P PocketQube as seen on Delfi PQ.

2.2. Existing PocketQubes and Deployment Configurations

Most PocketQubes launched prior to recent developments in miniaturized structures used body mounted solar panels and therefore there are only a few PocketQubes that have used deployable solar arrays. As of May 31, 2024, according to the Nanosatellite database and Wikipedia [6] [5], around 83 PocketQubes have been developed, a number of which were launched successfully and have either completed their mission or are still in orbit. An additional 61 are in development, accounting for a total 3.4% of nanosatellites launched. This can be seen in Figure 2.2

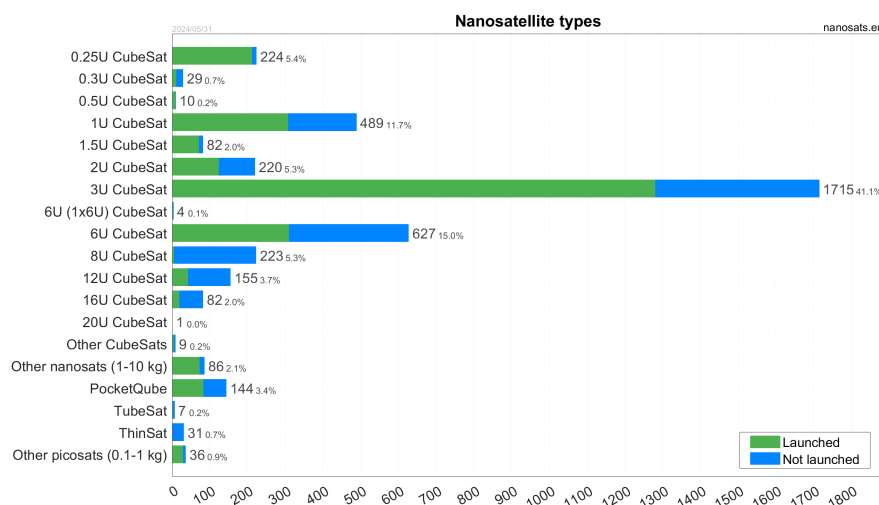


Figure 2.2: Nanosatellite Database -Types of Small Satellites Launched [5]

The majority of development has come since 2021 with Alba Orbital, GAUSS (Group of Astrodynamics for the Use of Space Systems), FOSSA Systems, and Libre Space Foundation being the preferred choice of deployer/broker. The developments have stretched from commercial earth observation satellites to university research focused on the feasibility and proof of concept for one or two subsystems. Figure 2.2 provides statistics on the percentage of nanosatellite developments that are PocketQubes.

A large number of PocketQubes have been launched with Alba Orbital's deployer made specifically for PocketQubes - AlbaPod. Details about the deployer dimensions and requirements have been provided in the PocketQube specification and standards in section 1.1. In some other missions, PocketQubes have been launched from CubeSat platforms, with notable mentions of StratoSat-TK1 that performed as a deployer for 6 PocketQubes [20].

Recent PocketQubes have been designed with deployable solar arrays to maximize power input. Instead of a singular body mounted face being exposed to solar radiation, these designs have the advantage of pointing multiple panels, increasing the total surface area. A number of these missions have been summarized in Table 2.1.

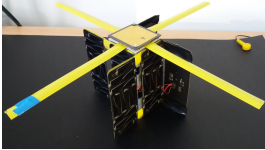
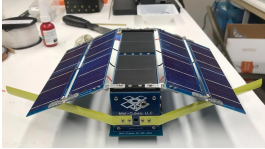
Mission	Organization	Size	Deployed Configuration	Mechanism and Peak Power
FossaSat-1	Fossa Systems	1P		Rigid Hinge Deployment *Peak Power = 3.55 W
FossaSat-2	Fossa Systems	2P		Rigid Hinge Deployment Peak Power = 9 W
Unicorn-1	Alba Orbital	2P		Tape Spring Deployment *Peak Power = 2.14 W
Unicorn-2	Alba Orbital	3P		Rigid Hinge Deployment Peak Power = 19.96 W
MDQubeSat-2	Innova Satellite	2P		Tape Spring Deployment *Peak Power = 3.20 W
Challenger	Quub/Intuidex	3P		Rigid Hinge Deployment *Peak Power = 12.25 W
Hello Sat	Hello Sat Turkiye	2P		Rigid Hinge Deployment *Peak Power = 7.47 W

Table 2.1: Overview of Satellite Missions and Deployed Configurations [5]

Note: Values marked with an asterisk (*) are approximations, estimated by assuming 30% cell efficiency and 80% packing efficiency (solar cell area/total surface area)

There are also a number of PocketQubes with deployable solar arrays that are currently in development and Table 2.2 gives insights on 4 of these by Mini-Cubes LLC, Space Team Aachen, The Flame Trench, and the Estonian Student Satellite Foundation.

Table 2.2: Overview of Various Mini-Cube Missions

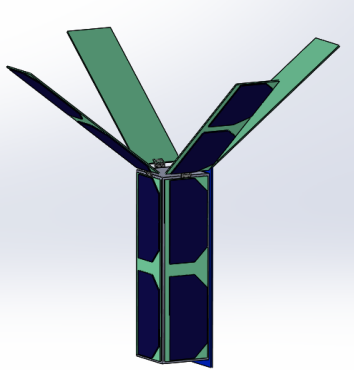
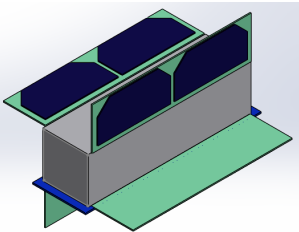
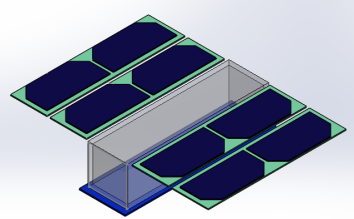
Mission	Organization	Size	Deployed Configuration	Mechanism
Mini-Cube 1	Mini-Cubes LLC	1P		Rigid Hinge Deployment
AQUIS	Space Team Aachen	1P		Rigid Hinge Deployment
TFTQube	The Flame Trench	1P		Flexure Hinge, Spring Tape w/ Electrical Connection
SUTS	Estonian Student Satellite Foundation	3P		N/A

What is seen in the heritage and upcoming missions is that a large number of these employ rigid torsional hinges in comparison to tape springs/flexure hinges, especially deployable arrays with multi-panel configuration. None of the existing missions feature multiple panels hinged on the shorter edges, and most feature multiple panels per array follow a 'wing' configuration. Additionally, there is no bias towards a particular PocketQube size, as deployable appendages are shown to feature on all PocketQube sizes 1P, 2P and 3P. An interesting development was that both Fossa Systems and Alba Orbital decided to go for a wing configuration in their newer satellite buses, also featuring pointing capabilities. Another noticeable trend was to utilize larger solar cells, at the expensive of packing area. MDQubeSat-2, FossaSat-2, Hello Sat and Unicorn-2 all decided to go for larger solar cells, that may have not had as much packing efficiency as visible on Challenger by Quub and this may be due to the complexity of the electrical setup pertaining to multiple individual cells.

2.2.1. Deployed Configurations

In all of these designs, there are numerous deployed configurations of solar arrays. However, most of the designs conform to 3 separate configurations, each suited to different mission profiles. The configurations provided below solely represent the change in deployed shape and attachment points of the panels, not the number of panels. The number of panels may vary for the different configurations, as will be seen later on.

Table 2.3: Different Deployed Configurations

Image	Description
 <p data-bbox="252 734 587 763">Configuration 1 (135° & 90°)</p>	<ul data-bbox="703 365 1396 745" style="list-style-type: none"> • Seen in many CubeSat and PocketQube missions including FossaSat-1, Mini-Cube 1 and TFTQube. Also featured on the upcoming Delfi-Twin Mission. • Favors 1 deployed panel per edge on either side of the satellite. • Can feature solar cells on multiple sides, enabling power generation at all phases in orbit. • Usually panels are deployed at a 45° or 90° angle to the PocketQube bus. Can have high peak power if hinge angle is 90 and 4 faces are exposed to solar radiation. • Maintains aerodynamic stability around flight vector. • Control of drag surface by changing panels' angle of deployment, in-orbit formation flying capabilities.
 <p data-bbox="325 1093 518 1122">Configuration 2</p>	<ul data-bbox="703 824 1396 1149" style="list-style-type: none"> • Configuration featured in first configuration of AlbaOrbital buses Unicorn-1 and various CubeSat designs. • Features uniform power generation by adding an additional surface for each face of the PocketQube and enabling power generation through most phases in orbit. • Aerodynamic stability around flight vector, center of mass is close to geometrical center. • Low peak power in comparison to other designs and large shadows inflicted, restricting use of optical payload. • Multiple hinge points per edge, greater structural integrity of deployed panels.
 <p data-bbox="325 1547 518 1576">Configuration 3</p>	<ul data-bbox="703 1227 1396 1664" style="list-style-type: none"> • Relatively new design for PocketQubes, featured on latest AlbaOrbital bus Unicorn 2, FossaSat-2 and Challenger. • Features multiple panels per wing, Z-folded or Roll-folded prior to deployment. • Highest peak power generated. • Low aerodynamic stability due to shifted center of mass. Could potentially be offset by batteries behind base-plate, as provided on Unicorn-2. • Requires greater ADCS capability to generate peak power. • Drag surface control possible enabling formation flying without propulsion. • Multiple hinge locations on long axis, greater structural integrity of deployed panels/wings. • Extremely difficult to stack multiple layers due to limited space within deployer.

It is essential to evaluate and compare the available configurations to identify the most suitable option for the design of deployable solar arrays. As outlined in the configuration descriptions, the selection process will depend on factors such as power generation capabilities, mission lifetime, aerodynamic stability, and structural integrity.

2.3. Deployment Mechanisms Overview

Deployable mechanisms have been featured on a large number of new small satellites, primarily for antennas, optical assemblies and solar arrays. Due to complexity, the primary focus has been avoiding

the use of moving parts, limiting the solutions to a small number of mechanisms and structures. The risk of failure of these deployment mechanisms on small satellites usually lead to total loss of the satellite (insufficient power/communication failure) [21].

Deployment mechanisms for solar arrays can cover a wide range of solutions:

- Actuation/Release Mechanism
- Guiding Mechanism
- Damping Mechanism
- Control Mechanism

While these are the major solutions that contribute to a deployable solar arrays, there are smaller peripherals that are essential to the design:

- Power distribution between panels
- Spacing/separation between panels/bus to avoid damage to cells
- Final blocking mechanism to lock panels post deployment

The main deployment mechanisms used for small satellites are discussed below with the components attributing to the main solutions mentioned above:

Spring-loaded mechanisms

Spring-loaded mechanisms represent the majority of deployment mechanisms for small satellites due to the simplicity, lack of need of active control, and low power, mass and volume requirements. These mechanisms usually incorporate a COTS HDRM or a burn-wire assembly that incorporates a thermal cutter and a tie-down cable as the hold down and release mechanism. Once power is supplied to the thermal cutter, it generates heat and cuts the tie-down cable, holding the spring loaded structures stowed prior to deployment. Once the tie-down cable is cut through, elastic energy is released deploying the appendages and locking them in place. The spring-loaded assembly or deployment guide could be made of a multitude of options such as torsion springs, tape springs, SMA hinges, etc.

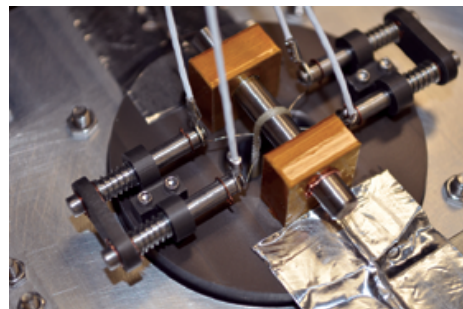


Figure 2.3: Adam Thurn's Burn Wire Mechanism [22]

Actuation/Release Mechanism	Thermal Cutter/ Burn Resistor, Pin Puller/ COTS HDRM
Guiding Mechanism (displacement)	Torsion Springs, Tape Springs (rotational), Conical Springs (linear), Compression Springs (linear), SMA Hinges (linear/rotational)
Damping Mechanism	Friction between hinge surfaces, Rotary Dampers
Hold Down Mechanism	Tie-Down Cable, SMA Release Nuts (DCUBED), Non-Explosive Actuators
Control Mechanism	Usually fixed at deployed state.

Coilable Booms & Inflatable Booms

Coilable and inflatable booms, despite being quite large, are a great option to enable large deployable systems on satellites. They provide great linear displacement and are ideal for separating sub-systems from the main bus of the satellite.

Coilable booms are usually thin-walled booms made of high-yield stress metal like stainless steel or carbon fiber reinforced plastic more recently. Provided a motor-driven or spring-loaded mechanism,

these can be packed extremely densely and deploy in multiple configurations, stem or bi-stem, with the later providing greater bending stiffness [23]. The booms have various packing configurations. They also provide a relatively stiff structure that could even have sensors mounted, requiring minimal movement. Coilable booms are proven on small satellites as seen on ExoTerra's Fold Out Solar Arrays (FOSA), that are facilitated by a roll-out composite boom.

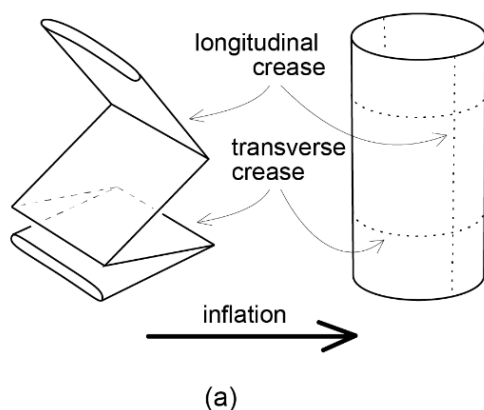


Figure 2.4: Inflation and Coilable Boom 1 [24]

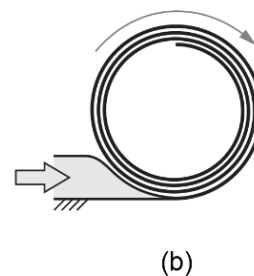


Figure 2.5: Inflation and Coilable Boom 2

Inflatable booms on the other hands look similar but are instead made of flexible material that can be inflated using a stored gas or sublimated (on-site) solid materials. These are usually made of fabrics coated with Mylar, Kevlar or similar strength materials to insure strength when inflated. These can achieve even longer lengths in comparison to deployable booms due to even higher packing density. These are folded in an origami driven approach or coiled up like the deployable booms, shown in Figure 2.5.

Actuation/Release Mechanism	Motor start or latch release (coilable), Valve release/opening (inflatable)
Guiding Mechanism (displacement)	Boom's intrinsic shape, curvature and stiffness. Often facilitated with a spool (linear)
Damping Mechanism	Valve acting as flow restrictors (inflatable)
Control Mechanism	Usually fixed at deployed state.

Active Motor Deployment

Active deployment mechanisms have also been considered in many space missions. Here, instead of a one-time deployment through a pre-loaded spring-based mechanism, rotary actuators and motors can be controlled to provide the rotational movement required to the deployed appendage. Electric motors are not so prevalent in the deployment of small satellite appendages due to their need to be close to the power distribution and control mechanism onboard the satellite. This is why they can only assist in the deployment of singular panels since they can't be placed in between consequent panels. Theoretically placing them between consequent panels in a Z-folded or roll-folded configuration would require power distribution to their location, and would entail additional wiring, etc. This issue is presented in Figure 2.7. Electric motors however have been vastly used in various Solar Array Drive Mechanisms (SADA) that help orient the arrays to the desired pointing vectors for maximum power generation and drag requirements. Such a SADA is shown in Figure 2.6.

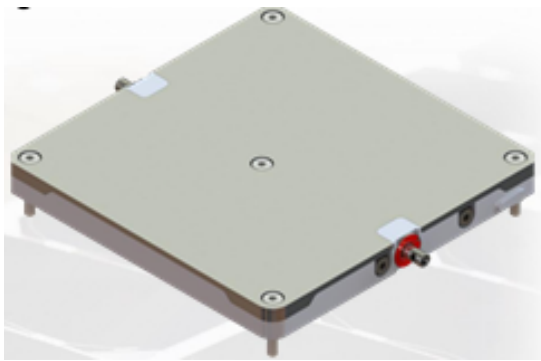


Figure 2.6: Solar Array Drive Assembly [25]

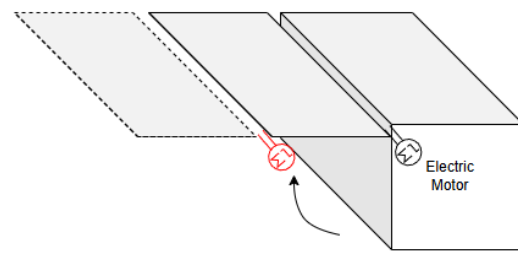


Figure 2.7: Electric Motor Deployment and Folded Panel Infeasibility

A combination of these have been used in deployment mechanisms prior and is also presented in two academic studies at Università di Roma by Fabio Santoni et al [26] [27] where they leverage the modifiable design of the innovative deployable panels and attach it to a rotating shaft controlled by a DC motor.

Actuation/Release Mechanism	Motor Start
Guiding Mechanism (displacement)	Hinge/Gear trains unfolding the panels.
Damping Mechanism	Not required due to controlled deployment speeds.
Control Mechanism	Motor driver w/ sensors to determine deployment angle.

Articulated Masts/Truss Booms

Articulated and coilable masts, such as those first developed by Astro Aerospace Corporation and later refined into designs like the Folding Articulated Square Truss (FAST) mast, utilize lattice columns and repeating cubic space frames to achieve lightweight, high-load structures. Pre-stress is applied using buckled fiberglass bows, which also facilitate the deployment of each bay. A coilable mast is shown in Figure 2.8, showing all phases of the deployable structure. Some notable modern solutions within this domain are provided by Orbital ATK [28]. Stowage length for coilable masts are between 0.5% and 2% of the deployed length, which is excellent for storage. However, the mast must be stored in a canister, the size of which may be too big for small satellites.

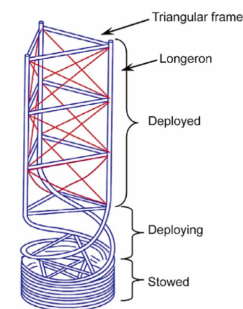


Figure 2.8: Coilable Masts

Actuation/Release Mechanism	Latch/pin puller facilitating canister release
Guiding Mechanism (displacement)	Mast extension through joints and linking elements (linear)
Damping Mechanism	Frictional elements or link material's energy dissipation,
Control Mechanism	Usually built into sequentially unfolding design, fixed at deployed state.

Summary

A summary of the deployment mechanisms and their advantages and disadvantages are provided in Table 2.4. These will be traded-off later in the design process as part of the 2nd research question.

Table 2.4: Deployment Mechanisms Overview

Deployment Mechanism	Type	Advantages	Disadvantages
Spring-Loaded	Passive	<ul style="list-style-type: none"> - High heritage, used in most small satellites including PocketQubes such as FOssaSat, Unicorn 2D, etc. - Low mass/volume required - No power required (apart from release mechanism) - Small radial size 	<ul style="list-style-type: none"> - Release mechanism required - No solar array control possible - Small force remaining at end of deployment - Limited to rigid solar panels
Coilable/ Inflatable Booms	Passive/ Active	<ul style="list-style-type: none"> - Large linear displacement (large arrays) - Heritage in large spacecraft, limited small spacecrafts such as InflateSail 3U. - High packing efficiency 	<ul style="list-style-type: none"> - Motor required to drive boom or heavily tensioned springs - Fluid required for inflatable (mass/volume) - Boom material is heavy, unjustifiable for PQs
Rotary Actuator/ Electric Motor	Active	<ul style="list-style-type: none"> - Retractable - Release mechanism not required - High heritage in small satellites, particularly cubesats. - Large torques achievable - Active control available, higher power generation 	<ul style="list-style-type: none"> - High power requirement - Additional control circuit required - High mass and volume required to mount to panel
Articulated/ Coilable Masts	Passive/ Active	<ul style="list-style-type: none"> - Large linear displacement (large arrays) - Rigid end of deployment, removing need for latching/locking. 	<ul style="list-style-type: none"> - Complex design and assembly - Large testing bench/space required

2.4. Hold Down and Release Mechanism

The HDRM is required to keep the solar arrays within the given dimensions of the PocketQube deployer prior to launch. The HDRM should be capable of withstanding all launch loads and keeping the solar arrays stowed prior to deployment sequence initiation. A number of HDRMs have been developed for space applications but they have mostly been limited to "burn wire" assemblies for small satellites where active control and heavy components such as NEAs are not feasible in mass, and pyrotechnics are not

allowed on board. In this section, burn-wire, Shape Memory Alloy (SMA), and Nano-Morphodynamic Muscle Strand Technology (NMD) solutions are discussed.

2.4.1. Custom Burn Wire Mechanisms

Burn wire solutions are simple, reliable, light, and inexpensive. This makes them prime candidates for small satellites. Typically, burn wire release mechanism consist of 2 main parts:

1. Thermal Cutter: The thermal cutter could be in the form of resistor or resistance wire like Nichrome and is usually what provides a thermal cut through the tied down cable. It is linked to an electronic circuit that provides the current required to heat up the cutting element.
2. Thermally cleavable tie-down cable: Prevents the deployable appendages from deploying. This will just be referred to as cable.

Key considerations are recommended by multiple studies done in developing burn wire mechanisms for smallsat deployable structures.

- Mechanism is required to have 100% success rate across a large sample space. A large sample space is necessary to ensure reliability and success in the real mission.
- Mechanism should be designed such that it does not warrant the disassembly of the satellite for integration and testing. This will make the design and testing campaigns easier.
- Thermal cutter should withstand multiple activation cycles. This allows for multiple attempts in case the cable is not cut through, and extensive functional testing in development.
- Design should avoid single-point failures. Incorporating redundancy in the design is crucial. If deployment of the solar arrays fail, the entire mission fails as there is no/minimal power generation and the optical payload is blocked.
- Design should indicate whether the solar arrays are deployed or not.

Theory

A burn wire setup can be treated as a simple heat transfer problem [29]. The equation that represents the thermal balance for a wire under various thermal interactions is given by:

$$A_{cs} \frac{\partial}{\partial x} \left(K_s \frac{\partial T}{\partial x} \right) + \frac{I^2 \rho_r l}{A_{cs}} - h A_s (T - T_0) - \sigma \epsilon A_s (T^4 - T_0^4) = c \rho V \frac{\partial T}{\partial t}$$

The cross-sectional area of the wire (A_{cs}) is given by πr^2 . K_s represents the thermal conductivity (W/m·K), while T is the wire's temperature in kelvin (K). The length of the wire is denoted by l and the applied electrical current by I . The wire's resistivity (ρ_r) is measured in $\Omega \cdot m$, and h is the coefficient of convective heat transfer (W/m²·K). The surface area exposed to the environment is A_s (m²), and T_0 represents both the ambient temperature and the initial temperature of the wire in kelvin (K). The Stefan-Boltzmann constant σ is taken as $5.6704E - 8$ W/m²·K⁴, and the emissivity ϵ is assumed to be 0.8. The specific heat capacity (c) is in J/kg·K, density (ρ) in kg/m³, and the volume of the wire (V) can be calculated as $A_{cs} \cdot l$. Time is represented by t (s).

The first term in the equation refers to conduction, which we can assume to be negligible to any surrounding surfaces. The second term is the energy due to the flow of current. The third term refers to convective heat transfer and the forth term refers to the radiative heat transfer. In a vacuum environment, we can assume convection and radiation to be negligible. Although ρ_r varies with temperature, this variation is compensated by a constant power model where the change in current (I) maintains a constant power P , calculated as $\frac{I^2 \rho_r l}{A}$. The reorganized equation becomes:

$$P = c \rho V \frac{T_n - T_{n-1}}{\Delta t}$$

If the energy balance is used for a vacuum environment and given a certain step size, one can then estimate the temperature of the wire incrementally. In a study by Chandler Dye at the University of Arkansas, even though the energy out is inaccurately considered to be 0, the rise in temperature with time for vacuum conditions in a test environment matches the analytical calculations well [29].

This calculation can be adopted for a resistor as well, as these are also viable thermal cutters in deployment mechanisms. It allows for judgment on how much current and for what duration the current must be passed for the thermal cutter to reach a viable cutting temperature and not overshoot to remove its reusability in case of failure.

Nichrome Burn Wire Release Mechanism

Resistance Wires have been used in numerous burn wire mechanisms for deployable structures in space. A widely used burn wire mechanism is one invented by Adam Thurn, an Aerospace Engineer at the U.S. Naval Research Laboratory [22] and it consists of Nichrome which is often used for its high electrical resistance. When a current is passed through the wire, it acts like a resistor and rapidly heats up due to joule heating. Due to its high melting point, the wire gets sufficiently hot to cut through the tied down cable without taking too much damage itself. This nichrome burn wire mechanism can be visualized in Figure 2.9.

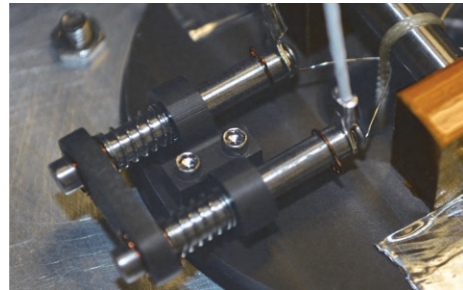


Figure 2.9: Adam Thurn's Burn Wire Mechanism [22]

Thurn's design incorporated a spring-loaded burn wire solution because it could be actuated with standard CubeSat bus power, it was simple to develop by university students, and it used low cost electronics to build. Compression spring system as shown in Figure 2.9 applies a force and a stroke to the nichrome burn wire. These compression springs are held between two saddles which are positioned on dowel pins using retaining rings. The dowel pins have a tapped hole for button head screw threads to go into. The nichrome wire is then tied around the threads. The free length of the nichrome wire is configured into a V shape with the apex in the V being the primary area for cutting through the tie down cable. The free length range is determined by a minimum length that avoids problems with heat sinking to rest of the mechanism, and a maximum length that will cause the wire to lose structural stability when heated as the tensile strength reduces.

This design by Thurn et al. proved to be an extremely viable and reliable solution to cut through tie-down cables. This study proposed the use of Vectran cables, but other cables might prove to be viable options. These will be discussed later in 3.3.2.

The electrical setup of the mechanism is shown in Figure 2.10. In this schematic, the DC-DC converter is used to step down the voltage from the input voltage, and to receive the enable command from the MCU (or NAND gate, etc). The inductor L1 then stores the energy when the switch of the converter is on. When the switch is off, the energy is released to the output through the flyback diode. The capacitor circuits C3, 4 and 5 are there to reduce any fluctuations in the input voltage that could be detrimental to the thermal cutter working effectively, also known as bypass filtering [30]. On the right most side, U2 is the assembly with the burn wire resistor setup that receives this heavily controlled voltage.

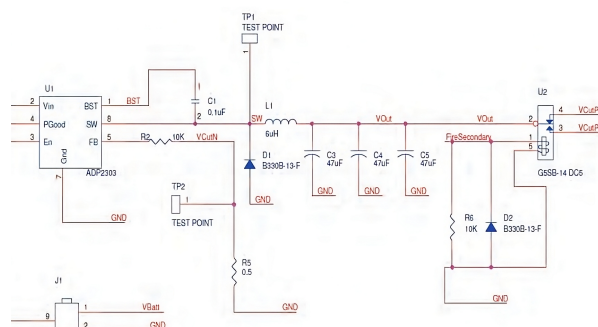


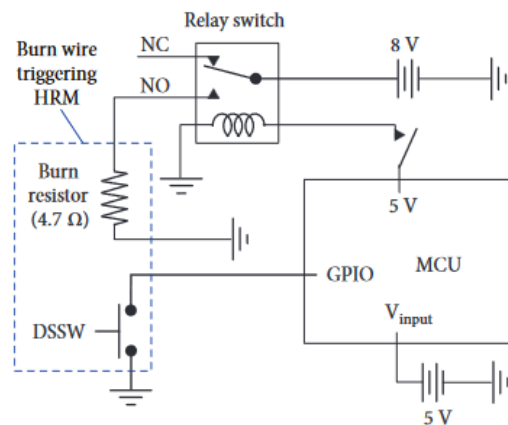
Figure 2.10: Nichrome Burn Wire Electrical Setup [22]

There are a number of advantages and disadvantages of using this or similar release mechanisms as discussed both in the study by Thurn et al.[22] and by Kailaje et al. [31] at Manipal Institute of Technology all shown in the summary at the end.

Resistor Based Burn-Wire Circuit

Instead of using a resistance wire like Nichrome, a resistor may also be used as the heat dissipating component to melt/burn through the tie-down cable. One such design is considered in [32] where they discuss implementing a burn wire deployment mechanism for a 6U cubesat. The proposed burn wire mechanism consists of two brackets, a PCB with a burn resistor and a Deployment Status Switch (DSSW). A surgeon's knot is used (as it is in pogo-pin mechanisms presented in the next section) to ensure reliability during stowage.

A PCB integrated with the burn resistor is mounted on a cubesat rail structure. The electrical and structural setups are presented in Figure 2.11.



(a) Electrical diagram of power cut off circuit for burn resistor

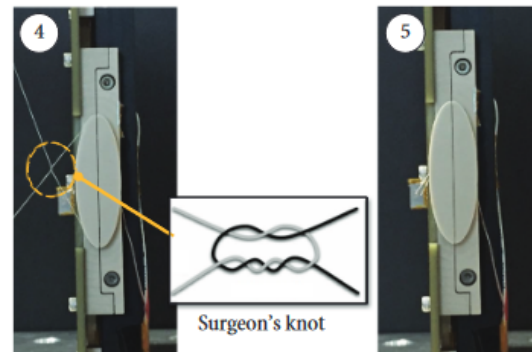


FIGURE 5: Optimized tightening process of nylon wire.

(b) Structural diagram of Surgeon's Knot

Figure 2.11: Resistor-Based Burn Wire Electrical Schematic and Tie-down Knot [32]

The electrical setup presented for this mechanism is much simpler than the ones proposed for the Pogo-pin based HDRM and Adam Thurn's HDRM due to a larger dependency on the MCU. In this circuit, the MCU provides an enabling input to the relay switch. This switch then allows the input voltage of 8V to be driven to the burn resistor. Once the DSSW provides a signal to the GPIO pin, the MCU can then de-activate the relay switch, opening the circuit once again.

An interesting experiment in the study related the release time of the HRM with the thickness and number of tie-down cable windings (which in the case of the study was nylon). The results provides that the number of windings has a more prevalent effect on the deployment time with higher thickness of the cable. At a low thickness of Nylon cable, the number of windings barely had any impact on cutting time. Another interesting consideration in the experiment was to constrain the mechanism along multi-plane directions of the solar panel for safely holding the panel in a launch environment.

Pogo-Pin Based Release Mechanism

A pogo pin, also known as a spring-loaded pin is a type of electrical connector where a spring inside the pin applies a constant normal force against a contact plate or electrode. It consists of a slender cylinder and spring-loaded pin. This is an enticing option for deployment mechanisms and studies have been done by Park et all and consequently developed by Oh et all [34] [35] to study the feasibility and possibility of such a design. The initial design is an evolution from the traditional burn wire mechanism. The pogo pins provide an electrical interface to provide power to the burn wire triggering resistor. The spring force applied by the pin also initiates the deployment guide of the solar panels. The design is shown in Figure 2.12.



Figure 2.12: Pogo Pin [33]

Mechanisms consist of a PCB, guide pins, burn resistors, spring-loaded pogo pins, and brackets. There is a primary and secondary PCB. The secondary PCB is mounted on the solar panel while the primary PCB

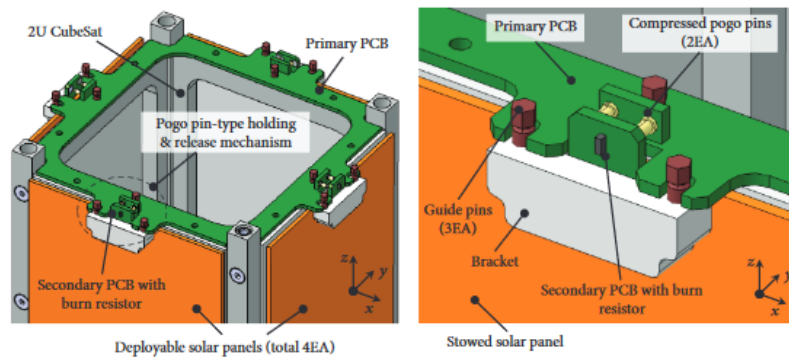


Figure 2.13: Pogo Pin Based Release Mechanism [35]

is on the smallsat bus. The primary bus provides the connection to heat up the resistor in a closed circuit. The guide pins, as shown in Figure 2.13, provide the contact points to wrap the tie-down cable around. In the study, a surgeon's knot is suggested to tie-down the cable in order to make sure that the not does not come lose.

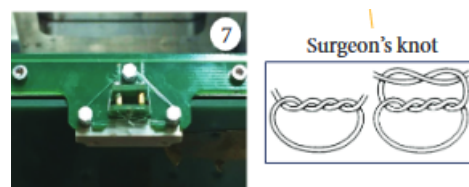


Figure 2.14: Pogo Pin Knot

The electrical setup used was fairly simple. A 5 Ohm resistor was used and multiple levels of voltages were passed down. 5V and 8V were used to see the change in release time of the solar panels. The change in current from 5V to 8V showed significant changes in release time as shown in their observed values, as 5V obtained release times ranging from 6 to 12 seconds and 8V obtained more precise release times around 1 second. A similar pogo-pin based HDRM was developed for a 3U CubeSat at the Space Technology Synthesis Laboratory [36].

2.4.2. COTS HDRMs

SMA-Based Release Nuts / Pin Pullers

SMA-based HDRMs represent a reliable and compact solution for the secure stowage and reliable deployment of deployable components, such as solar arrays or antennas. SMA materials have the unique ability to return to a predefined shape upon heating, making them suitable for release mechanisms where precision and repeatability are required.



Figure 2.15: DCUBED Nano Release Nuts [37]

A key feature of the DCUBED SMA HDRM is its integration of a low-power electrical circuit that

heats the SMA actuator. When current is applied to the circuit, the SMA material undergoes a phase transformation, causing it to contract and release the hold-down mechanism. This process is clean, efficient, and eliminates the need for pyrotechnic or spring-loaded alternatives, making it ideal for small satellites with strict debris regulations.

Figure 2.15 shows the NANO release nuts and pin pullers available at DCUBED that could fit within the volumetric constraints of PocketQubes. The Nano SmartPack Release Nut on the left fits within a volume envelope of $75 * 34 * 4 \text{ mm}^3$, and the ND3PP on the right fits within a cube envelope of $17 * 17 * 17 \text{ mm}^3$.

Gecko Release Mechanism

The Gecko release mechanism, designed by Thermal Management Technologies, was created to mitigate the effects of exposed tie-down cables and deployment failures for small satellites. Being somewhat similar to the DCUBED Smartpack, this mechanism is stored on a long, flat, and thin structure that incorporates both the hold-down and the release mechanism. However, it uses the traditional thermal cutting technology and also incorporates redundant release circuits within itself. This is shown in figure 2.16. The panel can be secured onto two types of hold-down structures, with the one on top being more suitable for limited volume. These mechanisms can be aligned to either long face of the PocketQube and fit within the dimensions. However, this would greatly impact the internal design of the PocketQube and favor differently stacked PCBs inside.



Figure 2.16: Gecko HDRM [38]

EXA Nano-Morphodynamic HDRM

Nano-Morphodynamic muscle strand technology is developed by the Ecuadorian Space Agency that does not require any moving parts [39]. It is only activated by resistive current or heat and has extensive flight heritage on dozens of missions dating back to 2013. These can be highly customized in terms of hold-down strength. These are usually designed for NanoSat applications and can have repetitive/resettable deployment, which is key in testing. Activation power required for these is 5W to deploy in 5s. That attributes to a large battery consumption required for activation. This technology is featured on EXA's Deployable Multifunctional Solar Array.

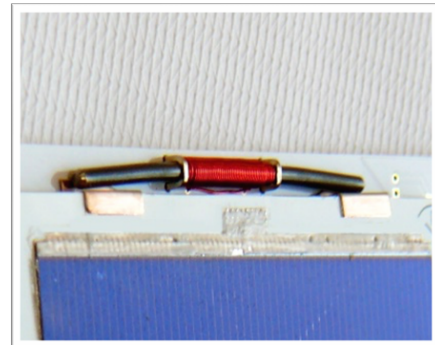


Figure 2.17: EXA NMD HDRM [39]

2.4.3. Summary

A summary of all the HDRMs discussed and found in literature is provided in table 2.5.

Technology	Advantages	Disadvantages
Nichrome Based Release Mechanisms	<ul style="list-style-type: none"> - Nichrome-based release mechanisms have been used in a number of missions and therefore they have proven reliability. - Most components are inexpensive. - Relatively simple design, easily manufacturable by university students. 	<ul style="list-style-type: none"> - Slow cutting process may result in re-fusing the tie-down cable, causing failure. This failure mode would prevent re-activation of the mechanism. - The burn mechanism produces smoke that could be harmful for nearby optical sensors. - Long lengths of the tie-down cable may entangle around surrounding subsystems or obstruct any optical imagery. - Assembly is highly dependent on workmanship that can involve human errors.
Resistor Based Release Mechanisms	<ul style="list-style-type: none"> - Less workmanship required as only one wire/cable component needs to be assembled, and the resistor is fixed. - Heat response is less complex to predict in analysis. - Simple design for manufacture by students. - Low heat dissipation to surroundings in comparison to Nichrome Wire. 	<ul style="list-style-type: none"> - Additional fixture/brackets required around the resistor to tie down the cable, increasing number of components. - Deployment failure if the tie-down cable is not tensioned onto the resistor properly, which is avoidable with Nichrome wire due to its draw. Also highly dependent on workmanship during assembly.
Pogo Pins	<ul style="list-style-type: none"> - Pogo pins maintain constant contact force, ensuring connectivity even if the tie-down cable loses tension during launch. - Their small size makes them ideal for compact spaces, such as in a PocketQube. - They feature blind mating and self-alignment and are resistant to vibration and shock, which is crucial during launch. - They can indicate deployment status; loss of contact with the secondary PCB signifies successful solar panel deployment. 	<ul style="list-style-type: none"> - Electrical contact point can fail if debris or dirt is present. - Limited current capacity may restrict their use in some deployment mechanisms. - Higher cost compared to other connectors. - Added complexity compared to traditional burn wire mechanisms.

Technology	Advantages	Disadvantages
COTS SMA- Based Release Nuts/ Pin Pullers	<ul style="list-style-type: none"> - Available in extremely compact sizes in new developments by DCUBED, can even fit inside PocketQubes. - Built in redundancy and high reliability since they are tested and approved for flight. - The time of release is controllable based on the amount of power supplied. - They can indicate deployment status. - Highly reusable, making them excellent for testing. Have a high number of use cycles and can be reset easily. 	<ul style="list-style-type: none"> - Fixed and large geometries limit integration on small satellites. Need space internally in the PocketQube bus. - Usually higher power requirement to activate. - Higher cost compared to other custom burn wire solutions.
NMD HDRM	<ul style="list-style-type: none"> - Their small size makes them ideal for compact spaces, such as in a PocketQube. - Available in custom sizes from Ecuadorian Space Agency. - They can indicate deployment status. - Built in redundancy and high heritage, contributing to high reliability. 	<ul style="list-style-type: none"> - Higher cost compared to custom HDRMs. - Lack of available information regarding NMD technology

Table 2.5: Comparison of different HDRMs

2.5. Deployment Guide

This section focuses on the mechanism that drives the solar panels to their final/deployed configuration, excluding the final blocking/locking mechanism. To provide the rotational movement that allows solar panels to unfold, a number of mechanical systems can be evaluated consisting mainly of passive mechanisms with rigid hinges and flexible hinges or active mechanisms with linear actuators and motors. Rigid hinges can consist of free hinges, torsion spring hinges while flexible hinges can consist of tape spring hinges or Shape Memory hinges.

Rigid hinges are similar to door hinges that are modified for space applications [40]. These typically contain 3 elements: 1) a pin and housing for solar array to pivot around; 2) a spring to provide the force for deployment (this can be obsolete given that there is another way to provide the push needed to unfold); 3) a latching mechanism to lock the panel in place once it's deployed.

Flexible hinges provide an alternative solution to rigid hinges by removing unnecessary parts and incorporating the driving force in the same material that would hold the structures together. This material could come in the form of SMA parts or tape springs, that provide the restoring force. While flexible hinges require less parts and can contribute to a simpler assembly, the lack of material specifications and unpredictability of the flexible material can lead to quite extensive testing requirements

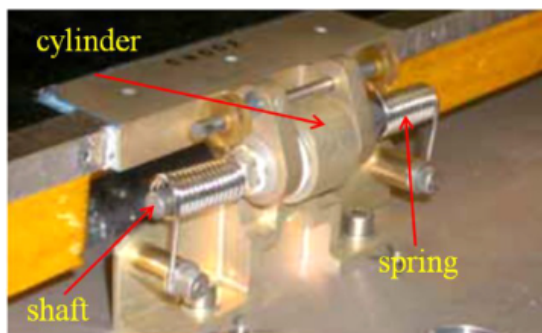
and non-linear analysis. It also has less heritage in comparison to rigid hinges for deployable structures.

Linear Actuators and motors provide active alternatives to the passive structures discussed where the deployment process could be controlled electrically. While these are appropriate for larger spacecraft, their mass, volume and complexity eludes their involvement in smallsats where miniaturized and light structures are preferred and there isn't much room available. For a small satellite mission, the end of life usually requires a de-orbit maneuver where the satellite completely ablates in the atmosphere. Therefore, retracting the solar panels into stowed configuration is not required and an active mechanism is redundant.

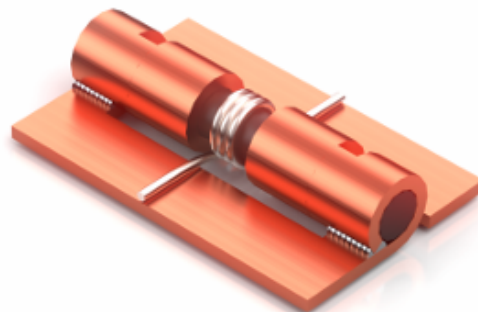
2.5.1. Rigid Hinges

Torsion Spring Hinge

Torsion spring hinges, also known as torque hinges and torsion hinges, are the most commonly used hinges in smallsat deployment mechanisms. Notable PocketQubes using rigid torsional hinge deployment mechanisms include FossaSat-2 and Unicorn-2. The conventional mechanism consists of many moving parts, such as springs, cylinders, and locking devices for the final blocking. 2.18a shows the setup of a torsion spring hinge as described by Ha et al at RMIT University [41].



(a) Torsion Spring Hinge [41]



(b) EXA Nano Hinge [42]

Figure 2.18: Helical Torsion Spring Hinges

Typically, a rod is placed through a torsion spring as the spring is not able to withstand all the torsional loads. The ends of the torsion spring are placed in two different housings, one that is attached to the stationary surface and one that is attached to the rotating surface. In the case of consequent panels, both surfaces would be rotating. COTS hinges are also available on the CubeSat market, similar to the one in 2.18b. However, usually custom solutions are preferred since COTS systems have specific separations, axis diameters and surface thicknesses that might all be different for different solar panel assemblies. These rigid hinges have high heritage in spaceflight and provide a solidified and controlled mechanism for deployable structures. However, they also contain increased number of parts that could be susceptible to higher mass, complexity and cold welding phenomena.

The torque relationship for torsion springs is linearly proportional to the angular deflection as seen in figure 2.19. After the maximum deflection (usually provided by the manufacturer) is reached, the torque gets exponentially unpredictable. Therefore, it is recommended to stay within the maximum torque deflection provided by the manufacturer, and that corresponds to the maximum internal bending stresses.

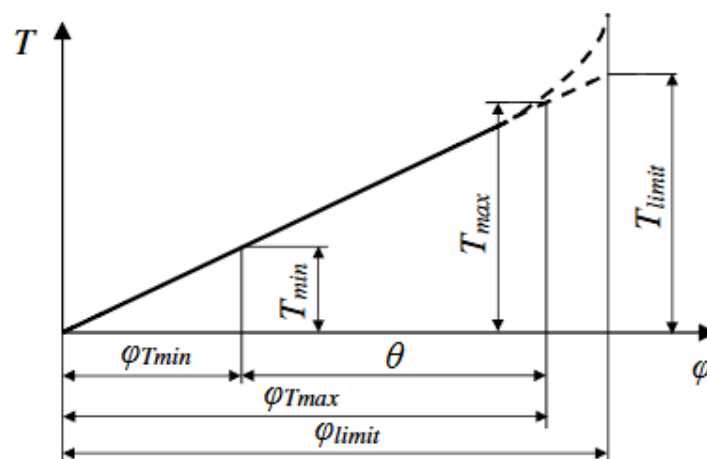


Figure 2.19: Helical Torsion Spring Torque & Angular Deflection Relationship [43]

2.5.2. Flexible Hinges

Tape Spring Hinges

A tape spring is a thin-walled structure that can incorporate a curved cross-section. A commonly used version of a tape spring is the Carpenter's tape. One might notice that when the carpenter's tape is folded, it contains elastically stored energy that is released to bring it back to its original position and the curved cross section assists with that. These come under the category of self-locking hinges as well since they may self stabilise the structure after deployment when equilibrium condition is satisfied [44]. Due to the relatively low stiffness of these elastic tape springs, their deployment behavior is extremely non-linear, and a number of oscillations might be required to reach this equilibrium/deployed state.

Typically, a tape spring consists of the following general parameters:

- Thickness (t)
- Transverse radius of curvature (R)
- Subtended angle of cross section (α)
- Length (L)

These are indicated in Figure 2.20.

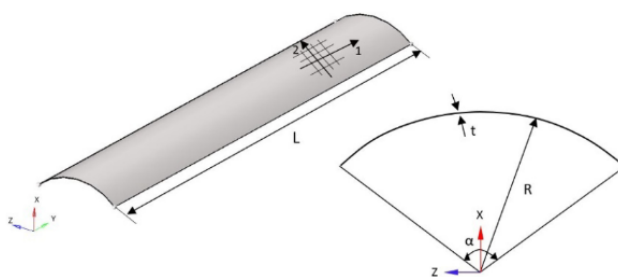


Figure 2.20: Dimensional parameters of the tape spring [44]

Due to space conditions, the choice of materials for space applications is limited to steel, aluminum, CFRP, GFRP, KFRP, and beryllium copper alloys. Due to the thin-walled nature of the tape spring, it is necessary to investigate its folding and deployment mechanics, as well as the storage of strain energy in stowed configuration.

Tape springs inherit two behaviors due to bending moments, depending on the location. Equal and opposite sense bending. If the direction of couple is opposite to the natural transverse curvature, the tape-spring produces a sudden snap-through buckling to form a reverse folding. If the direction of

processing. The lack of a separate burn wire release mechanism is also favorable. However, deployment mechanisms also require large recovering forces which can hinder release time. Power requirements for heating up the SMP material can also be much higher than burn wire mechanisms.

Shape Memory Polymer Composite (SMPC) hinges are shape memory polymers with fiber reinforcements that also have the strength of traditional reinforced polymers while still retaining the shape recoverability.

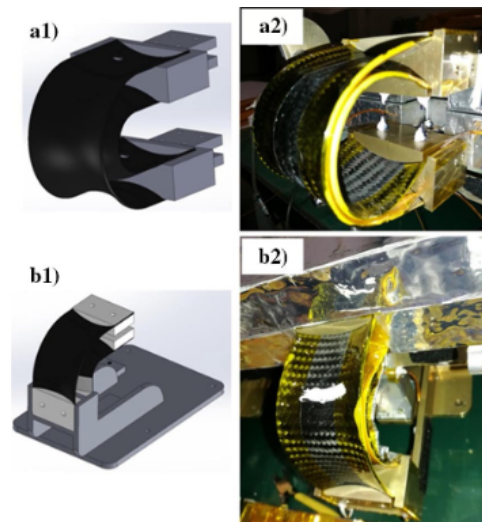


Figure 2.24: SMP Hinge 90 and 180 [45]

A study by Lan et al [45] delved into possible hinge configurations using SMPC hinges as shown in Figure 2.24. The SMPC hinges also use the shape of a carpenter's tape for increased bending stiffness.

While the tape spring hinges offer self blocking at the deployed configuration, SMPC hinges may require an additional self-locking mechanism to lock its deployed state rigidity, which would add additional mass.

Shape Memory Alloy Hinges

Filed under Patent No: 12,030,672, NASA Glenn Research Center has developed SMA hinges specifically for CubeSats and small satellites, providing a lightweight, reliable mechanism for release and deployment of solar arrays and antennas [46]. Unlike traditional mechanisms, these SMA-based systems are compact, low-power, and free from debris generation, as they do not require pyrotechnics or burn wires. The system uses an SMA-activated pin puller to disengage retention hooks, allowing SMA spring strips in the hinge to passively deploy the components once in orbit. This innovation has already been successfully used on NASA missions, showcasing its potential as a transformative deployment solution for small satellites. The new SMA spring strips can be visualized in figure 2.25.

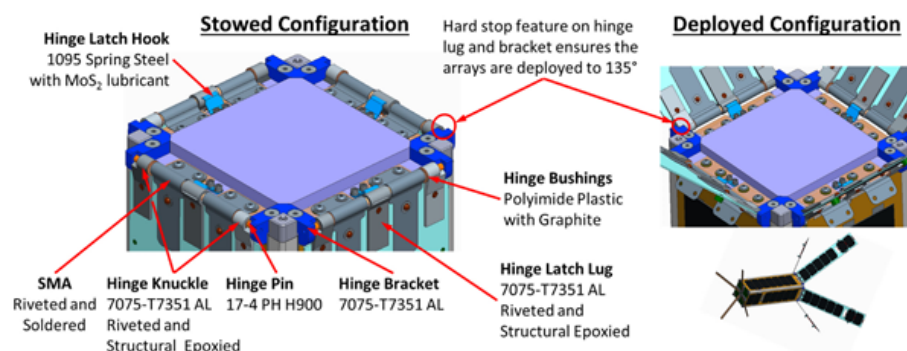
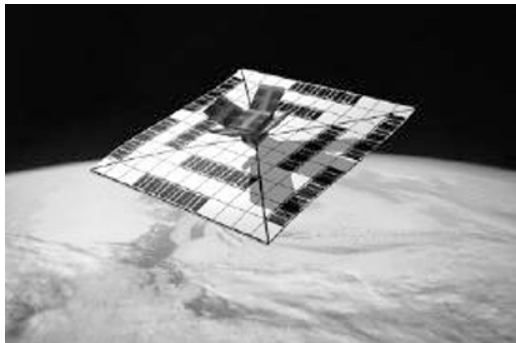


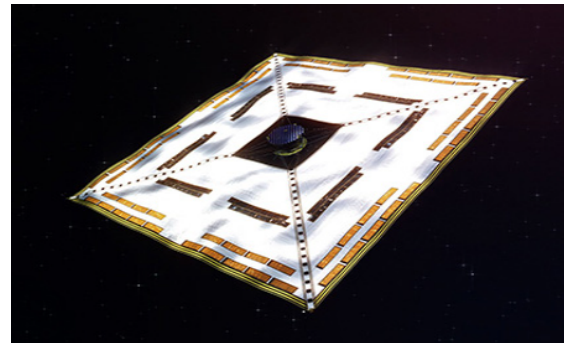
Figure 2.25: NASA Glenn's SMA CubeSat Hinge [46]

2.5.3. Spin-Stabilized Deployment

Spin of a satellite can be used for deployment of solar arrays as well. This deployment technique is particularly beneficial when considering the deployment of really large membranes, such as flexible solar arrays, solar sails. Suggested by ISSL's CubeSat project, they intended to experiment the deployment of large thin film solar cells using centrifugal force generated by spinning the satellite main body [47]. Another notable mission that utilized centrifugal force to deploy a large solar sail membrane was IKAROS by JAXA. Masses are attached to the four corners of the sail to keep tension on the sailed, and a low spin rate is maintained for this purpose as well. While this membrane was largely used as a means of propulsion, there were thin film cells attached for power generation possibilities as well. Both of these missions are visualized in figure 2.26a and figure 2.26b.



(a) Tokyo University CubeSat [47]



(b) IKAROS [48]

Figure 2.26: Notable missions featuring solar array/sail deployment by spinning or centrifugal force

2.6. Summary of All Options

Having reviewed all the options available for the different parts/stages of the deployable solar arrays, they can be summarized in table 2.6. Additionally, damping mechanisms found in the same academic papers reviewed have also been added. The table provides the sub-mechanism or function in on the left, with the available solutions identified for those in the preceding columns.

Table 2.6: Overview of Sub-Mechanisms and Solution Options

Sub-Mechanism	Solution Options					
Hold Down	Tie-Down Cable	Release Nut / Pin Puller	Gecko HDRM	EXA's NMD HDRM		
Release Mechanism	Resistor-based Burn Wire	Pogo-Pin Mechanism	Nichrome Burn Wire	Release Nut / Pin Puller	Active Motor Control	
Deployment Guide	Coilable / Inflatable Masts	Linear Actuator	Active Motor	Elastic Spring Hinge	SMA (Spring) Hinge	Spinning / Centrifugal Force
Final Blocking	Residual Spring Torque + Hinge Design	Active Motor Lock	Stable Tape Spring Position			
Damping	Fastener Torque	Friction Pad/Break				

2.7. Structural Analysis Theory

Designing structures and mechanisms for satellites requires addressing various environmental challenges encountered during launch. One of the primary concerns is mechanical loads, withstanding high acceleration, vibration and acoustic loads during launch. These are more stringent than in orbit loads, which consist of thermal stresses due to temperature extremes and oscillations induced by mechanisms. Analysis can assist in identifying material selection and optimizing mass, making sure that design selections can withstand launch and in-orbit conditions. Structural analysis of the final assembly plays a critical role in evaluating whether the assembly can endure the rigorous acceptance tests mandated by rideshare missions, ensuring the satellite does not pose a risk to other payloads or the launch vehicle.

2.7.1. Static Analysis

Static loads on spacecraft are the time-invariant forces experienced by the launcher during different phases of flight. These loads are usually quantified in axial and lateral accelerations. The structures should be simulated to withstand maximum load enveloped described by the launchers (axial $\pm 6g$ and lateral $\pm 3g$ for Falcon 9).

For static loads, the system is assumed to be time-invariant. Thus, velocity and acceleration are zero:

$$\dot{\mathbf{x}}(t) = 0, \quad \ddot{\mathbf{x}}(t) = 0$$

The equations reduce to:

$$\mathbf{K}\mathbf{x} = \mathbf{f}$$

2.7.2. Vibration Theory

During launch, satellites are subjected to various vibrational loads that can stem from vibroacoustic noise, booster ignition and burn out, engine vibrations, and countless other sources [49]. These disturbances travel through the rocket's structural frame, causing all attached components to also vibrate. These vibration loads can be great enough to shake critical components apart if they're not designed properly. In order to design spacecraft to survive launch loads, dynamic analysis is necessary. By performing dynamic analysis throughout the design process, we can establish certain confidence that the satellite can withstand the launch environment and still function afterwards.

On the theoretical side, vibration analysis often begins with a simplified single-degree-of-freedom model. Consider a mass m attached to a spring (stiffness k) and a damper (coefficient c) under an external force $F(t)$. The equation of motion is:

$$m\ddot{x} + c\dot{x} + kx = F(t),$$

where \dot{x} and \ddot{x} represent velocity and acceleration, respectively.

If no external force is present, the system's natural frequency $\omega_n = \sqrt{\frac{k}{m}}$ determines how it vibrates on its own, and the damping ratio $\zeta = \frac{c}{2\sqrt{km}}$ governs how quickly those oscillations die out.

Modal Analysis

Modal analysis is a way to understand the dynamic response of a structure into a set of independent modes of vibration, each characterized by a resonant frequency and a mode shape. Modal analysis begins by neglecting the damping and external forces and assuming free vibrations, resulting in the following:

$$\mathbf{M}\ddot{\mathbf{x}} + \mathbf{K}\mathbf{x} = 0,$$

where \mathbf{M} is the mass matrix, \mathbf{K} is the stiffness matrix, \mathbf{x} is the displacement vector, and $\ddot{\mathbf{x}}$ is the acceleration vector. Assuming harmonic motion, the displacement can be expressed as:

$$\mathbf{x}(t) = \boldsymbol{\phi}e^{i\omega t},$$

where ϕ is the mode shape, ω is the angular frequency, and t is time. Substituting this expression and its second derivative ($\ddot{\mathbf{x}} = -\omega^2\mathbf{x}$) into the equation of motion gives:

$$(-\omega^2\mathbf{M} + \mathbf{K})\phi = 0.$$

This can be rearranged as:

$$(\mathbf{K} - \omega^2\mathbf{M})\phi = 0.$$

The above equation represents an eigenvalue problem. For non-trivial solutions ($\phi \neq 0$), the determinant of the coefficient matrix must be zero:

$$\det(\mathbf{K} - \omega^2\mathbf{M}) = 0.$$

Solving this determinant yields the eigenvalues ω_i^2 , which correspond to the square of the natural frequencies of the system.

Random Vibrations

Random vibrations occur due to irregular, unpredictable forces acting on structures and are nondeterministic in nature. They do not have a repetitive, oscillatory nature like the sine vibrations discussed previously. Typically, a cluster of vibration intensities and frequencies exist, with a Gaussian distribution. The input to a random vibration analysis is given in terms of Power Spectral Densities (PSD). Usually the Root Mean Square (RMS) of the results are studied. Typically, the analysis is performed over a specific frequency range and in spacecraft design, this correlates to frequencies from 0 to 2000 Hz.

The Fourier transform is used in random vibration analysis to convert the equations of motion from the time domain to the frequency domain, due to their expression in PSD format.

Using Fourier transforms, the equations can be transformed into the frequency domain as:

$$[-\omega^2\mathbf{M} + i\omega\mathbf{C} + \mathbf{K}] \mathbf{X}(\omega) = \mathbf{F}(\omega)$$

A transfer function characterizes the dynamic behavior of a system by describing how the system responds to the input forces in the frequency domain.

$$H(\omega) = A(\omega) - iB(\omega)$$

where $A(\omega)$ and $B(\omega)$ are the real and imaginary components of the transfer function.

The relationship between the input and output PSDs in the frequency domain is given by:

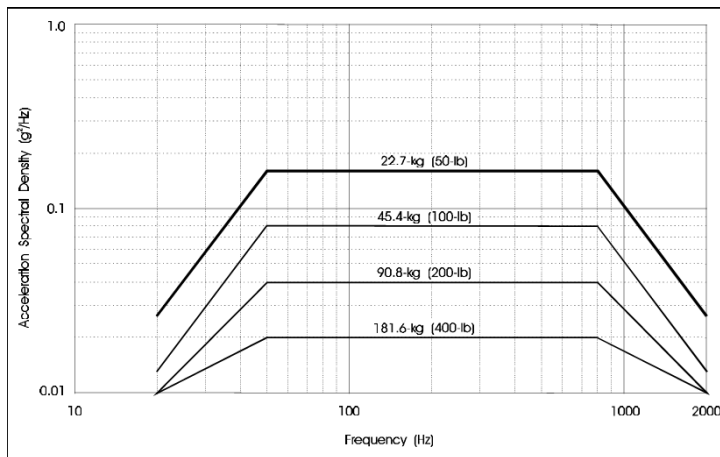
$$S_{\text{out}}(\omega) = |H(\omega)|^2 S_{\text{in}}(\omega)$$

The **Root Mean Square (RMS)** response is a key metric in random vibration analysis, representing the statistical magnitude of the response. It is calculated by integrating the output PSD over all frequencies:

$$\text{RMS} = \sqrt{\int_0^{\infty} S_{\text{out}}(\omega) d\omega}$$

To qualify certain sub-systems and small satellite structures for launch, certain profiles are used as the input PSDs to gauge the response, specifically evaluating the deformation and von-mises stresses.

National Aeronautics and Space Administration (NASA) created the General Environment Verification Standard (GEVS) to define a launch environment that matches/exceeds the baseline for most launch systems. This profile can be visualized in figure 2.27.



Frequency [Hz]	G Acceleration [G ² /Hz]
20	2.6e-002
50	0.16
800	0.16
2000	2.6e-002

Table 2.7: GEVS Qualification PSD

Figure 2.27: GEVS Vibration Qualification Profile

For this thesis, the random vibration module will be used alongside the modal analysis module within the Ansys Workbench and suite to determine the response from the stowed solar array assembly.

2.7.3. Explicit Analysis

Explicit dynamics is a numerical technique used to solve highly transient problems involving short-duration events, such as impacts, explosions, or crash simulations. In the case of this thesis, explicit dynamics will model the impact moment occurring at the end of panel deployment. Due to the extreme non-linearity of such events, achieving convergence using traditional implicit methods is infeasible. Explicit dynamics overcomes this limitation through uncoupled equations that can be solved directly, avoiding iterative matrix inversions and convergence checks.

Explicit analysis is typically based on the central difference method, a time integration scheme where displacements and velocities are computed explicitly at each time step using previously known values. This method is computationally efficient for short time steps but requires careful selection of time increment sizes to ensure numerical stability.

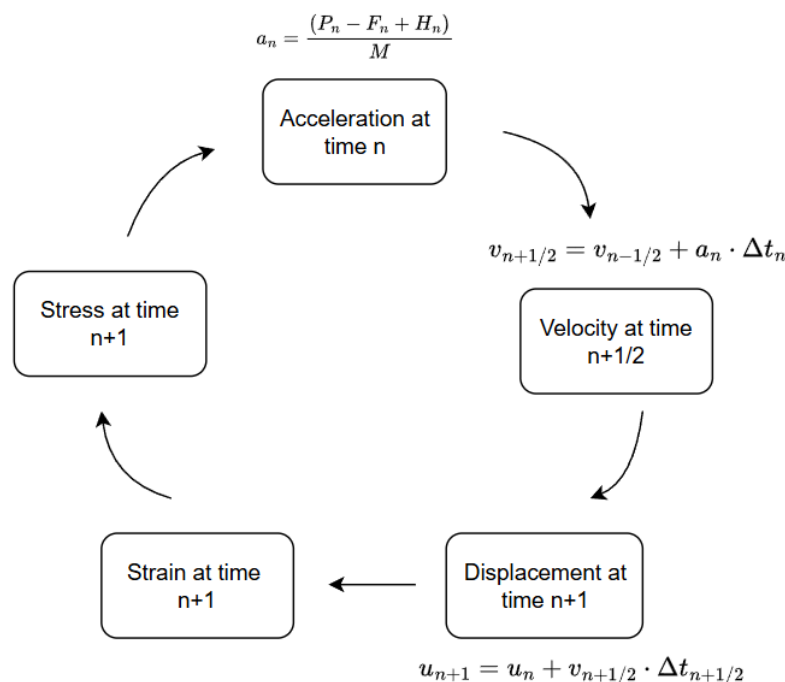


Figure 2.28: Explicit Dynamics Solution Process

Figure 2.28 outlines the solution process in explicit dynamics

To accurately simulate the impact at the end of deployment, Ansys LS-DYNA will be used instead of the Explicit Dynamics module. LS-DYNA offers enhanced capabilities, including the ability to account for rotational velocities and complex contact conditions, making it ideal for this purpose.

3

Design of Deployable Solar Arrays

The primary objective of this chapter is to develop a design for deployable solar arrays that can be utilized on 3P PocketQubes. At the outset of this thesis, a potential project within the Delfi Space Program involved developing deployable solar arrays for a 3P PocketQube in a wing configuration, also referred to as configuration 3 within the literature review section 2.2.1. This configuration is already featured on a number of missions using Unicorn 2, FOSSASat-2 and Challenger as seen in table 2.1. This configuration features high peak power generation due to the availability of a singular, large surface that can be exposed to the incident solar radiation.

The design process will incorporate structural analysis to ensure the chosen/designed components can withstand expected conditions. This chapter will lay the groundwork for future prototyping and iterations, enabling their integration into upcoming missions within the Delfi Space Program. The requirements for this design are detailed in 3.1, and the overall design process is outlined in 3.2.

3.1. Requirements

Generating requirements is a critical step in the design process as it provides measurable goals that guide the development and evaluation of the final design. For this design, the requirements are derived from established standards, including the PocketQube Standard and the AlbaPOD ICD. The PocketQube Standard provides guidelines for dimensions, weight, and functionality to ensure compatibility with the PocketQube framework [8]. The AlbaPOD ICD specifies critical interface parameters, such as deployment constraints and attachment mechanisms, ensuring seamless integration with the launch deployer [9].

Requirement ID	Requirement	Source
RQ-DC-01	All deployable appendages shall be constrained by the PocketQube and not by the deployer	PQ-Gen-01
RQ-DC-02	Deployment mechanism shall avoid flammable and hazardous materials.	PQ-Gen-03
RQ-DC-03	Stowed solar panels and deployment mechanism shall fit within total length of 192.0 ± 0.1 mm ($\pm z$).	PQ-Mech-06
RQ-DC-04	Stowed solar arrays and deployment mechanism shall fit within a 10.5 mm appendage volume on either side of the PocketQube ($\pm x$).	AlbaPOD ICD

Derived Functional Requirements

Aside from the requirements available directly from the PocketQube standard and the deployer ICD from AlbaOrbital, additional requirements are derived from reviewing academic papers regarding and ECSS standards, particularly "ECSS-E-ST-33-01C-Mechanisms".

Requirement ID	Requirement
RQ-FN-01	<p>Deployment mechanism shall lock the panels in place post deployment.</p> <hr/> <p>This requirement is derived from the review of all non-orientable solar arrays. Without the panels locking in place, there would be uncontrollable vibration effects and attitude control system would have to account for the unstably deployed solar arrays. This requirement is also derived from ECSS-E-ST-33-01_0820139 "Electrically actuated deployable items shall use positive latching or locking"</p>
RQ-FN-02	<p>Hold Down mechanism shall keep the solar panels secured until planned deployment</p> <hr/> <p>As derived from the Albapod ICD, solar arrays cannot touch the AlbaPod outer wall due to concerns of jamming the push plate. Therefore, they have to entirely be constrained by the hold-down mechanism.</p>
RQ-FN-03	<p>Deployment mechanism shall provide feedback telemetry on deployment status post attempt</p> <hr/> <p>This is necessary due to the planned start of other systems in the PocketQube deployment sequence. It is also outlined in ECSS-E-ST-33-01_0820135 "Unless monitored at spacecraft system level, the design of mechanisms shall include means to monitor the execution of its main functions."</p>
RQ-FN-04	<p>Release mechanism shall incorporate redundancy</p> <hr/> <p>Redundancy is crucial in release mechanisms/circuits because failure to deploy can result in mission failure due to insufficient or absent power generation. This can be included in the form of multiple burn resistors, etc. It is mentioned in ECSS-E-ST-33-01_0820454 "All single point failure should be eliminated by redundant components."</p>
RQ-FN-05	<p>In the event of deployment failure, solar arrays shall still be able to generate power in stowed configuration.</p> <hr/> <p>Deployment failures as studied in [50] are particularly prevalent in solar arrays and often result in mission failures. Redundancy in release mechanisms is not sufficient as failures can be attributed to tribology (frictional effects), inadequate torque margins, etc. An example is NASA's Galileo Spacecraft's high-gain antennas or ESA Beagle 2, which was declared lost due to lack of data transmission. While small satellites may be launched with minimally charged batteries, they are often sitting in deployers for long durations prior to launch. Due to depletion, PocketQubes may need to generate enough power in orbit to activate the release circuits.</p>

Requirement ID	Requirement
RQ-FN-06	<p>Deployable solar array assembly should be completely mounted on the exterior of the PocketQube volume.</p> <hr/> <p>This requirement was developed by reviewing existing COTS deployable assemblies. They can usually be attached to the exterior surfaces of small satellites utilizing fasteners and do not utilize any internal volume that may be required by important payload. This requirement does not include information flow as specified in 3.3.1.</p>

3.2. Design Process Overview

The design overview is provided in 3.1. Firstly, trade-offs will be conducted to determine the best concepts for the overall deployment mechanism, and consequently the HDRM and deployment guides. Following this, the PCB Assembly design to fit within the stowed envelope will be developed. This will include an evaluation of the present materials available and the possible layout to incorporate all required components. Furthermore, vibrational analysis will be done to determine the thickness and spacing combination that survives the most extenuating launch loads. Finally, a hinge design will be developed using constraints derived from the previous sections. Springs will be identified that are available in the market and provide relevant torque to deploy the panels instantly. Lastly, a hinges will be developed to support the springs and survive the shock experienced due to the impact at the end of deployment. Explicit analysis will assist in determining the survivability of the hinge during impact, and further vibrational analysis will be done on the final array design to assess their integrity against GEVS qualification loads.

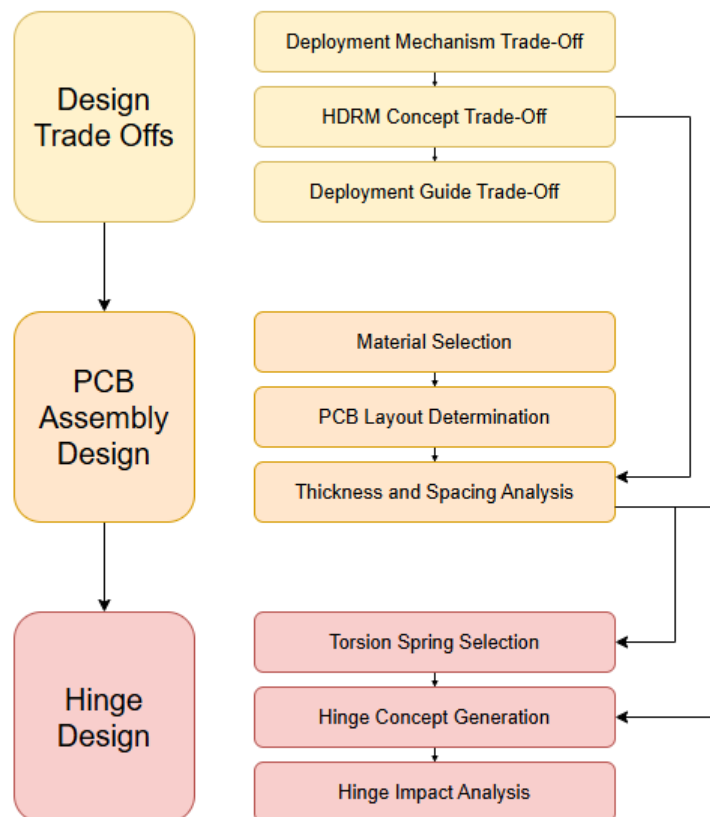


Figure 3.1: Design Process Overview

3.3. Deployment Mechanism and Subsystem Concept Trade-Offs

3.3.1. Deployment Mechanism Overview and Trade-Off

There were a number of deployment mechanisms studied in the literature review. These are spring-loaded, coilable/inflatable booms, rotary actuators/electric motors, and articulated/coilable masts. All four of these can be traded-off to pick the most suitable option for the deployable solar array design. A graphical trade-off is provided in Table 3.3 that evaluates these deployment mechanisms. Advantages and disadvantages given in table 2.4 are used to facilitate the trade-off.

Deployment Mechanism	Complexity	Reliability in Small Satellites	Size & Mass	Functionality
Coilable/ Inflatable Booms	<ul style="list-style-type: none"> Requires guide rails/ scissor mechanism. Pressurized system (inflatable) or motor (coilable) needed. 	<ul style="list-style-type: none"> Only 1-2 CubeSat examples launched. No COTS solutions available. E.g.: GASPACS, ExoTerra ROSA 	<ul style="list-style-type: none"> Need space inside PQ volume for gas/ motor to drive structure. Pressurized gas systems -> heavy. 	<ul style="list-style-type: none"> Can control speed and displacement length/ angle. Retractable design. No separate release mechanism required.
Rotary Actuator/ Electric Motor	<ul style="list-style-type: none"> Requires powered motor/ actuator. Complex control circuitry. 	<ul style="list-style-type: none"> Used abundantly in SADAs. Need gears to translate to rotational movement. E.g.: DHV SADA, Revolv SARA. 	<ul style="list-style-type: none"> Much larger than torsion springs. Unable to fit within folded panels. 	<ul style="list-style-type: none"> Unable to use with multiple panels. Speed/ displacement controllable. No release mechanism required.
Spring- Loaded	<ul style="list-style-type: none"> Requires housing & lubrication. Ground tests may not match orbit environment. Low number of components. 	<ul style="list-style-type: none"> High heritage in CubeSats/ PocketQubes. E.g.: Unicorn 1-2, FossaSat. 	<ul style="list-style-type: none"> Can be mounted completely externally. 	<ul style="list-style-type: none"> No control or retractability Needs locking + release mechanism
Articulated/ Coilable Masts	<ul style="list-style-type: none"> Many truss members; extremely complex geometry. Extensive testing and complex test setup required to mitigate gravity. 	<ul style="list-style-type: none"> Limited to large spacecraft. No known PQ usage. 	<ul style="list-style-type: none"> Space for canister/ support structures needed inside PQ volume. 	<ul style="list-style-type: none"> Can control speed/ displacement. No separate release mechanism required.

Table 3.3: Comparison of Deployment Mechanisms for Small Satellites. Ratings are color-coded as follows: Green meets requirements confidently, Yellow requires additional considerations to meet requirements, and Red is not expected to meet requirements.

Based on the graphical trade-off, the most suitable deployment mechanism for this project can be qualitatively determined to be a **spring-loaded mechanism**. Spring-loaded mechanisms propose light weight solutions that have a high heritage in spaceflight. Their complexity is quite large, but this can

be reduced by incorporating known burn wire designs, and utilizing COTS equipment for springs and tape springs. Inflatable and articulated masts, albeit with high heritage for large spacecraft, are not appropriate for this use case since they require a large volume and mass available to store these structures internally, violating requirements. Active mechanisms using rotary actuators and motors also have a high heritage in spaceflight, and can provide good control and retract-ability for certain in-orbit services. However, these require a lot of power, which might not be available prior to deployment with body-mounted arrays on PocketQubes. Additionally, they also require large components that cannot be incorporated between consequent panels and still adhere to the volume envelope available with the deployers. While a combination of motors and coilable booms are available on CubeSats in the form of ROSA by ExoTerra [51], they require large internal volumes to store the booms and motors, infeasible in a PocketQube volume. A breakdown of what encompasses a spring-loaded deployment mechanism is provided in the following figure 3.2.

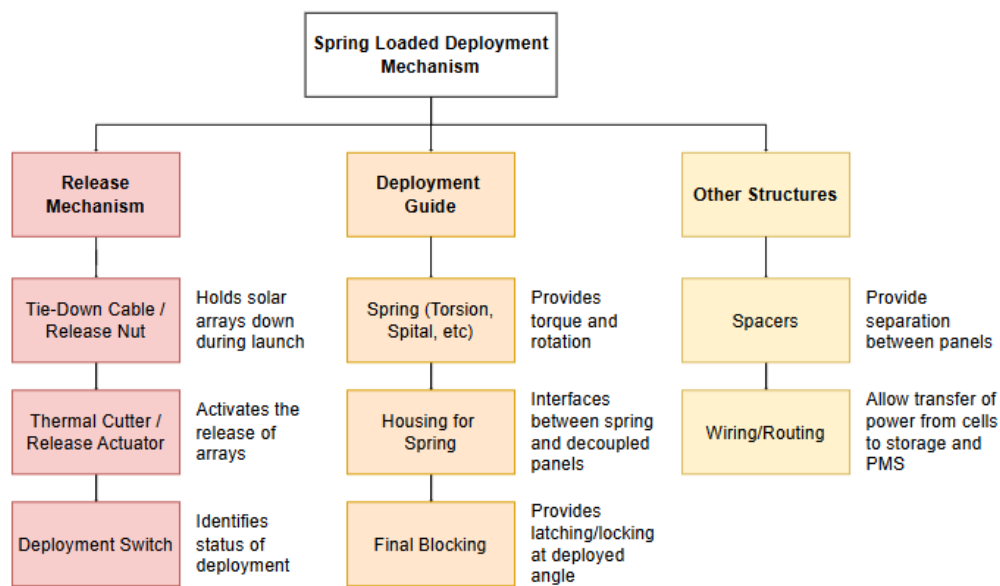


Figure 3.2: Spring Loaded Mechanism Breakdown

HDRMs consists mainly of a tie-down cable, release nut or alternative COTS hold down mechanism, a thermal cutter (burn wire) or release actuator for the hold down mechanism, and a deployment switch to indicate the status of deployment. The deployment guide usually exists of the spring/elastic element that stores the potential energy for deployment, the housing for this elastic element, and the final blocking. Other structures possibly contain spacers to facilitate the panel separation, and the electrical connection and routing through the PCBs. In the following sections, these will be evaluated and traded-off to provide the best solution to the design of deployable solar arrays.

Functional Overview

Mechanisms can be represented through a functional overview, highlighting how inputs are transformed into outputs. This approach is valuable for identifying the required structures and understanding how they contribute to the necessary functions of the system. For deployable structures, it is specifically outlined in the research study of "Conceptual Design of Deployable Space Structures" by Martin Hillebrandt [52] and an adjusted version of the functional diagram there is provided below. This is suited to the spring-loaded deployment mechanism selected previously.

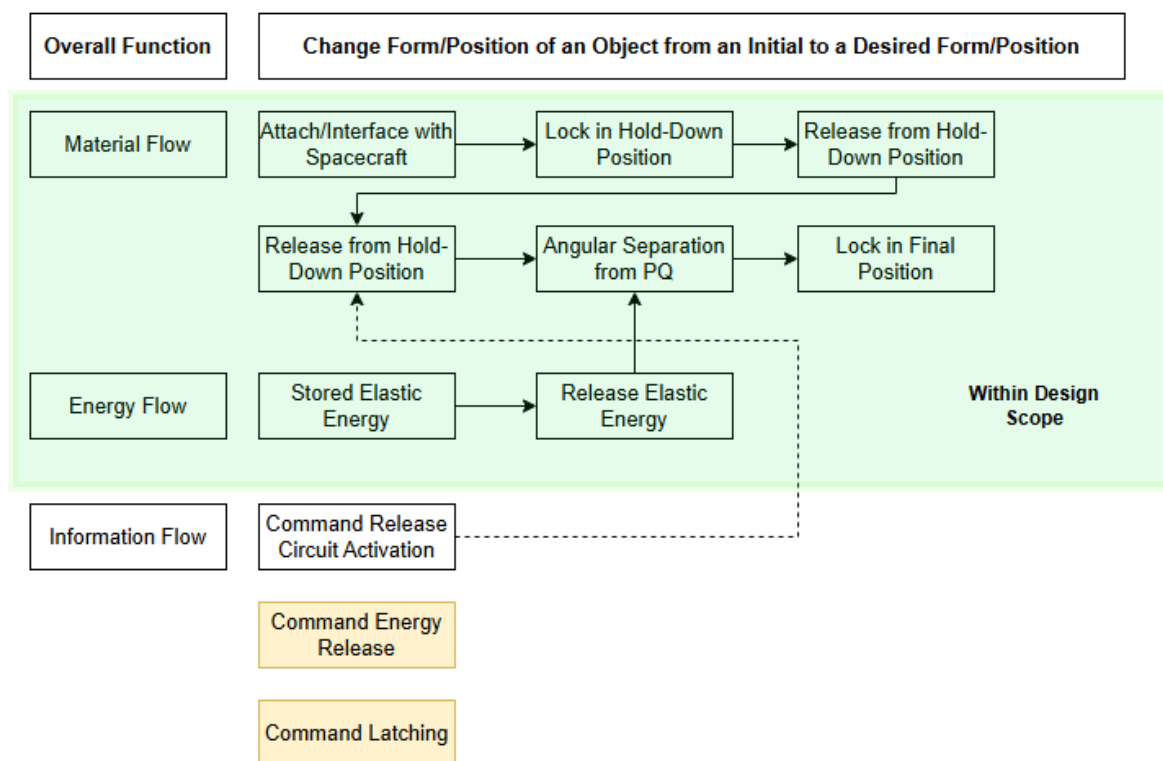


Figure 3.3: Functional Overview of Spring-Loaded Deployment Mechanism

In Figure 3.3, the scope of the thesis is also described, with both material flow and energy flow within the design scope. While the information flow, including the circuitry and communication for the release mechanism, is a very important aspect of the deployable solar panels, they will not be delved into. However, a brief overview of possible circuits and release techniques will be discussed.

3.3.2. Hold Down & Release Mechanism Concept Selection

This section will explore the development of an HDRM for this design's deployment mechanism. The requirements applicable to the HDRM are RQ-DC-01, RQ-DC-02, RQ-FN-03, and RQ-FN-04. Firstly, attributes and data regarding the release mechanisms from literature will be evaluated. Using these release mechanisms, certain hold-down concepts are shown that could facilitate the deployment mechanism. These hold-down concepts are then evaluated and traded-off to pick a concept of HDRM that facilitates the overall design. Following this, sample electrical setups and considerations regarding the tie-down cable are also provided, while not delving into detailed design.

Release Mechanism Review

There are a multitude of existing release mechanisms that have been used on small satellites. Some of these have been studied in the literature review. Table 3.4 summarizes the release mechanisms most suitable for the small satellite size. While values for burn wire mechanisms may vary drastically due to the choice of wire, thickness, supplied current and voltage, all values are provided from the relevant, cited sources.

Attribute	Dcubed Release Nut [37]	Nano-Morphodynamic Muscle Strand Technology (NMD) [53]	Nichrome Burn Wire [22]	Resistor-based Burn Wire Mechanism [32]
Average Actuation Time	3.6s (-60), 2.5s (0), 1.9s (22), 0.6s (70)	5s (20)	2.6 - 3s regardless of bus temp	0.4 - 4.5s (Varying with thickness and windings of tie-down cable)
Actuation Power (W)	1.80 - 4.4 (1.6 - 2.0 A & 0.7 - 1.1 Ω)	5	1.02 - 2.30 (0.4 - 0.9 Ω & 1.6A)	13.62 (8V, 4.7 Ω)
Max Energy Requirements (J)	15.84	25	6.912	10.62
Volume Envelope	Minimum (17 x 17 x 17), various options, smallest one	45 x 3 x 3	32 x 16.5 x 11.5	Custom
Mass (obtained from Literature)	>12g	1g	N/A	>2g
Cost (\$)	N/A	>300	>200	N/A
Important Factors	<ul style="list-style-type: none"> - Features re-activation (great for testing but unnecessary for flight). - Prequalified for spaceflight 	<ul style="list-style-type: none"> - Extremely small size but high power requirement. - No moving or burning parts. - Custom geometry upon consultation. 	<ul style="list-style-type: none"> - Successful cut times influenced by supplied current to nichrome wire. - Spring stroke all the way through cut extremely necessary, usually require 2 for redundancy. 	<ul style="list-style-type: none"> - Choice between Surface Mount Device (SMD) and through-hole, SMD resistors may de-solder if PCB temperatures are high. - Fixed thermal cutting location.

Table 3.4: Release Mechanism Attributes

Focusing on actuation time, power, and energy requirements is vital for the design of the release mechanism. While the release nuts from Dcubed provide different actuation times depending on the bus temperature, they demand a peak power of 4.4 W, potentially resulting in a high energy consumption of up to 16 J, depending on the release times. Similarly, NMD actuators from the Ecuadorian Space Agency exhibit even higher energy demands and require significant actuation power. In contrast, burn wire mechanisms emerge as the most suitable options due to their minimal power and energy requirements for deployment. Additionally, it is important to note that burn wire mechanisms are less influenced by bus temperature variations, as the temperature needed for thermal cutting is substantially higher.

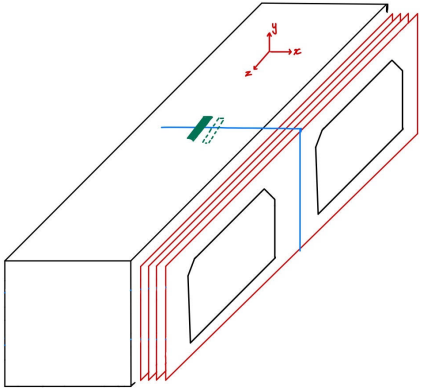
Volume and mass are critical considerations, particularly given the compact size of PocketQubes. While Dcubed's release nuts and pin pullers offer the smallest form factor for their type, they are still relatively large compared to the other available options and are also quite heavy, excluding the additional electrical components needed to supply power. Nichrome burn wire mechanism and resistor-based burn wire

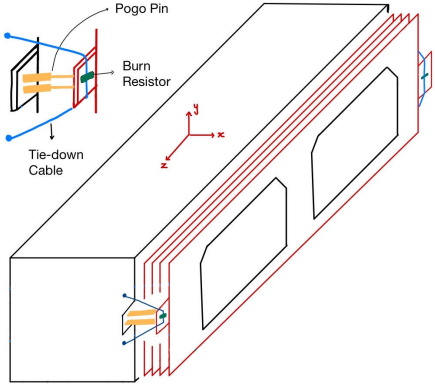
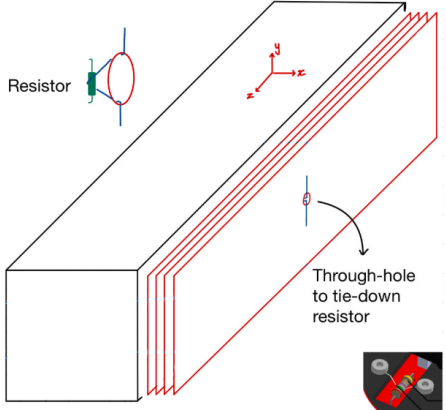
mechanisms offer greater flexibility, as they can be integrated in various locations, with the largest components typically being the nichrome wire/resistors and brackets used for securing the tie-down cable.

Lastly, complexity is important to consider as many PocketQube missions are university/high-school projects. For this purpose, the release nuts and NMD actuators offer the simplest solutions, since they are COTS components that can easily be incorporated into the design, given the available space and power required. Nichrome burn-wire mechanisms are highly complex as there are numerous parts and the release times/success rates are highly dependent on workmanship. Resistor-based burn wire mechanisms also introduce complexity into the design as they are highly custom. However, the replacement of a Nichrome wire with a resistor reduces the workmanship required due to the lack of an additional tensioned components, and consequently provides a simpler solution than Thurn's design [22].

Hold-Down Concepts

There are various ways to hold-down solar panels while they are in the stowed configurations. This section will study the four effective concepts to hold-down solar panels based on the literature study and existing deployable appendages on missions. These options and their advantages and disadvantages are provided in Table 3.5. It is important to assess multiple structures together for the same functionality, especially in small spacecraft where independent functionalities may not be the best option to minimize mass and volumetric constraints. Therefore, the hold-down mechanisms will be evaluated alongside release setups/assemblies as identified in the literature review.

Schematics of Concepts	Considerations	
 <p data-bbox="272 1682 719 1715">Option 1: Simple Encasing Tie-Down</p>	<p data-bbox="794 1021 1358 1339">Description: This option features a simple design where the encasing tie down cable is connected to both long faces on either side of the stowed panels. This is a common option featured on many small satellites, including AlbaOrbital's Unicorn 2D. The exception in their design is the inclusion of two tie-down cables that do not come into contact with the cells as none of them are facing outwards (a crucial requirement for this design).</p> <p data-bbox="794 1368 1334 1429">Release Mechanisms: Nichrome Burn Wire, Resistor-based Burn Wire</p>	
	<p data-bbox="810 1491 959 1525">Advantages</p> <ul data-bbox="810 1552 1078 1919" style="list-style-type: none"> - Simple design and assembly - Single Burn-Wire required - Minimizes contact with cells - Easy to incorporate redundancy 	<p data-bbox="1102 1491 1286 1525">Disadvantages</p> <ul data-bbox="1102 1552 1370 1827" style="list-style-type: none"> - Need additional deployment switch - Long tie-down may interfere optical payload - Limited face space for tie-down

 <p>Option 2: Pogo-Pin based Hold Down</p>	<p>Description: This hold-down option features constraining the panels from either side of the long edge (+z, -z). This can be assisted or improved by adding a pogo-pin based release mechanism setup, as featured in Park’s and Oh’s designs [32] [54]. This is a relatively novel concept as it has not been launched on PocketQubes in past missions.</p> <p>Release Mechanisms: Pogo-Pin and resistor based Burn Wire</p> <table border="1" data-bbox="794 622 1361 1198"> <thead> <tr> <th data-bbox="794 645 1082 678">Advantages</th> <th data-bbox="1086 645 1361 678">Disadvantages</th> </tr> </thead> <tbody> <tr> <td data-bbox="794 701 1082 896"> <ul style="list-style-type: none"> - Deployment status integrated in deployment sequence - Power to resistor automatically cut </td> <td data-bbox="1086 701 1361 1198"> <ul style="list-style-type: none"> - Low Torsional rigidity around z-axis - Hard to implement redundancy (multiple Pogo-pin setups) - Added complexity with No. of components and need to time simultaneous release - 4 Pogo-pin assemblies required for 2 deployed assemblies </td> </tr> </tbody> </table>	Advantages	Disadvantages	<ul style="list-style-type: none"> - Deployment status integrated in deployment sequence - Power to resistor automatically cut 	<ul style="list-style-type: none"> - Low Torsional rigidity around z-axis - Hard to implement redundancy (multiple Pogo-pin setups) - Added complexity with No. of components and need to time simultaneous release - 4 Pogo-pin assemblies required for 2 deployed assemblies
Advantages	Disadvantages				
<ul style="list-style-type: none"> - Deployment status integrated in deployment sequence - Power to resistor automatically cut 	<ul style="list-style-type: none"> - Low Torsional rigidity around z-axis - Hard to implement redundancy (multiple Pogo-pin setups) - Added complexity with No. of components and need to time simultaneous release - 4 Pogo-pin assemblies required for 2 deployed assemblies 				
 <p>Option 3: Through hole based Hold Down</p>	<p>Description: This hold-down option features a legacy setup used in my large deployable panels, where either the thermal cutter assembly (burn resistor) is mounted on the panels, or the tie-down cable is secured on the panels with brackets on the other end.</p> <p>Release Mechanism: Resistor-based Burn Wire</p> <table border="1" data-bbox="794 1547 1361 1839"> <thead> <tr> <th data-bbox="794 1570 1082 1603">Advantages</th> <th data-bbox="1086 1570 1361 1603">Disadvantages</th> </tr> </thead> <tbody> <tr> <td data-bbox="794 1626 1082 1821"> <ul style="list-style-type: none"> - Shorter tie-down cable and less - Uses same +x, -x faces for release setups </td> <td data-bbox="1086 1626 1361 1839"> <ul style="list-style-type: none"> - Need 1 or more burn assemblies for each side - Limited space available on the panel for PV cells </td> </tr> </tbody> </table>	Advantages	Disadvantages	<ul style="list-style-type: none"> - Shorter tie-down cable and less - Uses same +x, -x faces for release setups 	<ul style="list-style-type: none"> - Need 1 or more burn assemblies for each side - Limited space available on the panel for PV cells
Advantages	Disadvantages				
<ul style="list-style-type: none"> - Shorter tie-down cable and less - Uses same +x, -x faces for release setups 	<ul style="list-style-type: none"> - Need 1 or more burn assemblies for each side - Limited space available on the panel for PV cells 				

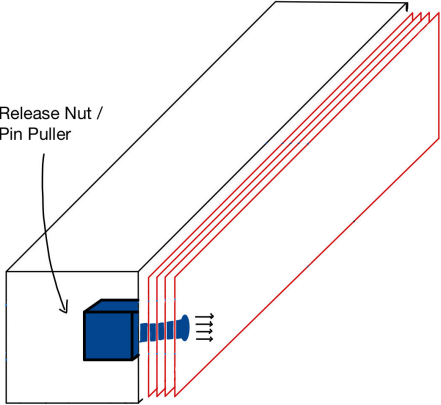
 <p>Option 4: Release Nut Hold Down</p>	<p>Description: This hold-down option features a release nut (specifically DCUBED Nano) also identified in the release mechanisms in the prior section, as it acts both as the hold-down and release. For such a setup, the release nut would be attached up until the other most panel, to which it would stay attached to post deployment.</p> <p>Release Mechanism: Release Nuts</p> <table border="1" data-bbox="794 593 1361 1014"> <thead> <tr> <th data-bbox="794 593 1086 645">Advantages</th> <th data-bbox="1091 593 1361 645">Disadvantages</th> </tr> </thead> <tbody> <tr> <td data-bbox="794 651 1086 1014"> <ul style="list-style-type: none"> - No tie-down cables to interfere with payload - Tested and reliable COTS options - Deployment status integrated by component - Built in reliability </td> <td data-bbox="1091 651 1361 1014"> <ul style="list-style-type: none"> - Large volume/Mass required inside PQ - Pricier than custom burn-wire assemblies </td> </tr> </tbody> </table>	Advantages	Disadvantages	<ul style="list-style-type: none"> - No tie-down cables to interfere with payload - Tested and reliable COTS options - Deployment status integrated by component - Built in reliability 	<ul style="list-style-type: none"> - Large volume/Mass required inside PQ - Pricier than custom burn-wire assemblies
Advantages	Disadvantages				
<ul style="list-style-type: none"> - No tie-down cables to interfere with payload - Tested and reliable COTS options - Deployment status integrated by component - Built in reliability 	<ul style="list-style-type: none"> - Large volume/Mass required inside PQ - Pricier than custom burn-wire assemblies 				

Table 3.5: Evaluation of Hold-Down Mechanisms

Having reviewed both hold down and release mechanisms and evaluating advantages and disadvantages of the concepts generated, it is important to trade them off with certain parameters that are crucial to the design of deployable solar arrays. These are as follows:

- **Mass and Volume:** Due to the limited volume and mass available on the pocketcube, this is the most important metric to compare the hold-down mechanisms.
- **Mountability:** While this is synonymous with mass/volumetric constraint, this criteria focuses on minimal intrusion of the payload volume available and the ability to attach to a PQ body in 'Plug & Play' format.
- **Reliability:** This is a very important trade-off criteria and is influenced by heritage, testing, and redundancy.
- **Complexity:** Reducing complexity and number of components is also an important trade-off metric as these can be cause for errors and consequently failures.

Table 3.6 summarizes the performance of these hold-down mechanisms for these trade off criteria.

Concept	Size & Mass	Mountability	Reliability	Complexity
Simple Encasing Tie Down	<ul style="list-style-type: none"> • Small and lightweight components. • 1 cable required to envelope both arrays. 	<ul style="list-style-type: none"> • Can be placed on custom mapping on either face of the PQ. • No intrusion in PQ payload volume. 	<ul style="list-style-type: none"> • High heritage. • Easily implemented redundancy with multiple burn resistor circuits. • TRL 7-9 	<ul style="list-style-type: none"> • High workmanship required.
Pogo-Pin Hold Down	<ul style="list-style-type: none"> • Small and lightweight components. • Requires at least 2 per array assembly. 	<ul style="list-style-type: none"> • Needs custom PCB mounts on ($\pm z$) faces of the PQ. • No intrusion in PQ payload volume. 	<ul style="list-style-type: none"> • Novel concept, no known flights. • Hard to implement redundancy. • TRL 4 	<ul style="list-style-type: none"> • Need to spec pogo pins with appropriate torque. • High workmanship required.
Through Hole Hold Down	<ul style="list-style-type: none"> • Small and lightweight components. • Requires at least one tie-down per assembly. 	<ul style="list-style-type: none"> • Needs space on panels to incorporate brackets/resistor. • No intrusion in PQ payload volume. 	<ul style="list-style-type: none"> • High heritage in large arrays. • Easily implemented redundancy with multiple burn resistor circuits. • TRL 7-9 	<ul style="list-style-type: none"> • High workmanship required.
COTS Release Nuts & Gecko	<ul style="list-style-type: none"> • Heavy; one-size-fits-all components. • Large volume and mass. 	<ul style="list-style-type: none"> • Requires volume inside PQ. • Attaching outside limits space for panels. 	<ul style="list-style-type: none"> • High heritage in larger arrays. • Includes redundancy within the mechanism. • TRL 9 	<ul style="list-style-type: none"> • Simple attachment to panels. • Low workmanship required.

Table 3.6: Hold-Down Concept Trade Off. Ratings are color-coded as follows: Green indicates optimal performance, Yellow represents suboptimal performance, and Red signifies unacceptable performance.

The clear winner is a simple encasing tie-down cable that constraints both solar panel assemblies. This allows for multiple redundant thermal cutting circuits, and is also a reliable and simple option in comparison to the other designs. Additionally, only 1 cable is required to envelop both/all arrays on the $\pm y$ and $\pm x$ faces, reducing the number of components and consequently points of failures in the design. While pogo-pin mechanisms are known to have numerous benefits in terms of providing initial deployment torque and maintaining stroke against the tie-down cable, there aren't any known missions using them, significantly halting the reliability. mechanism are great for testing, as they can be repeatedly reset (in comparison to burning through tie-down cables), but require large volumes inside PocketQubes. While an encasing tie-down cable is the best option, an additional deployment switch/monitor will need to be implemented that is in addition/standalone to the thermal cutting circuit and this is added complexity to the design. This switch will ensure that the power supplied to the burn resistor is stopped and prevents overheating. This hold-down option will be used in structural analysis of the PCB assembly in the upcoming sections.

Possible Electrical Setup

In the functional overview, it was discussed that the information flow is not part of the design scope of the thesis. However, the main electrical setups and release designs seen in literature will be outlined in

this section. The overall structure of the electrical design observed in numerous papers is quite similar and is presented in Figure 3.4.

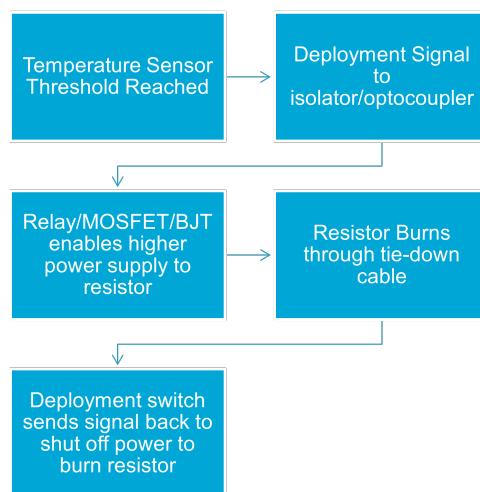


Figure 3.4: HDRM Electrical Setup

In the reviewed literature, it was essential that the signal and power circuits be isolated to prevent damage to the MCU pins. Therefore, a relay, optocoupler, MOSFET or BJT is used to provide this isolation and to drive the high power circuit for the burn resistor. Once a deployment signal is provided, the high power circuit will be activated and will short the burn resistor, providing the necessary heat dissipation to cut through the tie-down cable. Relays and optocouplers provide complete isolation between the signal and high power circuits, and may be connected in series with MOSFETS or BJT's to drive the higher power circuits. Two possible electrical schematics have been developed based on the designs from [34] and [55].

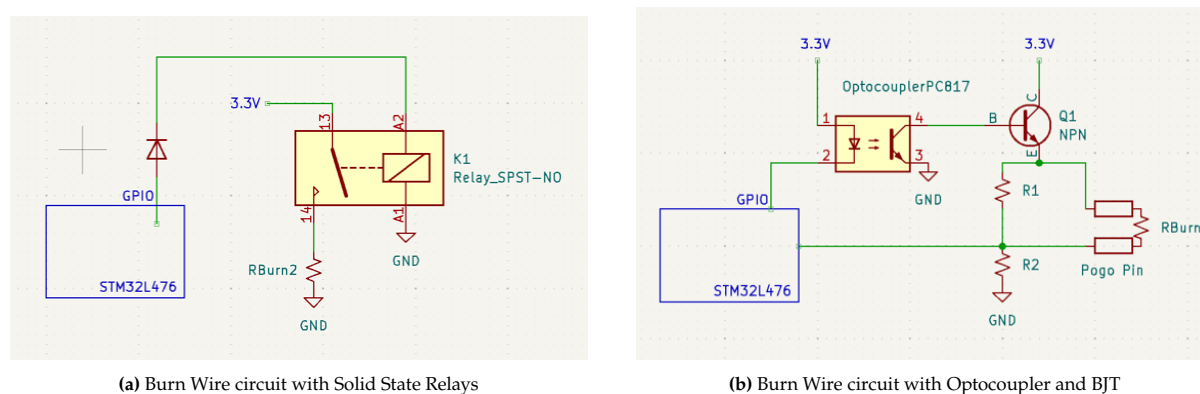


Figure 3.5: Electrical Schematics for Burn Wire Mechanism

Circuit 1 in figure 3.5a features a simple design where a GPIO pin from the MCU provides the activation voltage and current to electromagnetically switch on the high power circuit, which is then connected in series with the burn resistor to the ground. In this circuit however, the only way to detect the status of deployment and to stop providing power to the burn resistor is through a mechanical/external switch that reports back to the MCU. Failure of reporting back could lead to the resistor staying on and dissipating a lot of heat, potentially damaging other electronics and structures on board the PocketQube.

Circuit 2 in figure 3.5b features an optocoupler as a means of providing complete isolation and pogo pins as a means of circuit cut-off. When the GPIO pin provides a voltage of 3.3V, the Optocoupler provides a signal to the base of a BJT. This then drives the high current and voltage from the collector to the emitter. The emitter has a parallel path through the pogo pin and burn resistor, and a shunt/sensing resistor. When the high power circuit is on, the sensing resistor has barely any voltage drop due to the significantly low resistance. This allows the majority of power dissipation to happen through the burn resistor. When

the burn resistor cuts through the tie-down cable, the pogo pin circuit is disconnected. Due to the low voltage drop across the sensing resistor, the MCU is able to detect the input voltage of 3.3V/0V through a GPIO to see the status of deployment. This circuit does not require any additional mechanical/external switch.

While these electrical setups could be further investigated to provide considerations regarding release times, power supplied, redundancy and various other factors, **it is not part of the scope of the thesis.**

Tie-Down Cable Selection

There is an abundance of fibers and cables to choose from as the burn wire tie-down cable. However, they possess different mechanical properties and different characteristics that may impact the release time, hold-down strength and power required. Table 3.7 provides some of the cables suggested in the research papers discussed in this literature review:

Tie Down Cable	Melting Point (C)	Tensile Strength (GPa)	Tensile Modulus (GPa)	Density (g/cc)
Dyneema SK78 [56]	150	3.3 - 3.9	109 - 132	1.3
Nylon 6 Fiber [57]	210	0.58 - 0.61	2.9 - 9.65	1.14
Vectran HT [58]	330	3.2	75	1.4
Kevlar 49 Fiber [59]	560	3	112	1.44

Table 3.7: Tie-Down Cable Options

These parameters are extremely vital for the design of the release mechanism. A high tensile strength ensures that the cable can withstand launch loads and can keep the solar arrays in the stowed position. It is beneficial for the cable to deform as little as possible to not lose its tension and contact with the heating element, therefore the tensile modulus is also an important parameter. The melting point is important to indicate the temperatures that one might expect the cable to reach for it the heating element to cleave through it.

As can be seen, the parameters really vary across the board with the melting point ranging from 150 to 560 °C and the tensile strength ranging from 0.6 GPa up to 3.9 GPa. The density of the cables studied are relatively constant around 1.3 g/cc which shows that the tensile strength is a good indicator of specific strength.

The choice of cable is really dependent on mission requirements, power and mass available, and the subjected launch and deployment loads. As seen in [31], a number of other parameters are important in picking the right tie-down cable as listed below:

1. Toxicity to surrounding electronics and sensors.
2. Clean cut to prevent lose fibers from endangering components nearby.
3. Good abrasion and residual strength.

Keeping all considerations in mind, Dyneema SK78 is the selection for the design, as its melting point is considerably lower while it has great tensile strength. It also has high reliability in deployable appendages for small satellite applications, previously being used for the Delfi Space Program.

3.3.3. Deployment Guide Selection

Previously, a spring loaded deployment mechanism was selected due to its minimal power requirement and high heritage within small satellite deployable appendages. Having chosen spring-loaded designs, the deployment guides available are narrowed down to two primary choices: torsion spring hinges and tape spring hinges. Each offers distinct advantages and disadvantages, with their characteristics and performance differing significantly in nature. Table 3.8 below discusses provides a small comparison of

these hinges, summarizing their advantages and disadvantages. This is followed by a concept design for the hinge in section 3.5, that will further facilitate the design of deployable arrays.

Mechanism	Size & Mass	Reliability	Complexity	Locking Torque
Tape Spring Hinge 	<ul style="list-style-type: none"> • Transverse radius of curvature increases size (space between panels may not suffice). • Scaling to larger arrays may require thicker and heavy springs. 	<ul style="list-style-type: none"> • “Snap-back” phenomenon is hard to model; requires experimental study. [44] • High heritage in antennas and some solar panels (Unicorn 1, MDQubeSAT-1), but rarely used for multi-panel arrays. • Repeated testing can degrade elasticity. 	<ul style="list-style-type: none"> • Low part count (simpler design). • Extensive testing required due to highly non-linear deployment. • Support structure not necessary to support tape spring 	<ul style="list-style-type: none"> • Insufficient locking torque for multiple panels → lower natural frequency in deployed state. • No additional locking structures needed.
Torsion Spring Hinge 	<ul style="list-style-type: none"> • Micro manufacturing enables very compact designs. • Final hinge assembly mass is smaller than that of long tape springs. 	<ul style="list-style-type: none"> • High heritage in PocketQube (PQ) deployment (e.g., FossaSat-2, Unicorn 2D). • Hinge dynamics are more predictable and easier to simulate. • Deadlocking can prevent deployment, not a concern for tape springs. [60] 	<ul style="list-style-type: none"> • Provides structural separation between panels. • More parts, increasing potential points of failure. • Tedious to assemble. 	<ul style="list-style-type: none"> • Large locking torque yields a rigid deployed assembly, increases array fundamental frequency.

Table 3.8: Hinge Comparison. Green represents desirable performance, Yellow represents acceptable performance

Both tape springs and torsion springs provide optimal means of deployment guides for small satellites, as they are light, reliable, and have heritage on numerous missions. None of the options possess features that render them unfeasible for incorporation and both options can meet the design requirements set for deployable solar arrays on 3P PocketQubes. However, **torsion spring hinges** are the clear winner from the trade-off. Albeit being more complex than tape springs due to the increased number of components and requiring a tedious assembly process, these are more suited to multi-panel/large deployable arrays. Apart from not being utilized for any multi-panel arrays in heritage, tape springs also do not provide sufficient locking torque in comparison to torsion springs. High locking torque is particularly good for ensuring a higher fundamental frequency of the deployed arrays, which is particularly good for the ‘control bandwidth’ of ADCS system onboard small satellites. If the resonant frequency of the deployed structure is below or near this bandwidth, control actuators can inadvertently excite the arrays, causing uncontrollable oscillations.

3.4. PCB Assembly Design

PCB Design is an important aspect of designing deployable solar arrays for small satellites. This section focuses on deriving appropriate dimensions and spacing within the PCB assembly. PCBs' main functions on small satellites are:

1. Provide structural support to solar cells and maintain their integrity throughout launch.
2. Support wiring connections and routing for power transfer.

There are some existing space companies that provide information regarding the material, applicable platform, thickness, and temperature range. These are provided in Table 3.9.

Supplier	Platform	Substrate Material	Thickness	T Range
DMSA EXA	1U	FR4-Tg180	1.25/1.50	-80 + 130
AAC Clyde Space	3U - 12U	FR4 w/ Al	N/A	-40 + 80
DHV Tech	3U	Polymide w/ Kapton coverlay	1.6	-50 + 125
ISI Space	1U-3U	Aluminum Substrate	1.8	-40 + 125

Table 3.9: Solar Array PCB Suppliers [61][62][63][64]

The PCB design process is inspired by the methodology presented in [65], which focuses on the design of a solar array substrate for a GEO satellite. Although their design is tailored for a much larger, rigid deployable array, the same approach can be adapted for the rigid arrays used in PocketQubes. This approach begins by estimating the dimensions and thickness of the solar panel substrates. It then evaluates material properties through dynamic analysis and thermal assessments, considering the substantial mass fraction of the substrates relative to the overall deployable arrays. Subsequently, potential layouts and geometries of the substrates are identified, including the locations of the HDRM and relevant constraints. Finally, a random vibration analysis is performed to evaluate the performance of these configurations. Random vibrations determine how the structure behaves under diverse frequencies, and are particularly critical in driving the design of secondary structures, such as the deployed PCBs supporting the solar cell assemblies. Sine vibrations are less critical because they occur at lower frequencies, below the expected natural frequencies of the final PCBs and final structural assembly. As a result, the risk of resonance and excessive displacement is minimized. Therefore, while sine vibrations are still considered, they do not have as great an impact on the overall structural design compared to random vibrations.

Figure 3.6 illustrates the variables used to represent the dimensions of the solar arrays in our design that are ideally obtained at the end of the section:

- L_a : Length of the solar panel.
- L_b : Width of the solar panel.
- t_p : Thickness of the solar panel.
- t_s : Spacing between subsequent.

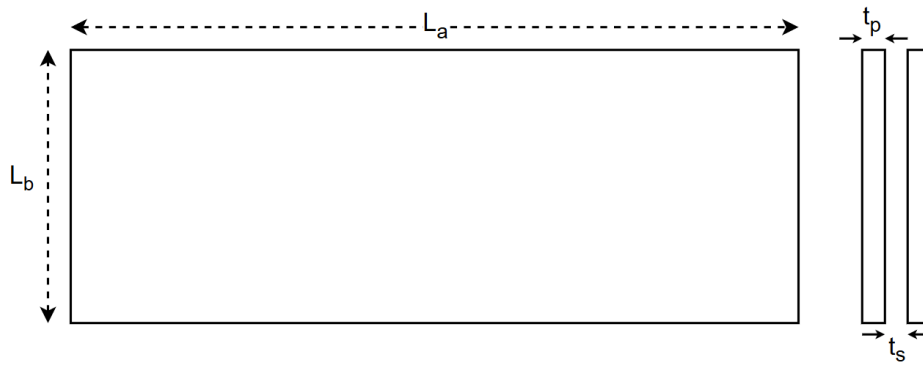


Figure 3.6: PCB Dimension Variables

A flowchart of this design process is provided in figure 3.7.

Firstly, material for the panel substrate/PCB is evaluated from existing materials that have flight heritage in the specific use case of solar arrays. The selection of material for the PCB is critical due to its significant contribution to the overall system mass. This high mass sensitivity necessitates careful consideration of material properties to optimize performance while minimizing weight. Their structural performance will be compared by initially assuming fixed dimensions for L_a , L_b , and t_p by doing modal analysis for rectangular flat plates. Consequently, a random vibration profile will be applied to understand the deformation of these plates with the assumed parameters, to identify whether additional constraints are required in the assembly. Finally, a material will be chosen based on the desired structural response and thermal considerations for the PCB to support the design.

Following the material selection, a PCB layout is developed with the overall dimensions to incorporate the solar cells, hinges, and tie-down cable. This layout is essential to determine the available space for the said components and consequently to determine the constraints and model for the vibrational analysis that will help determine the final dimensions for the stowed assembly, particularly the thickness of the panels and spacing in between them.

The thickness, spacing, and width of the panels within the stowed assembly are determined through vibrational analysis. Options will be developed to fit within the 10.5mm with available thicknesses of PCBs online. Based on the vibrational response, an option is selected that is able to incorporate the most number of panels with deformations and stresses that prevent the solar cells and panels from being damaged during launch. Based on the thickness and spacing, the maximum diameter of the hinge is determined, which directly drives the width of the panels since these hinges are situated in the $\pm Y$.

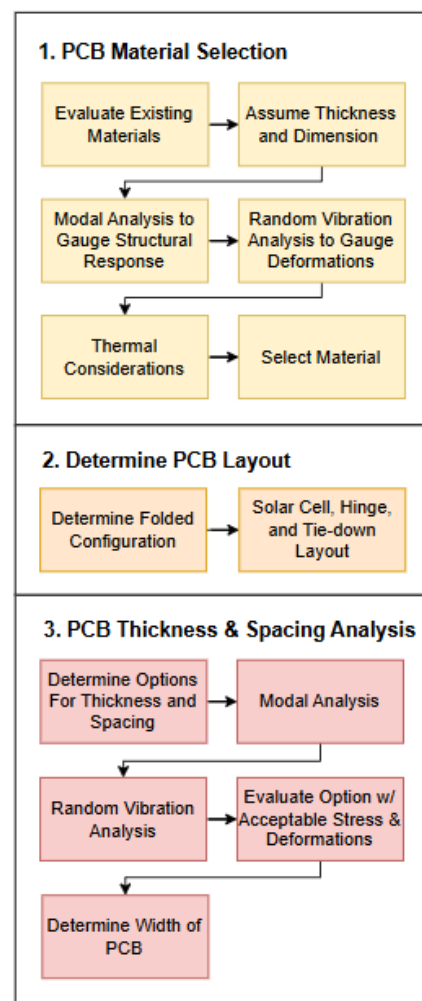


Figure 3.7: PCB Assembly Design Process

3.4.1. Material Selection

Selecting the material for the PCB substrate is a vital part of the PCB design. There are a variety of factors that can affect the choice of a substrate material, many of which are provided at [66].

1. **Thermal Conductivity:** Determines the ability to dissipate heat generated by electronic components

during operation. Higher thermal conductivity is great to have uniform heat distribution and to prevent hot spots throughout the mission. Aluminum or copper PCBs provide great thermal conductivity.

2. **Coefficient of Thermal Expansion:** A low coefficient of thermal expansion is preferable as deformation/expansion on the array may damage the cells and lead to mission failure.
3. **Strength-to-Mass:** Having a high strength to mass ratio is preferred minimize the mass of the PCBs.
4. **Flexural Rigidity:** Elastic properties correlate highly to the deformation in and out of the plane during launch. A high flexural rigidity is preferred to prevent damaging the solar cells. A balance between elasticity and rigidity is crucial to minimize stress on the PCBs; they should be flexible enough to withstand vibrations and shocks without becoming brittle and breaking under mechanical excitation.
5. **Outgassing:** Wave soldering defects can cause cavities or blowholes that have the potential to impair the PCB performance. Composites such as polyimide and PTFE (teflon) have little to none outgassing.
6. **Glass Transition Temperature:** High T_g is necessary to maintain mechanical and electrical properties at elevated/extreme temperatures. Ceramic-based substrates such as alumina and aluminum nitride provide good solutions for high T_g materials. High T_g FR4 has also been developed.

A key aspect of choosing between materials is also the type of structure desired for the solar arrays. Typically, solar array substrates can be rigid or flexible panels.

Type	Description	Advantages and Disadvantages
Rigid	Rigid Panels typically consist of crystalline cells that are mounted onto a solid substrate, usually made of aluminum or glass. This solid substrate takes up large volume and typically requires complex folding assemblies for deployable solutions. They are usually hinged together or wrapped around the outside of the satellite [67].	<p>Advantages:</p> <ul style="list-style-type: none"> • Cells typically feature higher efficiencies and more power generation. • Stiffer designs with high natural frequencies. • Deployment mechanism usually smaller (tiny hinges). • Durability against meteoroidal impacts. <p>Disadvantages:</p> <ul style="list-style-type: none"> • High volume and mass. • Typically high cost of crystalline cells.
Flexible	These typically consist of thin-film cells, such as amorphous silicon, cadmium telluride, or copper indium gallium selenide (CIGS). They are usually roll up or extendable boom structures.	<p>Advantages:</p> <ul style="list-style-type: none"> • Lightweight and flexible substrate. • Accommodates complex shapes and modular designs. <p>Disadvantages:</p> <ul style="list-style-type: none"> • Generally lower efficiency. • Less resistant to harsh space environment and impacts. • Complex deployment mechanisms like booms that are hard to accommodate in small satellites. • Attitude control system needs to accommodate low natural frequencies of deployed arrays as oscillations have minimal environmental dampening.

Table 3.10: Comparison of Rigid and Flexible Solar Panels for Spacecraft

Dynamic Response and Vibrations

This section begins with hand calculations for a simply supported plate to establish baseline natural frequency and deflection. Subsequently, an ANSYS response analysis is conducted for a plate with clamped corners under the GEVS profile, providing detailed insights into deflection and stress distribution.

The selected materials, listed in Table A.2 with their mass, density, Young's modulus, and Poisson's ratios, are sourced from various academic papers and the EuroCircuits materials page, a trusted European PCB manufacturer [68, 69]. Materials highlighted in yellow are readily available from Euro-Circuits, enhancing their likelihood of integration due to their reliability and prior use in the Delfi space program.

Flexural rigidity and natural frequency for simply supported rectangular plates are evaluated using a fixed plate thickness of 1.25 mm, length of 178 mm, and width of 50 mm. Although the thickness remains constant in this analysis, it will be varied in section 3.4.3 to identify the optimal value that minimizes stresses and deformations while accommodating four panels within the 10.5 mm appendage volume.

Table A.3 provides the results based on equations provided at [70] for thin rectangular plates. Figure 3.8 visualizes these results.

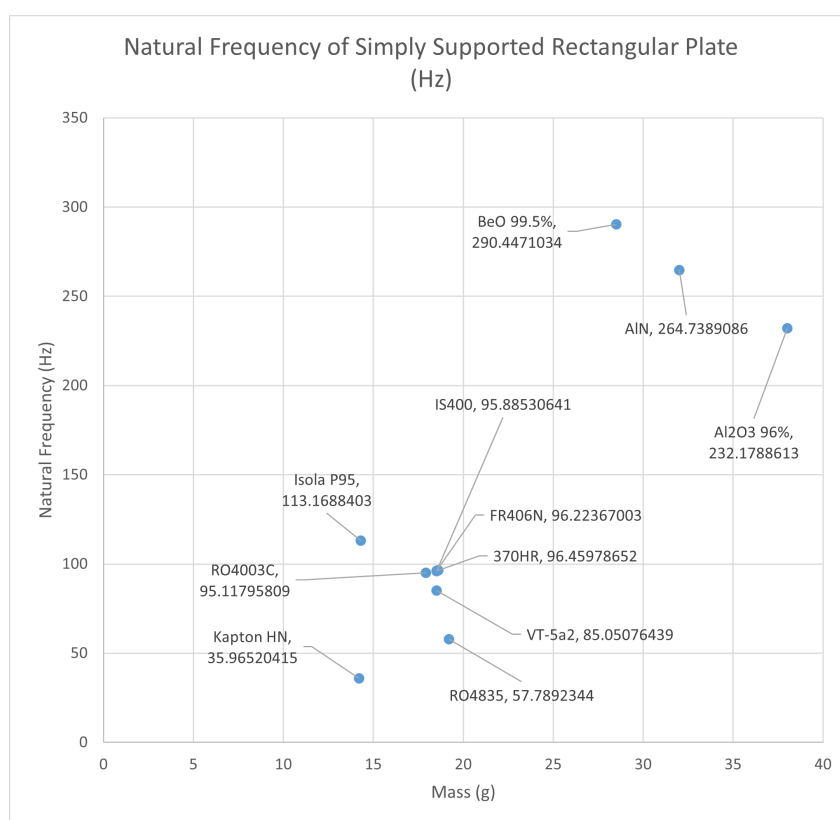


Figure 3.8: Natural Frequency of Simply Supported Rectangular Plate

The scatter plot shows the relationship between the mass and natural frequency of various materials used for a simply supported rectangular plate. Generally, materials with lower mass, such as Kapton HN (35.97 g) and RO4003C (95.12 g), exhibit lower natural frequencies, while materials with higher mass, like Al₂O₃ 96% (232.18 Hz) and BeO 99.5% (290.45 Hz), display higher natural frequencies. This indicates that materials with higher density and stiffness tend to have greater natural frequencies, making them less prone to deformation under vibrational loads. The clustering of materials around similar frequencies (e.g., IS400, FR406N, and 370HR) suggests comparable dynamic behaviors.

To gain a more accurate understanding of the PCB's dynamic response during launch, analysis will be done using ANSYS modal and random vibration tools. The corners of the plate are clamped to represent the studs/hinges typically used to secure the folded panels and provide separation between them. A random vibration profile based on the General Environmental Verification Standard (GEVS) will be applied, providing a more representative model of the launch loads. This will be further explained in 3.4.3. The GEVS vibration profile is provided in A.7.

	Mode 1 (Hz)	Deflection (95.45%) (mm)
Al ₂ O ₃ 96%	232.16	0.648
AlN	261.05	0.547
BeO 99.5%	287.26	0.474
VT-5a2	86.031	2.87
IS400	96.72	2.413
370HR	97.427	2.384
FR406N	96.889	2.406
RO4003C	86.611	2.89
RO4835	52.621	6.066
Kapton HN	34.625	7.877
Isola P95	114.05	1.884

Table 3.11: Natural Frequency and Deformation Under Random Vibration Loads

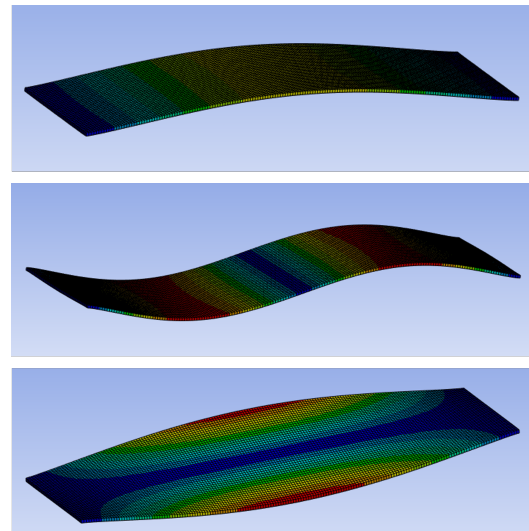


Figure 3.9: Mode Shapes 1, 2, 3

What can be identified from looking at the first three eigenfrequencies of the modal analysis with fixed corners, is that there are large resonances occurring in the center of the panel and this area is most likely to deform or be subject to oscillations. The modal analysis also yielded values close to the ones predicted from the analytical solutions. Although ceramic-based PCBs exhibit minimal deformation, the materials available from EuroCircuits undergo relatively large deformations exceeding 2.0 mm. These significant deformations can cause the stowed panels to collide with the inner walls of the deployer or with adjacent panels, potentially damaging the solar cells. Consequently, it is essential to secure the panels using tie-down cables or to incorporate spacers to prevent such collisions.

Thermal Considerations

As mentioned earlier, it is critical to evaluate the thermal properties of substrate materials to see if they could withstand the temperature extremes experienced in LEO. Given eclipsed or non-eclipsed orbits, certain materials could be more favorable. Section A.2 in the appendix provides the data. Thermal Conductivity and coefficient of thermal expansion can have orthotropic data and values in X,Y,Z are inserted where available. Otherwise, the default value is in the long dimension.

When comparing different materials based on their Glass Transition Temperature (T_g), Coefficient of Thermal Expansion (CTE), and Thermal Conductivity (TC), ceramics like Aluminum Nitride (AlN) and Beryllium Oxide (BeO) offer significant advantages. AlN has a high T_g of 1726°C, making it ideal for applications that require stability at extreme temperatures. It also has a low CTE (5.6 ppm/°C), which minimizes thermal stresses, useful for protecting electrical components and the solar cells. The TC of ceramics is significantly higher than , which aids in efficient heat dissipation, although it may come at a cost in terms of weight and cost, which can be significant.

On the other hand, Mid- T_g and High- T_g FR4 materials, such as IS400 or FR406N, offer a balance between thermal performance and cost-effectiveness. With T_g values around 150°C to 180°C, these materials are lighter and well-suited for moderate temperature ranges typical experienced in LEO. However, their CTE values, such as IS400's 0.36 ppm/°C, indicate a higher propensity for thermal expansion compared to ceramics, which may introduce mechanical stresses. Additionally, the thermal conductivity of FR4 materials is relatively low (e.g., IS400 at 0.183 W/m·K), making them less suitable for applications where rapid heat dissipation is critical. This makes ceramics like AlN superior for high-temperature and high-thermal-conductivity applications, while FR4 materials remain a cost-effective choice for less demanding thermal environments.

Chosen Material

Although Isola 370HR exhibits lower natural frequency and greater deflection compared to ceramic-based PCBs, it offers significantly superior thermal performance and reduced mass. Additionally, this material is readily available from EuroCircuits, a trusted European supplier, and outperforms traditional FR-4

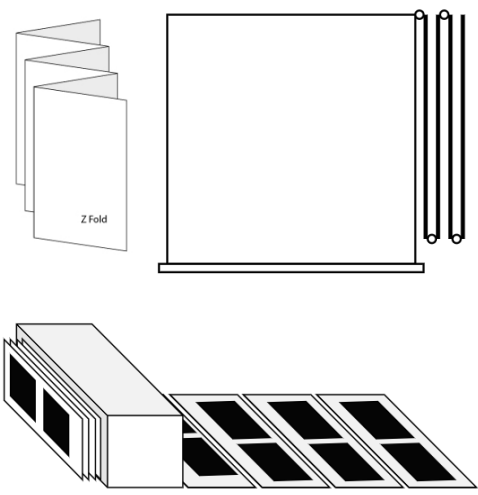
materials with its high glass transition temperature (T_g), low coefficient of thermal expansion (CTE), and excellent thermal conductivity. Given these advantages, and its comparable mass and cost to other fiberglass-reinforced epoxy laminates, **Isola 370HR** is the chosen material for the design. However, other fiberglass-reinforced epoxy laminates remain viable options, and a more detailed thermal analysis, beyond the scope of this design, could further refine the material selection process.

3.4.2. PCB Layout

This section will evaluate the PCB layout, starting with the folding configuration of the panels in their stowed assembly and assessing the dimensioning of the PCB with respect to the cells, hinges, and tie-down cable.

Folded/Stowed Configuration

Folding deployable panels can be done in numerous ways, similar to brochures. Just like brochures have many folded configurations, rigid panels can also be stored in multiple ways to reduce their aperture to the size of a singular face on the PocketQube. However, two of these are most popular, as seen in [71] and those are z-folds and tri/roll-folds. These are both presented in Table 3.12 alongside the relevant missions and their advantages and disadvantages.

Schematics of Options	Considerations
 <p data-bbox="319 1523 638 1568">Option 1: Z-folded Panels</p>	<p data-bbox="766 873 1388 1198">This is the most commonly used folding technique for rigid panels in deployable solar arrays. Solutions known to using this arrangement are Nanosatellites M12P, EnduroSat 3U deployable array and AAC Clyde Space’s Photon arrays. This features many advantages. Since no panels fold in on themselves, the hinge designs can be identical for all panels. Furthermore, due to a 1 degree of freedom deployment (in the ideal scenario), there is no jamming as the panels do not intersect during deployment.</p> <p data-bbox="766 1220 1388 1668">However, using z-folded panels in a 2 or 4 panel options provides a limitation on where the solar cells are facing post deployment. Due to RQ-FN-05, there have to be solar cells facing outward in the stowed configuration. This limits the deployed configuration of cells to be facing towards the PQ body as displayed in the figure below or the inclusion of 2 additional cells. The first option reduces the power generated as the PQ body provides a larger shadow on the cells throughout the orbit if they aren’t sun-pointing, and the latter increases the total cost of the assembly. Additionally, cells on adjacent panels can be facing each other in the stowed, potentially damaging them due to vibrations.</p>

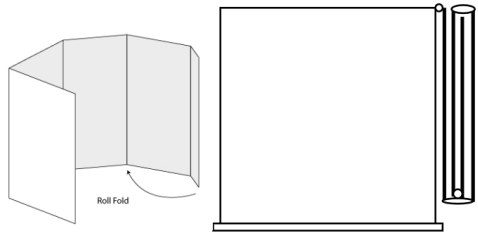
 <p>Option 2: Roll-folded Panels</p>	<p>This folded configuration features multiple folds in on themselves in a roll formation. This is also similar to tri-folds where there is a central panel onto which panels from either side fold inwards. In this configuration, RQ-FN-05 is satisfied even with the solar cells facing away from the PQ body, leading to greater power generation. However, there are a number of issues associated with this option. There are multiple DOFs during deployment, causing possible jamming or interaction of panels within themselves. Furthermore, due to the panels folding inwards, the folds cannot be identical, leading to more complex designs. The hinges also cannot be identical, as the hinge gap changes.</p>
--	--

Table 3.12: Folded Deployable Panel Configurations

Due to the large added complexity and increased number of different parts needed for roll-folded panels, **z-folded panels** are chosen for the design. Despite the slight reduction in power generation due to the deployed positioning of solar cells, it is vital to reduce the number of different parts to minimize analysis and testing of them. Furthermore, jamming or interaction of panels is also prevented in z-folds, leading to a much more reliable design. Due to the large shadow imposed by the current folding configuration, the last panel will feature cell assemblies on either side of the 2-layer PCBs to meet requirement RQ-FN-05.

Solar Cell, Hinge and Tie-down Layout

Given that the pocketcube size is 3P, the maximum dimensions available for the PCB are 178mm * 50mm. As previously mentioned in 2, for the upcoming TU Delft PocketQube missions, Azur Space’s 3G30CA have been procured with the dimensions 80mm x 40mm [19]. Given the overall dimensions of the PCB, figure 3.10 and figure 3.11 demonstrate the two ways that that could incorporate possible hinges, solar cells, and tie-down cable to secure the panels.

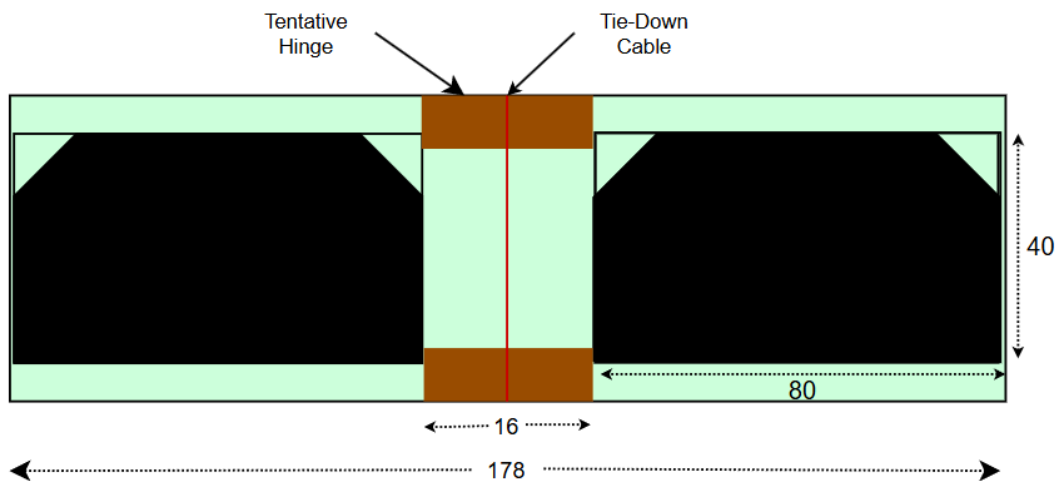


Figure 3.10: PCB Layout 1

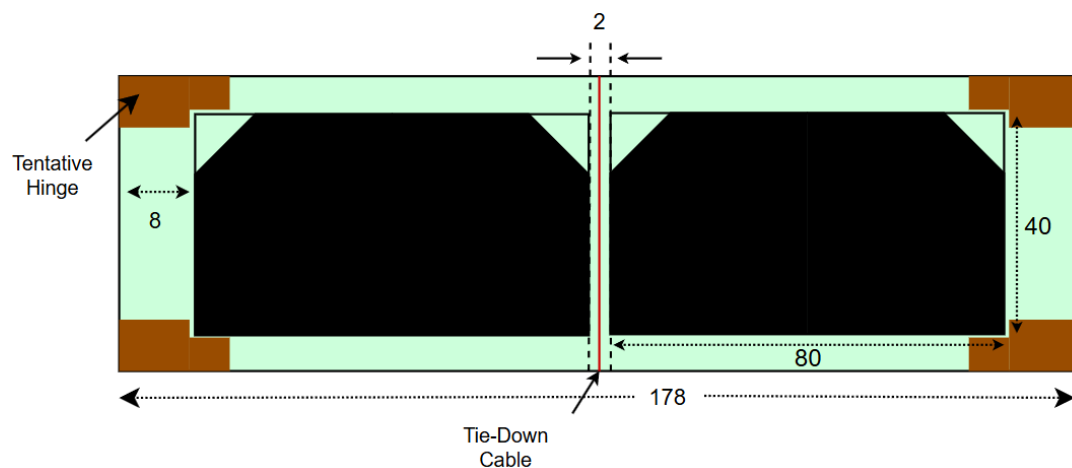


Figure 3.11: PCB layout 2

Even though it is possible to incorporate more than 2 hinges per side, none of the existing designs launched or studied in academic papers featured more. This is mostly due to the lack of space available and the increased number of components. While incorporating 3-4 hinges per side would provide added stability, the limited space would result in smaller structures, leading to added complexity in manufacturing.

While both of these options satisfy the dimensions available for the PCB, they offer different functionality to the overall design. Option 1 features one hinge located centrally between the two solar cells per long edge. This would enable a much larger hinge to be incorporated, and the possibility of including COTS hinges such as EXA's hinge Nano [39], which features overall length of 15mm. However, this reduces the structural integrity of the structure as either ends of the panels are not joined mechanically to adjacent panels. This would cause greater deformations due to the vibrations experienced during flight. Option 2 features two smaller hinges (8mm length maximum) located on either ends of the long edge, mechanically joining the ends of the panels and leading to increased torsional stability of the panels. Both options feature a tie-down cable through the middle to constrain the panels in their hold down configuration, as chosen in 3.6. Layout 2 will be chosen to proceed with the thickness and spacing analysis of the PCB assembly to find the number of panels, thickness of panels, and spacing between the panels that will withstand the major vibrational loads experienced during flight.

3.4.3. PCB Thickness and Spacing Analysis

In the final assembly of the stowed solar panels, their volume envelope limits the thickness and spacing between the panels. The combined thickness of the panels and the spacing between them shall not exceed 10.5mm as given in the requirements and provided by AlbaOrbital [9]. In this section, Dynamic analysis will be required to assess the different thicknesses and spacings to see which options provide deformations and stresses that are lower than the expected values. In Figure 3.12, the overall assembly structure is portrayed with 4 panels.

In figure 3.12, a cross-section view of the space between the PocketQube Wall and the Deployer wall is shown for a 4 panel assembly. As can be seen, the thickness of the panels is represented by t_p and the spacing between the panels is represented by t_s . A combination of these has to be less than 10.5mm as the equation represents for simplicity. In theory, all of the spaces in between panels and the pocketqube bus and deployer could be different, making the complexity of the design and analysis much greater. Therefore, the required spacing between the PocketQube wall and the first PCB, and consequently between the PCBs, is set to t_s while the space between the final PCB and the deployer wall is set to $1/2 * t_s$. This is because the maximum allowed deflection due to vibrations of the PCBs is limited to $1/2 * t_s$ as any more than this would cause neighboring PCBs to collide and damage the solar cells.

As realized in the fixed corner analysis of rectangular shell in the material selection section 3.4.1, large deformations occur either in the center or the edges of the of the panels. This shows the need for spacers/standoffs to separate the panels and reduce this deformation. These spacers are shown in the image and will match the separation used in the analysis. The spacers used for these separations are

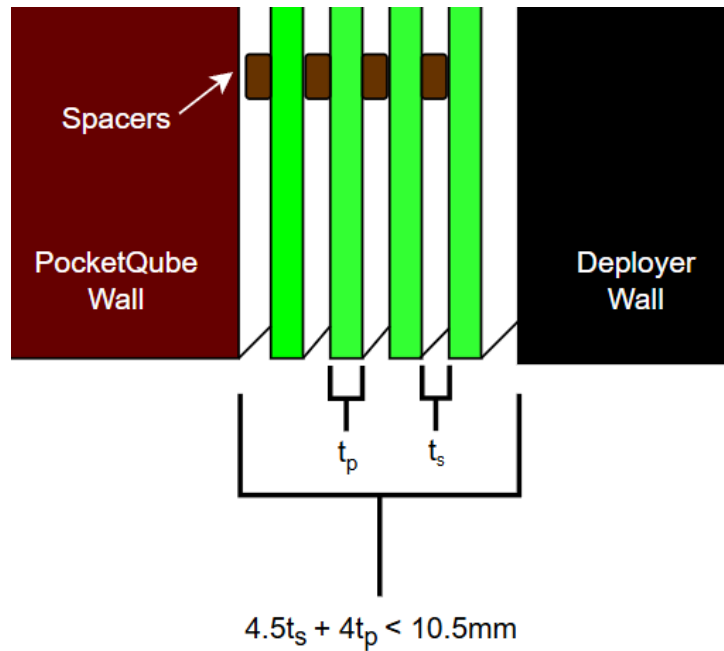


Figure 3.12: PCB Stowed Assembly Schematic

‘SMT Spacers’ provided by Wurth Elektronik. See Figure 3.13 and Table 3.13. SMT spacers allow for easy installation While it is beneficial to chose COTS spacers due to the lower cost and available documentation regarding the solder mask, etc, one cannot outlook the ease of manufacturability for such a component. Mentioned on the website, these fasteners mount on PCBs in the same manner and at the same time as other surface mount components prior to the automated reflow solder process. The fasteners simply become another board component.



Figure 3.13: Wurth Elektronik WA-SMSI SMT-M1.6 [72]

Attribute	Value
Supplier	Wurth Elektronik
Model	WA-SMSI SMT-M1.6
Separation Length (mm)	1.5
Hole Diameter (mm)	2.1
Min Board Thickness (mm)	0.7
Land Pattern Diameter (mm)	4
Material	Steel
Solderable	Yes

Table 3.13: WA-SMSI SMT-M1.6 Specification [72]

Eurocircuits is a trusted PCB supplier in Europe and they provide various options for PCB with the ability to select the number of layers, thickness, base material, color of solder masks, legends, surface finish and many other parameters. While most of these are out of scope of this project, the parameters in Table 3.15 have been chosen to meet the minimum requirements of deployable solar panels. Consequently, the price of different thickness and order quantity is shown in Table 3.14.

Thickness (mm)	Quantity 8	Quantity 16
0.80	666.96	672.32
1.00	322.16	366.40
1.20	666.96	672.32
1.55	262.80	327.20

Table 3.14: Price (€) for 7 Day Lead Time [68]

Parameter	Value
Number of Layers	2 (double-sided)
PCB Size (mm)	174.00 x 50.00
Base Material	IS370HR
Material Tg	170-180°C
Outer Layer Copper	18 μm

Table 3.15: PCB Specifications

As clearly evident, the pool-able options are with thicknesses of 1.00 mm and 1.55 mm. This means that they are manufactured (or cut) from larger sheets accommodating multiple orders. This is not the case for the other two thicknesses available, drastically impacting the cost of the panels. While the difference in the cost is large, they are all relatively affordable for small satellite projects, in comparison to other subsystems.

Using the equation below, different thicknesses and spacings can be analyzed and simulated in ANSYS to see the structural response. A sample of these combinations is provided in Table 3.16. Due to the aim of incorporating 4 panels for this particular design, spacer separation was reduced from the assumed 1.5 mm (due to the available COTS spacers) to 1.4 for option 2, to have an option available with 1.00 mm thick PCBs as these are provided with pool-able options. There are no viable options for 4 panels with thicknesses > 1.00 mm as these would exceed the 10.5 mm envelope available with minimal spacing in between.

$$T_w \leq (n_p + 0.5) * t_s + n_p * t_p \leq 10.5 \text{ mm}$$

Option	Number of Panels n_p	Thickness t_p (mm)	Panel Separation t_s (mm)	Total Width T_w (mm)	Clearance to Wall (mm)	Total Mass of Panels (g)
1	4	0.80	1.50	9.95	1.3	52.9728
2	4	1.00	1.40	10.3	0.9	66.216
3	3	1.20	1.50	8.85	2.4	59.5944
4	3	1.00	1.50	8.25	3	49.662

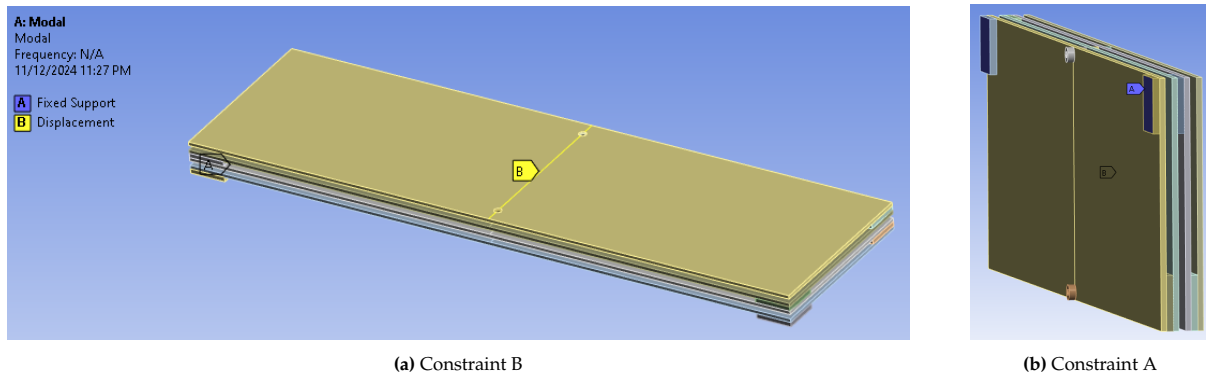
Table 3.16: Sample of Thickness and Spacing Combinations Analysed in ANSYS

If the deformation between consequent panels were to exceed $1/2 * t_s$, that would mean that the panels could potentially collide with each other or the deployer wall, causing permanent damage to the solar cells and jeopardizing the mission.

Model Generation

In order to find the thickness and separation combination that adheres to the requirement mentioned above, a representative model of the panel assembly is developed in Ansys with the options mentioned in Table 3.16. This model can be seen in Figure 3.14 alongside the constraints that are relevant to the analysis. The model adopts a 3D mesh approach, ensuring that all structural and load-bearing components are represented with their primary contributing dimensions accurately captured. This philosophy prioritizes precision by considering the critical geometrical and material properties that

influence the overall structural behavior. A list of the key considerations in this model are provided below:



(a) Constraint B

(b) Constraint A

Figure 3.14: 3D Model for Structural Analysis

- Hinges are modeled as flat plates according to the Z-folded configuration chosen earlier, and are used to separate the panels on the short edges.
- Hinges connecting the closest panel to the PocketQube body are chosen as fixed supports. This is shown as constraint "A" and are the first two hinges at the bottom of the model.
- To replicate the tie-down cable option selected in the Hold-Down section 3.6, a displacement constraint is used along the middle of the outermost panel to constrain the movement out of the plane. This is shown as constraint "B".
- Mesh was generated using 'Edge sizing' with 2mm elements defined along the edges of the panels. Additional mesh parameters were defined to increase resolution around cutout elements and adapting sizing was also used to increase the resolution for separation elements (hinges, spacers). Overall resolution was set to '5'.

Modal Analysis

Firstly a modal analysis was done in order to understand the natural frequency of the system and the mode shape, indicating where structure is likely to deform and what the response is like. An image of the first 1st mode shape is provided in Figure 3.15. The other mode shapes are available in appendix A.2.1

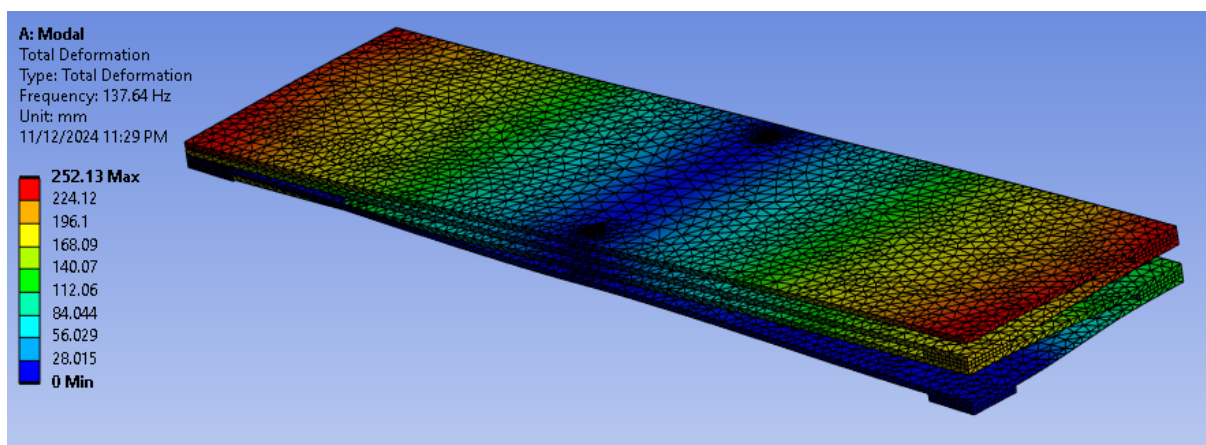


Figure 3.15: Modal Analysis of Panel Assembly

The mode shape illustrates that the outermost panels are most susceptible to deformation, particularly at either ends of the long edges, which experience the highest displacement under oscillation. The central region of the panels remains relatively stiff and experiences minimal deformation, likely due to the reinforcement provided by the tie-down cable or constraint 'B.' This is a consistent pattern across all thickness and spacing combinations and suggests that the outer edges of the panels are the primary areas of concern for managing vibrations.

A worst case scenario is considered for the minimal natural frequency of the panel assembly. Essentially, the oscillations are transferred to the PocketQube via the backplate. Since the panels are mounted on the outer surface of the PocketQube body, the worst case assumption is that these oscillations are also transferred directly to the panel assembly, without any dampening. This means that the natural frequency of the structure must be greater than 100Hz to pass the structural requirement for small satellites. All combinations of thicknesses and separations have a higher natural frequency, and are therefore considered stiff enough.

Random Vibration Analysis

Random Vibrations refer to unpredictable and non-repetitive oscillations caused by a multitude of outputs. They do not have a predictable sinusoidal impact but are generally characterized by statistical representation such as PSD. Section 2.7 introduces random vibration analysis and delves into the GEVS profile that is used for the random analysis. The deformation and stress concentrations observed for option 2 from 3.16 are shown in Figures 3.16 and 3.17.

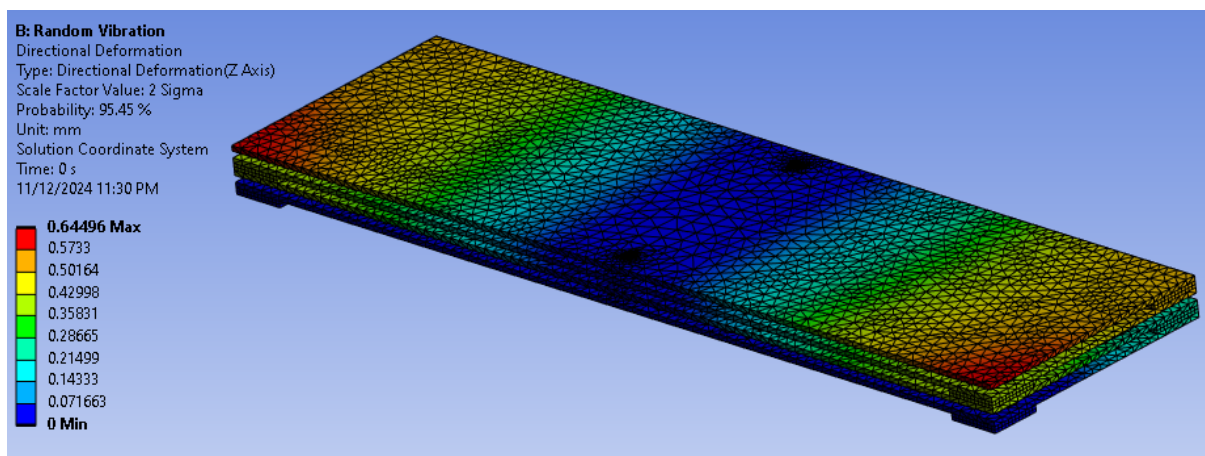


Figure 3.16: Panel assembly deformation

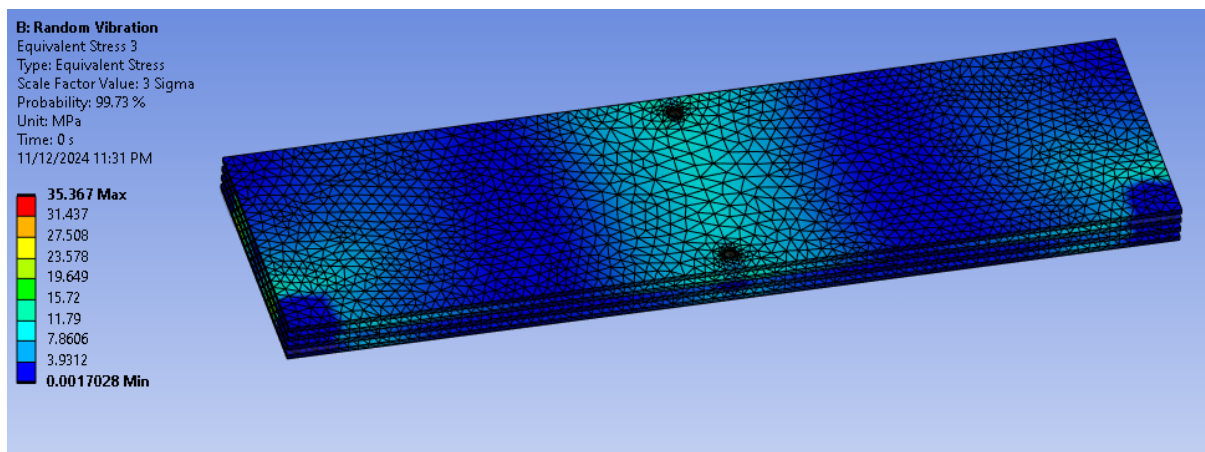


Figure 3.17: Panel assembly Von-mises stresses

These figures present the deformations and stresses resulting in the chosen combination that passes the requirement mentioned earlier, where the maximum deformation is less than half the spacing between consequent panels. The results of the analysis are summarized in Table 3.17.

Option	Number of Panels	Thickness (mm)	Panel Separation (mm)	Max Deformation-z (2σ , mm)	Von Mises Stresses (2σ , MPa)
1	4	0.80	1.50	0.89907	
2	4	1.00	1.4	0.64496	35.367
3	3	1.20	1.50	0.44092	19.6878
4	3	1.00	1.50	0.62941	29.102

Table 3.17: Comparison of Panel Configurations with Deformation and Stress Metrics

Apart from option 1 with 0.8 mm panels, all other options pass the criteria for maximum deformation, and can be used in a multi-panel assembly. The margin of safety is calculated as specified in the ECSS Mechanisms Handbook. The Design Allowable Load is the maximum load the structure can withstand, while the Factor Of Safety (FOS) accounts for uncertainties within the model. A conservative FOS of 1.4 was chosen due to the simplifications in the model.

$$\text{MarginOfSafety(MOS)} = \frac{\text{design allowable load}}{\text{design limit load} \times \text{FOS}} - 1 \quad (3.1)$$

Based on the analysis, the design that maximizes the number of panels and still meets the criteria for avoiding contact between consequent panels is option 2, with 4 panels of 1.00 mm thickness and 1.4 mm spacing in between consequent panels. A noticeable trend is that while decreasing the PCB thickness does allow for greater separation between consequent panels, the deformation increases exponentially, making it infeasible to incorporate thinner PCBs in the assembly.

Option	Von Mises Stresses (MPa)	Factor of Safety	Yield Strength (MPa)	Margin of Safety
2	35.37	1.4	385	6.78

Table 3.18: Summary of Von Mises Stresses, Factor of Safety, Yield Strength, and Margin of Safety for each Option.

Determining L_b

Based on the chosen option, parameter L_b (width of PCB) needs to be adjusted to match the available envelope for the solar array assembly. This is directly driven by the choice of torsion spring hinges, the maximum diameter of the spring that can be incorporated, and the available envelope in $\pm Y$

As seen in figure 3.18, the maximum length available in the AlbaPOD ICD to incorporate the solar arrays is 54.5 mm. This includes the overall length of the panels and the hinges on either side of the panels. The maximum diameter $D_{o,max}$ of the spring (and consequently the hinges) can be visualized in figure 3.19, driven directly by the previous thickness and spacing analysis of the pcb assembly.

$$D_o \leq 2t_s + 2t_p$$

This yields that a conservative value of 4.8 mm can be chosen for the maximum diameter of the spring. Utilizing this relationship, the maximum value for L_b can be obtained by the following relationship:

$$L_b + 2 * D_{o,max} \leq 54.5 \text{ mm}$$

The maximum value of $L_b = 44.9$ mm. Having obtained this new length, the random vibration analysis needs to be conducted again to see whether deformations are still under specified requirements to prevent the collision of consecutive panels.

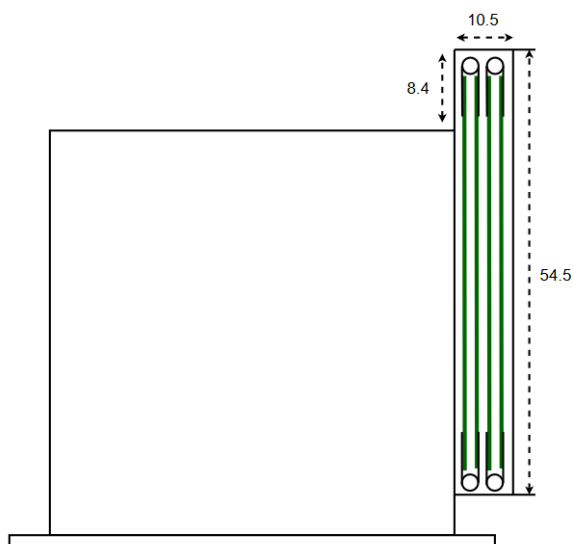


Figure 3.18: Solar Panel Envelope

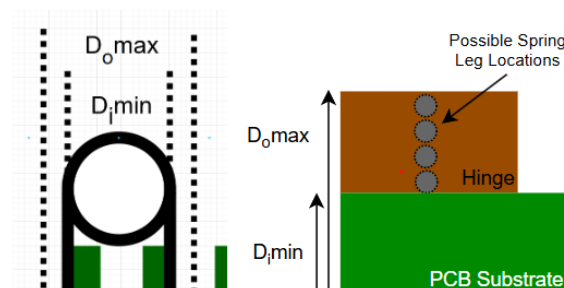


Figure 3.19: Minimum and Maximum Spring Diameter

Modal analysis and Random Vibration analysis were consequently done with the adjusted panel dimensions of 178 mm * 44.9 mm. The maximum deformation observed was 0.544 mm and the maximum stress was 22.22 MPa at a 2σ scale factor. These results fit the criteria described earlier. The final specifications and results for the PCB assembly from this section are provided in table 3.19.

Parameter	Value
Length L_a	178 mm
Width L_b	44.9 mm
Spacing t_s	1.4 mm
Thickness t_p	1.00 mm
Mass per Panel	14.86 g

Table 3.19: Table of Parameters and Values

3.5. Hinge Design

3.5.1. Torsion Spring Selection

The result of the trade-off in section 3.3.3 yielded that torsion spring hinges are the most appropriate to support the deployment mechanism design. In order to design the hinge, a torsion spring needs to be selected initially. This will allow us to design a structure to support the spring and interface between panels and the PocketQube body.

A comprehensive guide to spring design is provided by Associated Spring [73] and a lot of key parameters and considerations are provided regarding torsion springs, most of which are summarized in the list below.

- Available in single or double bodied options.
- Stressed in bending.
- Should always be loaded in a direction that causes body diameter to decrease. This is because residual forming stresses are favorable in this direction.

- Clearance must be maintained between tube at all times to prevent binding. Ideal shaft size is $\leq 90\%$ of the internal diameter when the spring is fully deflected.
- Spring index $C = D/d$ is recommended to be 4-12. Low spring index can result in high stiffness and compact solutions with the cost of high internal stresses. High spring index gives one the opposite.
- Avoid special/bent ends to minimize stress and failure of torsion springs.

Materials

Torsion springs are usually available in 2 materials, properties of which are provided in table 3.20.

Property	Music Wire	SS304
Type	High Carbon Steel	Stainless Steel
Density (kg/m^3)	7750	8027
Tensile Strength (MPa)	1585 - 2751	896.3 - 2241
Modulus of Elasticity (GPa)	206.8	193
Maximum Temperature ($^{\circ}C$)	121.1	287.8
Description	Highly magnetic, generally great fatigue life due to high tensile strength	General heat resistant spring wire, slightly magnetic and mostly used in marine applications

Table 3.20: Comparison of Properties for Music Wire and AISI 304 [74]

What is noticeable is that music wire will tend to have a higher spring rate, and provide slightly greater torque in comparison to the stainless steel alternatives. This is mainly due to the high longitudinal modulus of elasticity as seen in the equations provided. However, it is also highly magnetic, which may interfere with the magnetometers and attitude control sensors on board. For less magnetic, high temperature resistant options, stainless steel is usually the material preferred. While these have low tensile strength, it is not a critical factor due to the single use application.

For this design, **Stainless Steel** spring options will be evaluated as this is the preferred material due to its high temperature stability, and heritage use in corrosion prone circumstances such as marine applications.

Torsion Spring Equations

As discussed earlier, a torsion spring is a mechanical spring that works by exerting torque when it is twisted along its axis. The spring is typically made of high carbon steel, stainless steel, or other non-ferrous metals such as bronze and copper.

The torque of a linear torsion spring can be calculated by the following equation [75]:

$$T = k\theta \quad (3.2)$$

Where:

- T = torque of a torsion spring [N-mm]
- k = torsional spring constant [N-mm/rad]
- θ = angular deflection of the torsion spring [rad]

The torsional spring constant, also known as the torsional spring rate, is an indication of the spring's stiffness or resistance to twisting and rotation. This determines the amount of torque needed to achieve a given angular deflection, or in our case, the amount of torque generated by pretensioning the spring

to a given angular deflection. As can be seen in the equation above, the spring constant is directly proportional to the torque generated and is therefore a crucial parameter. The spring constant can be calculated by the following equation:

$$k = \frac{d^4 E}{64 D N_a} \quad (3.3)$$

Where E is the longitudinal elastic modulus of the spring material [N/mm²], d is the wire diameter [mm], D = mean coil diameter [mm], and N_a = number of active turns in the spring [unitless]

Finding the right spring or developing the right custom spring for the deployment mechanism is a challenging task due to the following reasons:

1. Spring has to fit in a small volumetric envelope and therefore cannot have extremely large coil diameters or a large number of coils.
2. The angular rate of deployment should be limited to reduce the impact shock at the end of deployment.
3. Spring has to maintain torque at the end of deployment to insure final blocking.

The stress of a round wire torsion spring can be calculated by the following formula:

$$\sigma = K \frac{32T}{\pi d^3} \quad (3.4)$$

K is a unitless parameter that aims to correct geomtric deviations in the wire during deflection that causes the neutral axis to shift towards the center of curvature. Therefore, the inner surface of the spring experiences higher stresses than the outer surface. The parameter can be calculated by the following equations where C is the spring index (D/d):

$$K_i = \frac{4C^2 - C - 1}{4C(C - 1)} \quad (3.5)$$

$$K_o = \frac{4C^2 + C - 1}{4C(C + 1)} \quad (3.6)$$

One can calculate the impact velocity for the impact moment of deployment by looking at the angular kinetic energy equation [76]:

$$E_{\text{rotational}} = \frac{1}{2} I \omega^2 \quad (3.7)$$

As outlined in the paper, the work done (energy) by the torsion spring can be represented as the following:

$$E = \int_{\theta_0}^{\theta_1} T(\theta) d\theta; \quad (3.8)$$

$$E = \int_{\theta_0}^{\theta_1} k(\theta_1 - \theta_0) d\theta = \frac{1}{2} k(\theta_1 - \theta_0)^2; \quad (3.9)$$

The moment of inertia can be estimated as the following for a rectangular plate (solar panel) when the axis of rotation is parallel to the short edge of the plate:

$$I = \frac{mb^2}{3} \quad (3.10)$$

Where m = mass of the panel and b = Length of the Short edge of the panel (m)

By using the angular kinetic energy equation, the angular velocity for the impact moment can be calculated by the following relation:

$$\omega = \sqrt{\frac{2 \left(\frac{1}{2}k(\theta_1 - \theta_0)^2\right)}{\frac{mb^2}{3}}} \tag{3.11}$$

By calculating the spring force required and the maximum impact moment possible due to the induced shocks, one can start designing the torsion spring needed in the torsion spring hinge for such a deployment mechanism.

Spring Selection

From the panel assembly chosen and designed, there are multiple constraints that can be derived that limit the scope of available options for torsion springs in the market. Ideally, due to high manufacturing complexity, **only COTS springs will be evaluated for the design**. Many of these can be found at two trusted spring manufacturers, Tevema and Lee Springs and therefore their catalog will be studied.

Seen in Figure 3.20, the spring locations are identified. Tevema and Lee springs, like most manufacturers, provide set free positions of the springs and these are shown in Figure 3.21. Based on these, Table 3.21 summarizes the stowed angular separation, angular displacement, and the recommended free positions.

Spring ID	Stowed Position (°)	Angular Deflection (°)	Recommended Free Position (°)
S _t 1	90	90	180
S _t 2	0	180	210, 270
S _t 3	0	180	
S _t 4	0	180	

Table 3.21: Spring free positions and deflections

A key consideration here is that it is crucial to maintain residual torque in the latched position, as minimal environmental damping is available in space to reduce oscillations. Without this residual torque, the panels may not lock securely, leaving them susceptible to oscillations when the spacecraft rotates or experiences other dynamic conditions. If the springs lose stiffness due to thermal effects, this would also make the panels subject to uncontrollable oscillations. Therefore, the free position of the springs is recommended to be beyond the final angular separation of the spring legs.

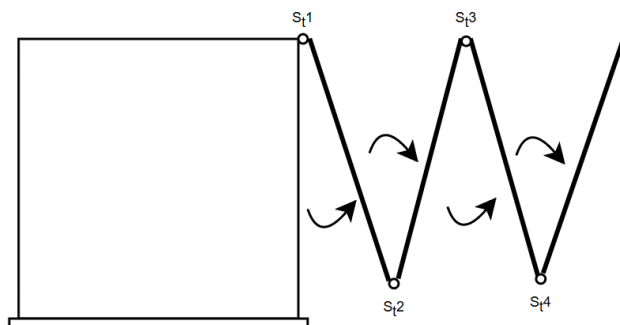


Figure 3.20: Spring Locations

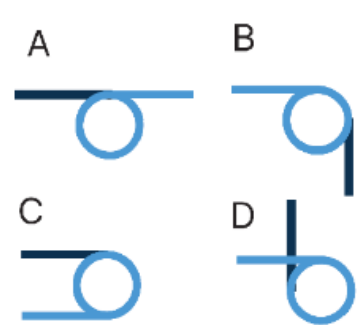


Figure 3.21: Spring Free Positions

From the panel assembly, the outer diameter of the spring is limited as shown in Figure 3.22. This concept maximizes the diameter of the spring by utilizing the outer surface of the panels to mount on. Otherwise,

the panel separation width identified of 1.25mm would be required for the maximum outer diameter for the spring, largely limiting available options.

This results in:

$$D_i \geq t_s + 2t_p \geq 3.40 \text{ mm}$$

While this is the minimum internal diameter of the spring between consequent panels, the maximum outer diameter is limited by the distance to the next spring as seen in 3.4.3. This results in:

$$D_o \leq 2t_s + 2t_p < 4.80 \text{ mm}$$

This will allow 2 springs to be placed next to each other in the stowed configuration without making contact. Based on these requirements, there were a handful of helical torsion springs that fit the criteria, specifically from the more comprehensive catalog of Lee Springs. These springs all have varying levels of torque when deflected to the angular positions as mentioned in 3.21. All the torque values have been calculated using the equations above.

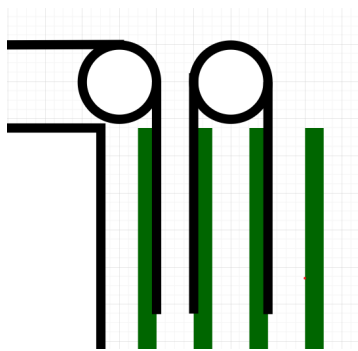


Figure 3.22: Spring Position Concept

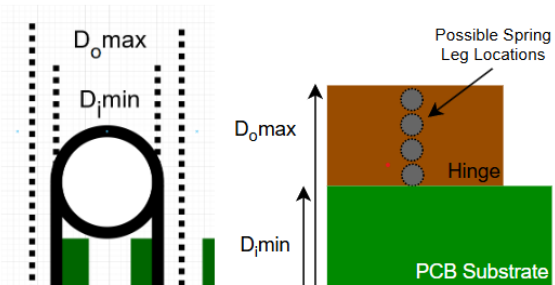


Figure 3.23: Dimension Limitations

The preferred spring out of the ones identified is **LTR012A 05 SS** and the characteristics for it are provided in table 3.22. This spring deemed most suitable as it has a compact body length of 2.18 mm, and the impact velocity is also the least, as shown in table 3.25.

Table 3.22: LTR012A Specifications

Outside Diameter (mm):	4.34
Wire Diameter (mm):	0.3
Max Torque (N-mm):	5.3103
Deflection to Max Torque:	270.00
Radius (mm):	6.35
Free Position of Ends:	270
Length of Leg (mm):	12.7
Body Length (mm):	2.18
Total Coils:	5.75
Material:	Stainless Steel

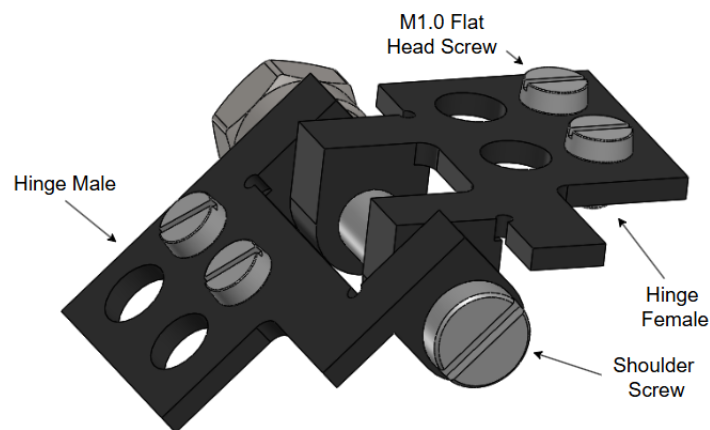
3.5.2. Hinge Assembly

As noted in the hinge trade-off analysis, torsion springs require additional housing/encasing to structurally support their contact between the different appendages and to support the internal diameter of the spring with a shaft. This subsection will delve into developing a concept for such a hinge structure, that facilitates the springs and also provides final blocking/latching, as specified in the requirements of the hinge. Certain design constraints are posed by previous sections that contribute to the design of the hinge. These are as following:

Table 3.23: Hinge Design Constraints

Description	Value	Source
Minimum shaft diameter: Calculated by the relationship obtained from the Associated Spring guide. The interior diameter for the spring is 4.04 mm, reduced to 3.56 mm under deflection (coiling). To provide clearance, the diameter should be less than this value.	< 3.20 mm	Torsion Spring
Minimum Width for Torsion Spring Body Length: Based on the preferred spring (LTR/LTL 012A), this is 2.025 mm.	> 2.025 mm	Torsion Spring
Hinge Mounting Plate Thickness: Limited by the clearance between subsequent panels, calculated as 1.40 mm. Therefore, the hinge plate thickness is half this value.	0.70 mm	PCB Assembly Design
Hinge structures should prevent jamming due to thermal expansion and manufacturing tolerances.	-	-
The design should be manufacturable using precise CNC machining, limited to ISO 2786 fine guidelines. This is essential to be able to manufacture in house, or to procure from numerous suppliers in the market, such as PCBWay, ProtoLabs, etc.	-	ISO 2786

Based on these considerations and design specifications, three hinge assemblies were developed to facilitate the attachment of panels and the PocketQube body. These assemblies focus on minimizing the type and number of separate parts that need to be manufactured.

**Figure 3.24:** HP2P: Hinge Panel To Panel

This hinge (HP2P) is designed to interface between consequent panels. The hinge assembly features 4 parts: Hinge Female, Hinge Male, Shoulder Screw and Lock Nut. The male and female hinge bodies also provide a structure for locking at final deployed position.

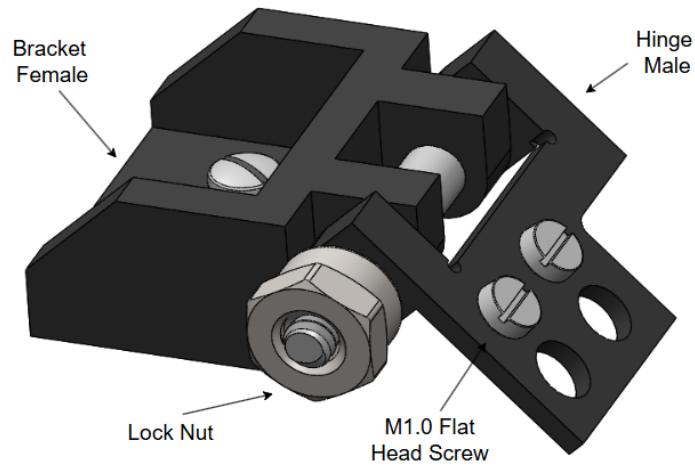


Figure 3.25: HP2PQ1: Hinge Panel To PQ 1

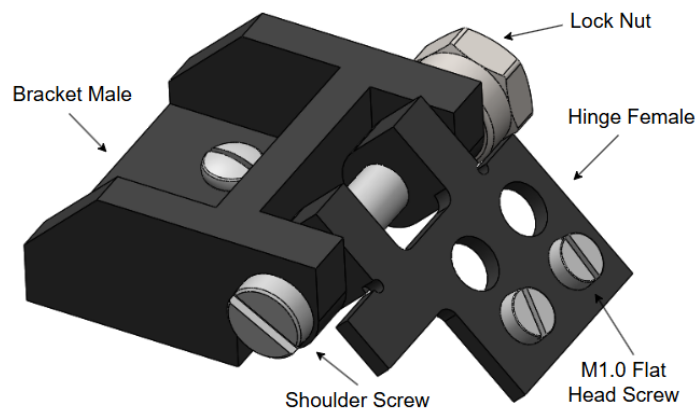


Figure 3.26: HP2PQ2: Hinge Panel To PQ 2

These two hinges, HP2PQ1 and HP2PQ2, are assemblies that mount the solar arrays to the PocketQube body. They consist of an additional 2 bodies, the male and female brackets. The brackets are mounted on the +Y face of the PocketQube, at either end of the long edge. All the individual parts used in these assemblies are outlined in table 3.24.

Table 3.24: Parts Used in Hinge Assemblies [5]

Part (Supplier)	Description	Image
Bracket Male & Female (Custom)	These brackets are responsible for the panel to PQ hinge assemblies. The design for these brackets is inspired from the brackets observed in FossaSat-2. To fasten with the PQ body, they contain two M1.2 tapped holes.	

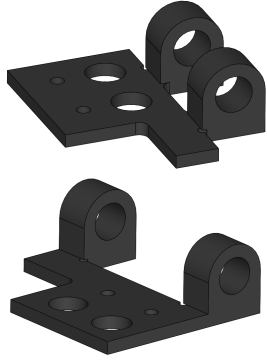
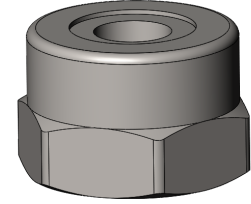
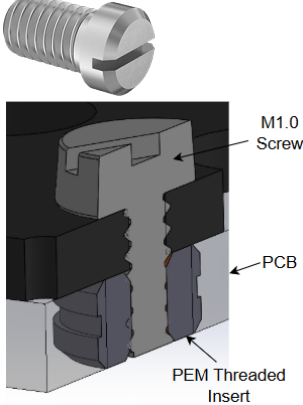
Part (Supplier)	Description	Image
Hinge Body Male & Female (Custom)	These hinge bodies are seen in all three hinge assemblies. While the overall planar dimensions of the bodies is 12mm x 8mm, they contain cutouts to enable the incorporation of solar cells with the PCB layout determined earlier. The total thickness of the bodies is 0.7 mm, as the maximum separation determined in the PCB assembly design is 1.4 mm and two hinges will stack up between consequent panels. To fasten these to the PCBs, they contain M1 tapped holes.	
Shoulder Screw (McMasterCarr)	Rather than conventional hinges consisting of a pin, this hinge consists of a shoulder screw as this provides the structure to support the spring, and can be constrained on the other end by a lock nut, resisting any movement or failure due to vibrations. This is similar to the design observed in Unicorn 2 PocketQubes. The shoulder diameter and length are 2mm and 12mm respectively, and the thread is 1.6mm.	
Lock Nut (Accu)	This lock nut is used to fasten and constrain the shoulder screw on the opposite end of the hinge. The internal thread diameter is 1.6mm, and is cushioned with nylon inserts to prevent loosening due to the vibrations experienced during launch.	
M1 Flat Head Screws (ACCU)	M1 screws are used to attach the hinge bodies to the PCBs. While the thickness of the hinge body is only 0.7 mm, the screws pass through the hinge body and are fastened into the threaded inserts attached to the PCBs. This matches guidelines recommended by NASA [77], where the length of the thread engagement must be at least 1x the nominal diameter of the thread.	

Table 3.24: Parts Used in Hinge and Bracket Assemblies

Hinge Body Material Selection

For developing the additional structure and shaft to encase the torsion spring, it is important to consider the materials that are available for such structures in small satellites. Properties for these are provided in the appendix in table A.5. The four most prominent materials used in mechanisms and structures in small satellites are aluminum alloys, titanium alloys, beryllium copper alloys, and stainless steel, each of which offers unique advantages and disadvantages. For example, BeCu 172, also known as Alloy 25 in the industry, has heritage in the only nano-scale hinge available in the market by EXA [39]. This is due to its relatively high strength, extremely good corrosion resistance, and high manufacturability. However, it is fairly expensive, highly toxic (although the Beryllium content is 2%) and hard to obtain compared to Al7075 or SS302/304, which are readily available in most markets. Alloy 25 does offer additional

capability with single-channel electrical conductivity, reducing the complex wiring between subsequent panels, despite the high electrical resistance.

Highest strength-to-weight ratios are provided by titanium alloys, however they are costly and hard to manufacture due to the relatively low stiffness. Since the mass of these hinges will be a relatively low percentage of the system mass and contribute negligible changes, it's relevance is less in this comparison. Due to easy of procurement and other characteristics discussed, **AL7075** is the chosen material. A hinge impact analysis will be conducted in the next section to deem whether the stresses observed will cause failure due to the aluminum alloy chosen, and the dimensions chosen for the hinge structure.

Hinge Body Separation Analysis

The two hinge bodies should ideally be locked together to prevent unwanted vibrations. However, a separation between the two hinge bodies t_b , specifically the concentric structures, is necessary to prevent jamming prior to deployment. This separation is visualized in figure 3.27. This jamming/locking can occur due to thermal expansion and manufacturing defects. In order to prevent this jamming, a separation between the two hinge bodies will be determined by evaluating the deformation due to thermal expansion to conservatively high temperatures gradients experienced in orbit, and by evaluating the linear tolerance under the ISO 2768 'fine' standard.

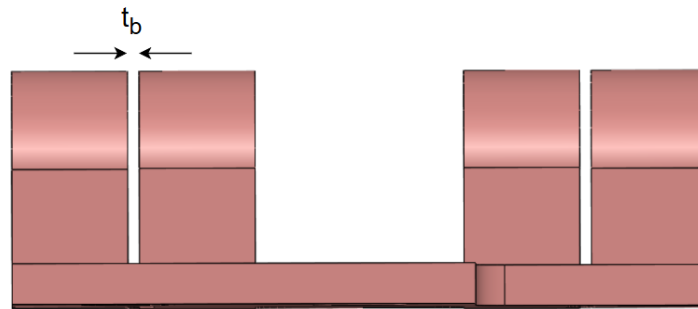


Figure 3.27: Hinge Body Separation t_b

The thermal analysis was done in Ansys Mechanical's 'Static Structural' tool on both hinge bodies. They were constrained around the bolted down surface and initial and final temperatures were applied of 22 °C and -40, 80 °C respectively. These final temperatures are conservative values obtained from most sources regarding the minimum and maximum surface temperatures experienced on small satellites in LEO [78]. It also assumes maximum conduction between the PQ outer surfaces and the hinges. The following results were obtained:

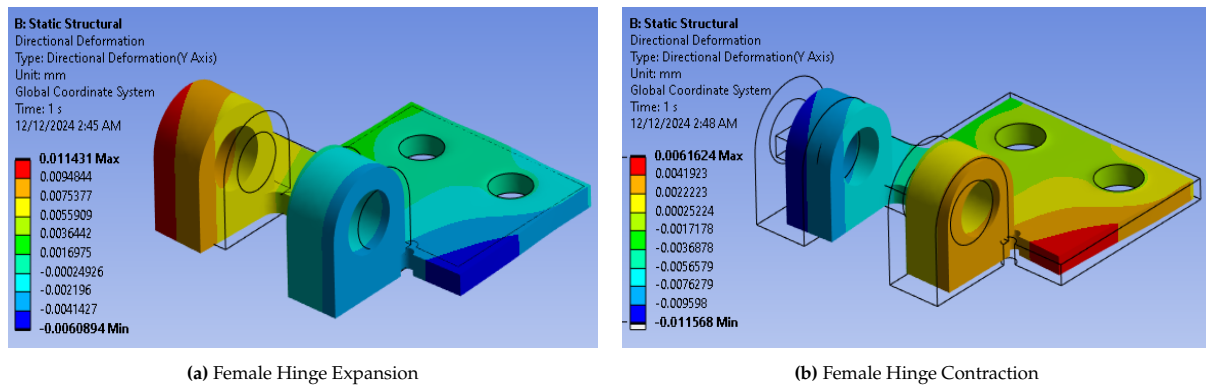


Figure 3.28: Thermal Deformation Observed on Female Hinge Body

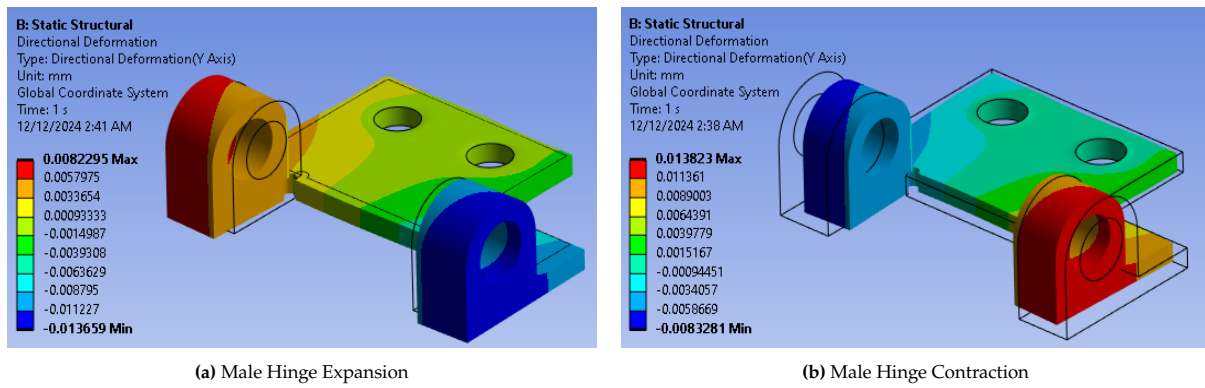


Figure 3.29: Thermal Deformation Observed on Male Hinge Body

The results for this analysis are summarized in table below.

Temperature (\degree C)	Directional Deformation (um)					
	Female Body			Male Body		
	Min	Max	Total	Min	Max	Total
-40	-11.57	6.16	17.73	-8.33	13.82	22.15
80	-6.09	11.43	17.52	-13.66	8.23	21.89

The total deformation observed in the hot and cold cases are 0.0394 mm and 0.0399 mm respectively. The tolerance for 3 axis CNC machining provided by most manufacturers according to the ISO 2768 standards are 0.05 mm, leading a total possible overlap of 0.1mm by both hinge bodies. This results in a minimum value of the following:

$$t_b > 0.1399mm$$

Due to ease of manufacturing and to introduce some clearance for this minimum separation between the two hinge bodies, a value of ($t_b = 0.2mm$) is chosen for the assembly.

3.5.3. Hinge Impact Structural Analysis

Simulating the impact of the hinge at the end of the deployment is crucial to the design, as this is where the structure is most likely to fail. This simulation should validate the use of the concept designed if it were to survive impact shock and loading.

For each spring location, the worst and best case is considered for moment of inertia. The worst and best case is considered by evaluating situations where all consequent panels are still stowed or fully deployed. This can be seen in Figure 3.30. Using the minimum and maximum inertia values, the angular impact velocity can be calculated using the equations outlined previously. This is an important calculation because it determines the state of the collision of the hinge/locking structure, and consequently drives sizing and material recommendations for it. This approach is adopted from [76], which also delved into the design of deployable solar arrays on PocketQubes. The minimum and maximum impact velocities can be calculated and are provided in Table 3.25.

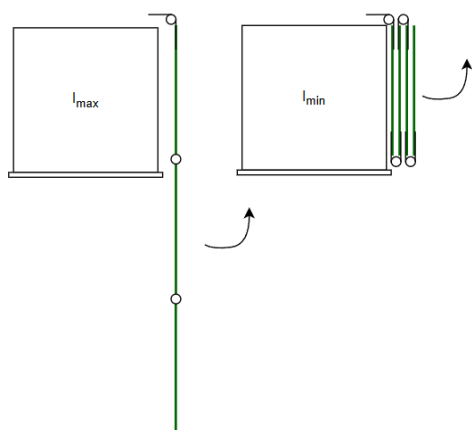


Figure 3.30: Minimum and Maximum Moment of Inertia Conditions

Spring ID	LTR017C 03 MW	LTR012A 05 SS	LTL020D 03 S
Spring Rate	2.992E-03	1.014E-03	4.524E-03
Max ω_{S_t1} (rad/s)	12.207	7.105	15.009
Min ω_{S_t1} (rad/s)	3.052	1.776	3.752
Max ω_{S_t2} (rad/s)	28.191	16.409	34.662
Min ω_{S_t2} (rad/s)	9.397	5.470	11.554
Max ω_{S_t3} (rad/s)	34.526	20.097	42.452
Min ω_{S_t3} (rad/s)	17.263	10.049	21.226
ω_{S_t4} (rad/s)	24.414	14.211	30.018

Table 3.25: Spring Impact Velocity. S_t1 , S_t2 , S_t3 and S_t4 represent the torsion springs, starting with the one attached to PQ Bracket.

Using explicit analysis through LS-DYNA is necessary as it can accurately model the non-linear effects caused by the impact angular velocity. This angular velocity can be derived from the characteristics of the torsion spring selected earlier in the design process. Explicit analysis is preferred over implicit analysis for simulating highly dynamic events, such as the impact of a hinge, because it is better suited for handling short-duration, non-linear phenomena. This is further detailed in section 2.7. It requires no convergence checks or inversion of large matrices. However it is essential to model the problem properly and as simply as possible to reduce the computational time and focus on the main structure being analyzed.

LS-DYNA Results

For the analysis, Spring LTR012A 05 SS was chosen, as this provided the least angular velocity at impact. The most conservative calculation of 20.097 rad/s was also chosen as the final impact velocity for the analysis, resulting from the deployment of a 2 PCBs of mass 14.9g and dimensions of 178mm * 44.9mm each. The chosen values and characteristics for the analysis are given in table 3.26.

Parameter	Value	Description
Time Step	0.0005s (Automatically Determined by LS-DYNA)	Defines the time increment for solving the explicit equations; should satisfy the CFL condition for stability.
Total Run Time	0.01s	The total duration of the simulation, ensuring complete event capture.
Hourglass Coefficient	0.1	Controls numerical stabilization for low-order elements, reducing artificial energy modes.
Average Mesh Size	0.3 mm / Element	Size of elements in the mesh, affecting accuracy and computational efficiency.

Table 3.26: Explicit Dynamics Simulation Parameters

An end time of the simulation was chosen as 0.010 seconds as this was adequate to achieve the maximum stress during impact and reduce the computational time to the minimum. One side of the hinge (male/female) was modeled as attached to a rigid PCB through the tapped holes, while the other (female/male) was attached to a rotating PCB through the same tapped holes at the specified angular rate.

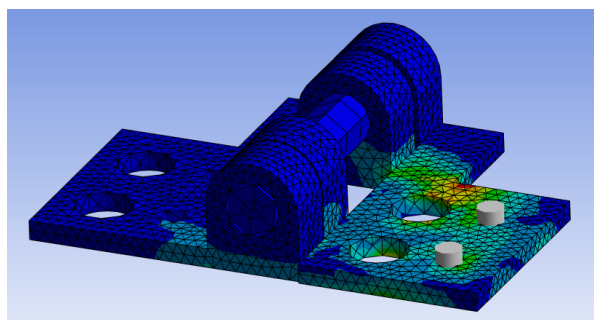


Figure 3.31: Stress Concentrations During Simulation - AL7075 Hinge

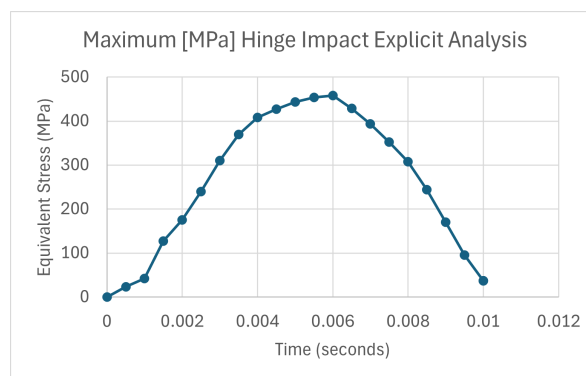


Figure 3.32: Stress Plot AL7075 Hinge

Firstly, the simulation was run using Al 7075 alloy as the material of choice for the hinge body. The largest stresses observed throughout the runtime of 10 ms were observed to be around the internal corners of the hinge bodies, with the maximum stress being 458 MPa. This is observed in figure 3.31 and figure 3.32. This value will be compared with the ultimate tensile strength of Al7075 [79], specifically for sheets ranging 0.305 - 0.991 mm. This is the maximum stress a material can withstand before breaking and is a better indicator than yield strength in this analysis. A conservative factor of safety is again used for this analysis due to manufacturing inconsistencies of the spring and inaccurate predictions of the impact moment. The margin of safety is obtained using the equation 3.1 and found to be -0.183. While the stresses observed may be less than the ultimate tensile strength, inconsistencies within the model and manufacturing could lead to material failure.

However, it is important to understand this maximum stress is only observed for a duration of 0.004 seconds, enough to inflict minor plastic deformation in the structure, and not necessarily break the hinge. Furthermore, a simple fillet would largely reduce the stresses observed, and the analysis proves that this hinge is capable of withstanding the loads during deployment impact.

Maximum Stress (MPa)	Factor of Safety	Ultimate Tensile Strength (MPa)	Margin of Safety
458	1.4	524	-0.183

Table 3.27: MOS Hinge Impact Analysis

Future Work for Hinge Design

Evaluating spring forces for small satellite applications presents significant challenges due to the unique and extreme conditions of the space environment. As a result, the design and validation of such mechanisms rely heavily on a test and prototyping approach. Iterative testing in simulated space conditions is often necessary to gather reliable data on the performance of these components and to identify and address potential issues.

For the purposes of this thesis, I will not delve further into the detailed design and testing of these hinges and spring mechanisms. However, the process outlined in this section can be adapted and expanded upon in future work by estimating and applying friction factors, damping coefficients, and other variables. A general torque margin recommended in [71] is 3 as inadequate torque was a major contributor to the failure of deployable systems as studied in [50]. ECSS Mechanisms handbook suggests the following equation for calculating the minimum torque to prevent deployment failure:

$$T_{\min} = 2 \times (1.1I + 1.2S + 1.5H_M + 3F_R + 3H_Y + 3H_A + 3H_D) + 1.25T_D + T_L$$

where:

- I is the resistive inertial torque applied to a mechanism subjected to acceleration in an inertial frame of reference (e.g., spinning spacecraft, payload or other).

- S is the resistive torque due to springs in the mechanism.
- H_M is the resistive torque due to magnetic effects.
- F_R is the resistive torque due to friction.
- H_Y is the resistive torque due to hysteresis in the mechanism.
- H_A is the resistive torque due to harnesses or cabling within the mechanism.
- H_D is the resistive torque due to adhesion between contacting surfaces.
- T_D is the internal resistance torque caused by the worst-case acceleration mechanism specified by the customer at the mechanism level.
- T_L is the deliverable output torque, when specified by the customer.

3.6. Final Design and BOM

This section contains the final assembly of the deployed solar arrays. It also contains the parts used to assemble all the different structures together, that haven't previously been identified in the hinge design chapter. The render of the final deployed and stowed solar arrays can be found in figure 3.34 and 3.37. A close up of the attachment to the PocketQube body is observed in 3.35 and the attachment of panel to panel hinges is provided in 3.36. Additionally, the mass and cost budgets are also provided for the final assembly.

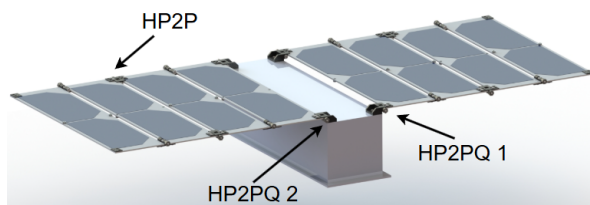


Figure 3.33: Render of Deployable Arrays - Deployed

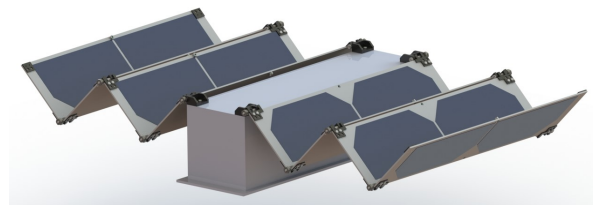


Figure 3.34: Render of Deployable Arrays - Deploying

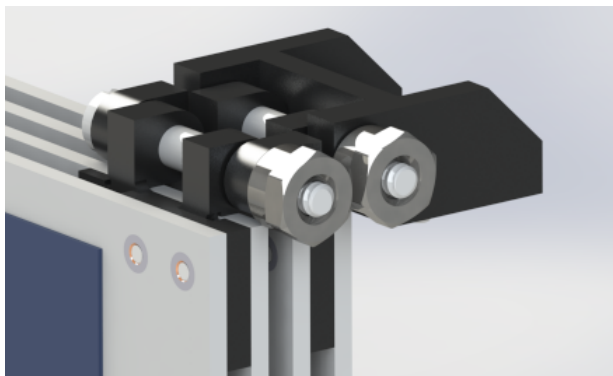


Figure 3.35: Render of HP2PQ and HP2P in Stowed Configuration

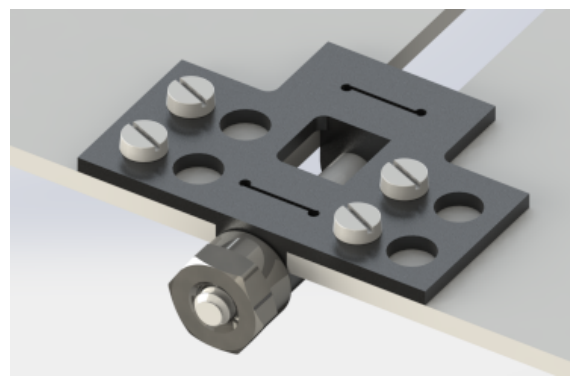


Figure 3.36: Render of Panel to Panel Hinge

While the design was developed in accordance to the dimensional constraints provided by the AlbaPOD deployer and PQ standard, it's still possible to overlook certain aspects, which can result in a design that ultimately doesn't fit within the deployer. Therefore, it is essential to evaluate the cross section of the final PocketQube model within the deployer structure. AlbaPod ICD also specifies that the deployables may not maintain contact with the deployer wall, due to concerns of jamming with the pusher plate during deployment. For this purpose, a 3d model of the deployer was modeled, and figure 3.38 shows that the PocketQube perfectly fits within the volumetric constraints of the deployer.

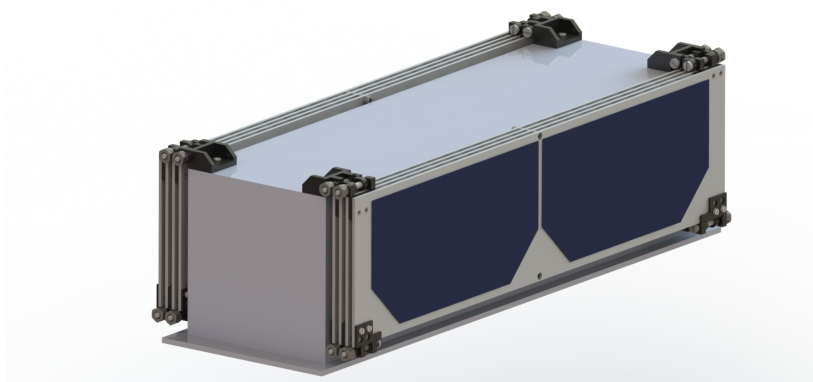


Figure 3.37: Render of Deployable Arrays - Stowed

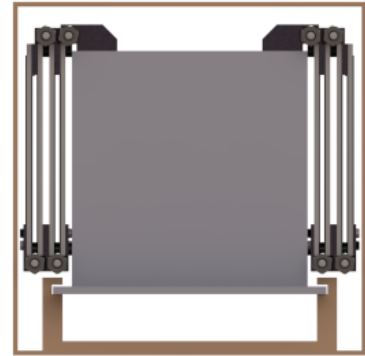


Figure 3.38: PocketQube Within AlbaPOD V1

Other than the parts outlined in table 3.24, the following parts are used to complete the assembly.

Table 3.28: Additional Parts Used in Deployable Solar Array Assembly [5]

Part (Supplier)	Description	Image
Panel PCB (EuroCircuits)	The PCB was designed to be 178mm * 44.9mm with a thickness of 1mm. It is procured from the trusted European supplier EuroCircuits.	
M1.2 Flat Head Screws (McMasterCarr)	M1.2 screws are used to mount the brackets onto the PQ body.	
PEM M1 Threaded Insert (PEM)	PEM threaded inserts provide a durable, reusable metal thread for fasteners in plastic components, overcoming the inherent weakness of plastic or FR4 in threaded applications, especially pertaining to microscrews. These are usually installed using heat-staking processes and will interface between the M1 screws and hinge bodies.	
Dummy Hinge (Custom)	This flat hinge structure is used to support the final PCBs in the assembly. It provides the separation alongside the male and female hinge bodies to act as a spacer on either end of the panel, and prevents the edges of the panels from oscillating and bending.	

3.6.1. Structural Analysis of Array Assembly

This section presents the structural analysis conducted on the final array assembly designed in this chapter. It outlines the model preparation steps used behind the analysis within Ansys Mechanical, and consequently presents the results obtained.

Model Preparation

To prepare the model for the structural analysis, it is important to simplify the geometry to reduce the computational time and temporary memory being used, while still maintaining high accuracy and confidence in the results obtained. The analysis employed a 3D mesh method, enabling an accurate representation of the stresses and deformations observed within the hinges and PCBs.

Fasteners: Modeled as beam elements within SpaceClaim, with a cross sectional diameter equal to their respective sizes. They are remotely attached to the concentric surfaces using fixed joints.

Boundary Conditions: Boundary conditions are developed to accurately represent the launch environment for the solar arrays in their stowed configuration, and to transfer the loads from the representative points. The supports are also shown in figure 3.39.

1. Fixed Support 1: Applied to the tapped holes of the brackets mounted to the PocketQube.
2. Compression Only Support 1: Provides a displacement constraint in -y restricting movement of the bottom bracket surface into the PocketQube wall.
3. Compression Only Support 2: Provides a displacement constraint in +z for the SMT spacers, preventing their movement into the PQ wall.
4. Fixed Support 2: Applied to the tie-down cable, with a frictionless contact to the outer panels to prevent movement in -z.

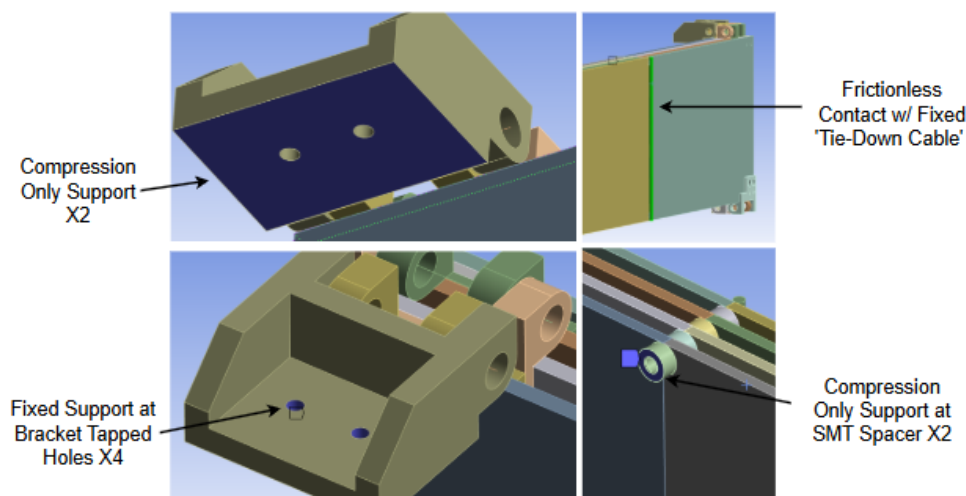


Figure 3.39: Boundary Conditions for Structural Analysis

Mesh: An adaptive meshing approach is used within Ansys mechanical with a high resolution. This method automatically refines the mesh in regions of higher geometric complexity (hinge, spacers), ensuring accurate capture of stress concentrations while avoiding unnecessary element growth. The final mesh comprised of 574,129 nodes and 241,220 elements. Hinge bodies consisted of elements ranging from 0.1 mm (near tapped holes) - 0.5 mm. Mesh sizing was described for the PCBs, fixing element size to 2.0 mm.

Modal Analysis

The modal analysis was conducted for up to 50 modes to ensure the inclusion of an effective number of modes that contribute significantly to the cumulative effective mass relative to the total mass across all six degrees of freedom. Additionally, the analysis accounts for modes up to the frequencies experiencing PSD accelerations. Modal results for modes representing the highest mass fractions are provided in table 3.29, capturing the most significant dynamic variations in the structure. Figure 3.40, 3.41, 3.42, 3.43,

3.44 and 3.45 show images of these mode shapes. The structure’s fundamental natural frequency was determined to be 192.6 Hz, demonstrating its high rigidity and reflecting a stiff overall design.

Mode	Frequency (Hz)	Type
1	192.90	Global Torsion
2	206.01	Global Bending
9	479.16	Localized Bending
11	631.37	Localized Torsion
12	768.37	Global Bending
21	1020.2	Localized Torsion/Bending

Table 3.29: Modal analysis results for final array assembly

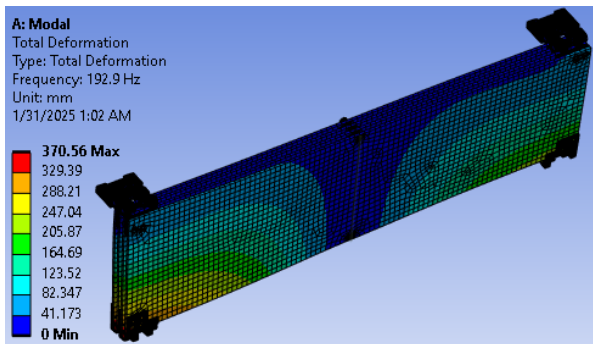


Figure 3.40: Final Array Mode 1

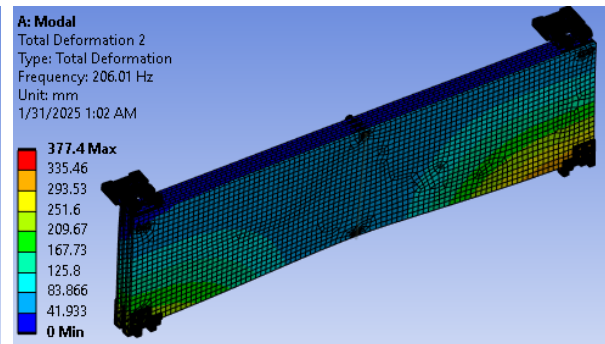


Figure 3.41: Final Array Mode 2

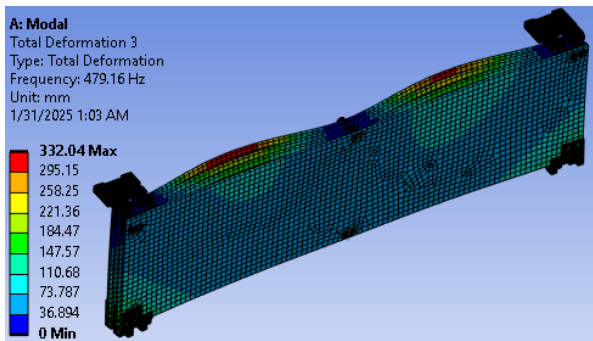


Figure 3.42: Final Array Mode 9

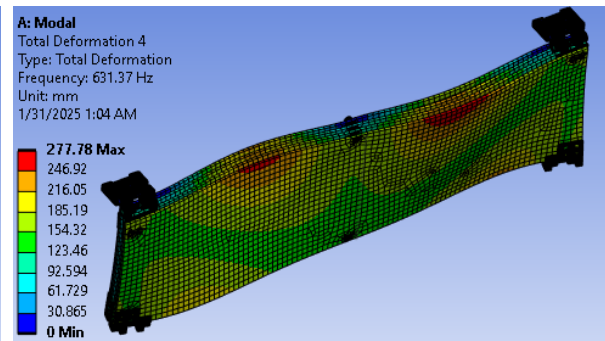


Figure 3.43: Final Array Mode 11

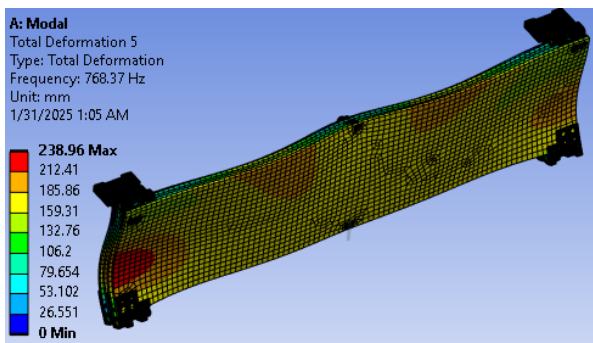


Figure 3.44: Final Array Mode 12

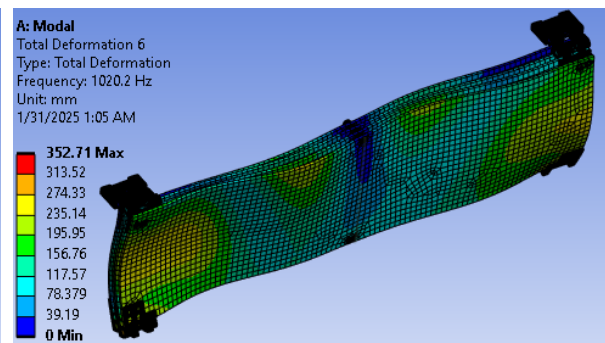


Figure 3.45: Final Array Mode 21

Random Vibration

Due to the structure’s high fundamental natural frequency, sine vibration inputs, albeit still resulting in stresses, will not resonate the structure. This makes the random vibration environment the primary driver to looking at stress and displacement responses in launch conditions. Random vibration analysis was performed in ANSYS using the built-in random vibration module. The input consisted of PSD acceleration values in g, derived from GEVS qualification levels presented in 2.27, applied in all principal axes (X, Y, and Z). The boundary conditions were defined to reflect the actual support constraints, ensuring realistic simulation of the random vibration environment.

As observed in figures 3.46, 3.47 and 3.48, the deformations are largely experienced in and out of plane of the solar panels ($\pm Z$) and are negligible in X or Y. A maximum deformation of 0.779 mm is observed for the bottom parts of the array assembly, closest to the base-plate of the PocketQube. The results suggest that while the PCB won’t collide with the inner walls of the PocketQube deployer, the hinge has a high probability of doing so since it is closer, and may need additional tie-down cables along the length of the panel to reduce the deformations. Additionally, to help reduce the deformations observed under random vibration, viscoelastic stiffeners can be used on the PCBs. Viscoelastic materials’ inherent damping properties absorb and dissipate vibrational energy, lowering resonance peaks and minimizing overall displacement.

Additionally, the maximum stresses were observed in the bracket assembly, close to the tapped holes and the root of the hinge as visualized in figure 3.49. A maximum stress of 177.85 MPa was observed, proving great structural integrity of the hinge during launch. Using the material properties, the MOS is 0.983. Negligible stresses are observed in the PCBs.

Maximum Stress (MPa)	Factor of Safety	Ultimate Tensile Strength (MPa)	Margin of Safety
177.85	1.4	493.8	0.983

Table 3.30: MOS Hinge Impact Analysis

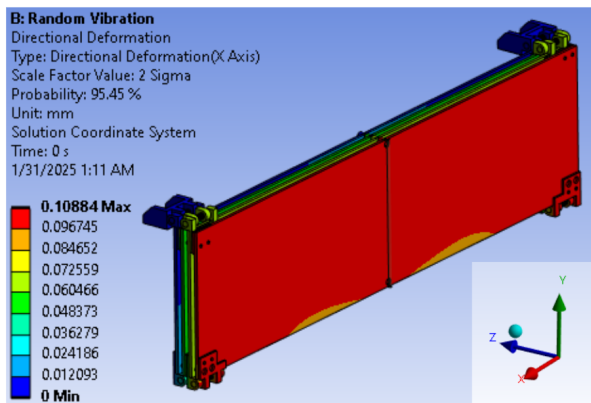


Figure 3.46: Random Vibration Deformation x-axis 2σ

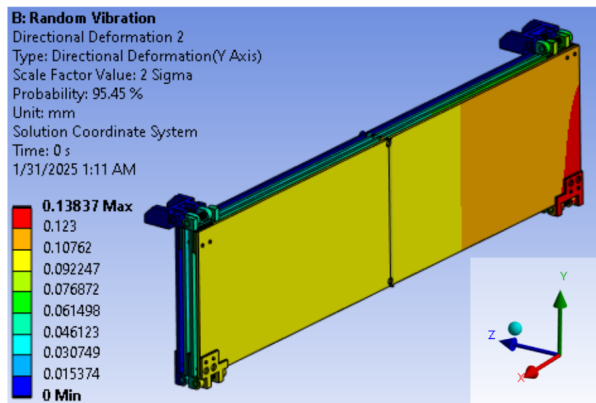


Figure 3.47: Random Vibration Deformation y-axis 2σ

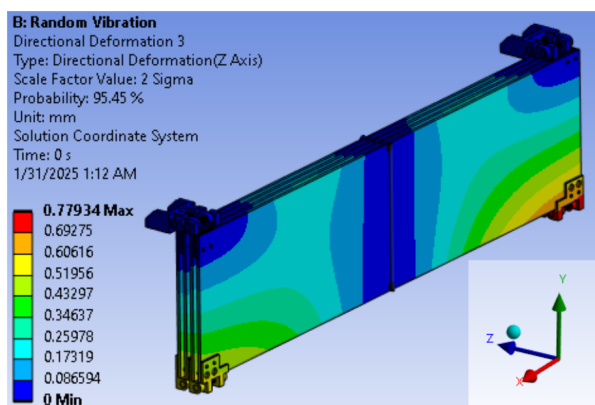


Figure 3.48: Random Vibration Deformation z-axis 2σ

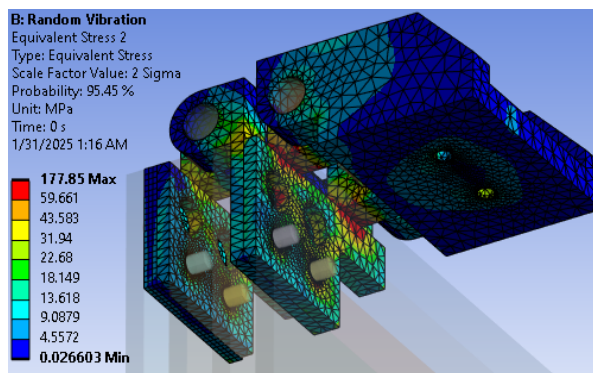


Figure 3.49: Random Vibration Equivalent Stresses 2σ

3.6.2. Failure Modes and Mitigation Strategies

This subsection examines common mechanical failure modes, including fastener detachment, hinge deadlocking, pin fracture, and insufficient preload in tie-down cables. Each failure scenario is analyzed in terms of its root cause, potential impact on the system, and mitigation strategies. Proven solutions such as advanced coatings (e.g., Keronite, hard anodizing), solid and liquid lubricants (e.g., MoS₂, PTFEs), precision assembly processes, and space-qualified adhesives (e.g., Loctite 242/271) are discussed. Implementing these countermeasures enhances performance and reliability of deployable arrays in the extreme space environments. The potential hazards are obtained from studies on reliability and failure assessments of heritage deployable mechanisms [60] [80]. Table 3.32 summarizes the faults and mitigation strategies. Severity ratings are as follows:

Level	Final effect	Explanation
I	Catastrophic	Cause the loss of satellites
II	Critical	Cause the satellite system damaged, or cause the missions failed
III	Marginal	Cause the satellite missions degraded or delayed

Table 3.31: Failure Classification Levels [60]

Part	Fault	Cause	Effect to Upper Mechanism	Final Effect	Severity	Mitigation
Burn Resistor	Cutting Failure	Insufficient current/voltage, Insufficient stroke from tie-down cable	Panel Deployment Failure	Limited PQ power generation	2	-Multiple burn-wire assemblies -Meticulous assembly process - Repeated breadboard testing.
Hinge	Fastener Failure	M1 screw breaks or detaches due to deployment impact	Hinge disassembly	Solar array detachment, hazardous debris creation	1	-EP53TC, Loctite 242/271 epoxy threadlockers (Used previously by NASA, low out-gassing) [81].

(Continued on next page)

(Continued from previous page)

Part	Fault	Cause	Effect to Upper Mechanism	Final Effect	Severity	Mitigation
	Pin Fracture/ Failure	Vibration due to separation of hinge bodies	Hinge disassembly/bending	Solar array detachment, peak power reduction, hazardous debris creation	1	-Solid/Liquid Lubrication to prevent frictional wear, MoS2, PFPEs, PAOs [82].
	Deadlocking/ Cold Welding	Thermal expansion or debris jamming	Panel deployment failure	Limited PQ power generation	2	- Hard Anodizing - Keronite (PEO) Coating (provides long-term durability, wear resistance, and cold welding prevention [83] -Powdered graphene [42], other lubricants.
Torsion Spring	Insufficient Drive Torque	Friction forces	Panel deployment failure	Limited PQ power generation	2	-Powdered graphene, other lubricants.
Tie-Down	Insufficient Preload	Insufficient tension during assembly	Excessive panel vibrations, hitting deployer wall	Solar panel failure/break, PQ deployment failure, debris during deployment	1	-Meticulous assembly process, surgeon's notes. -Observation after multiple sweep tests.
PCB	Warping/ Cracking	Extreme thermal cycling	Bending/misalignment of deployed array, solar cell efficiency reduction	Reduced power generation	3	-Orbital thermal simulation and thermal coatings.

Table 3.32: Failure Modes and Mitigation Methods

Mass and Cost Budgets

This section will delve into two important budgets associated with the design, mass and cost. Calculating the final mass of the assemblies will allow the investigation of the Specific Power (W/kg) of the solar arrays as this is an important metric to allow comparison with industry solutions. It will also help understand how much mass is available for the payload, and other sub-systems. The mass budget is provided in table 3.33. The cost is also an important metric to evaluate to make sure that the development of the PocketQube stays within budget. For non COTS parts, the costs are estimated from external manufacturers like ProtoLabs and PCBWay. This is provided in table 3.34. The cost estimates presented herein include only manufacturing and purchasing expenses. Labor (man-hours) and procurement costs are excluded from this budget.

Quantity	Parts	Material	Mass (g)
8	PCB	Isola 370HR	14.86
14	Hinge Male	7075 T-6 Al	0.225
14	Hinge Female	7075 T-6 Al	0.226
2	Bracket Male	7075 T-6 Al	0.956
2	Bracket Female	7075 T-6 Al	0.996
4	Dummy Hinge	7075 T-6 Al	0.102
16	Shoulder Bolt	304 Stainless	0.385
16	Lock Nut	304 Stainless w/ Nylon	0.0489
16	Torsion Spring	304 Stainless	0.15
72	M1 Screws	304 Stainless	0.0214
8	M1.2 Screws	304 Stainless	0.0412
18	Azur 3G30A	GaNP/GaAs/Ge	3.561
		Total Mass (g)	204.8

Table 3.33: Mass Budget

With a total mass of 204.8g and a peak power generation of 19.7 W as estimated in 4.1, the specific power calculated for these deployable arrays is **96.2 W/kg**. This is comparable to Blue Canyon Technologies' quadruple deployed 3U rigid arrays (108 W/kg) and Ecuadorian Space Agency's DSA/1A 1U rigid arrays (107 W/kg) as shown in NASA's Power State of the Art 2021 report [17].

Part	Supplier	Quantity Required	Cost Per Part (€)	Cost at Quantity (€)	Total Cost (€)
PCB	EuroCircuits	8	160.62	39.2	313.6
Hinge Male	PCBWay (Est.)	14	37.35	20.1	281.4
Hinge Female	PCBWay (Est.)	14	37.35	20.1	281.4
Bracket Male	PCBWay (Est.)	2	37.36	33.65	67.3
Bracket Female	PCBWay (Est.)	2	37.36	33.65	67.3
Dummy Hinge	PCBWay (Est.)	4	37.59	28.96	115.84
M2.0 Shoulder Bolt	McMaster-Carr	16	7.4	6.3	100.8
M2.0 Lock Nut	ACCU	16	6.6	4.45	71.2
Torsion Spring - LTR012A 05 SS	Lee Springs	16	8.06	8.06	128.96
M1.0 Cheese Head Screw	ACCU	64	1.34	0.57	36.48
M1.2 Cheese Head Screw	ACCU	8	1.38	0.76	6.08
PEM Threaded Insert MSIA-M1-100	ACCU	64	0.19	0.148	9.472
Total Cost					1479.83

Table 3.34: Cost Breakdown of Components

A complete list of the COTS parts within the design are provided in the appendix section A.9. The total cost of the structures (excluding cell arrays) amounts to 1479.83 Euro.

4

Evaluating Deployment Configurations and Their Impact on a 3P PocketQube Mission

Various configurations of deployable arrays on PocketQubes have been launched, with the three most common ones discussed in the literature review in table 2.3. The 'configuration' purely refers to the locations at which the solar panels are attached to the PocketQube body. Unlike larger satellites, which can adjust their configurations throughout the mission using deployable appendages, small satellites are constrained by their limited size and power. In particular, PocketQubes lack the capability to orient solar panels and may rely solely on passive stabilization. Therefore, selecting the appropriate configuration requires careful consideration of the mission's primary objectives, requirements, and functional constraints. This chapter explores the effects of these configurations on power generation and mission duration specifically, offering a detailed analysis to guide researchers and designers in choosing the most suitable option for their deployable arrays. The configurations examined are illustrated in Figure 4.1.

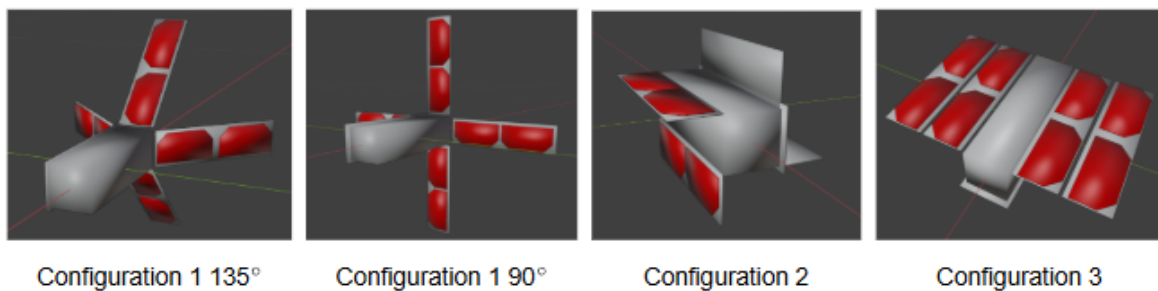


Figure 4.1: Panel Deployment Configurations

These four configurations were specifically selected due to their high prevalence in small satellite missions. Among PocketQubes, these represent the only configurations implemented in past or planned missions, and for CubeSats, a significant proportion follow these configurations.

4.1. Power Generation

Power generation is a key factor when selecting the right configuration for a small satellite, as it significantly affects the instrumentation and communication capabilities. For satellites like Unicorn 2 that feature active Attitude Control System (ACS) and pointing, configurations with singular large surface areas are generally more effective. On the other hand, satellites with passive ACS, which primarily support de-tumbling and limit rotation along specific axes, benefit from configurations with distributed power surfaces. This section analyzes the chosen configuration's power generation capabilities and how they vary across different orbits and throughout the year. For this section, the spacecraft will be modeled as a velocity aligned, spinning satellite, representing the passive aerodynamic

stabilization commonly employed by small satellites below 500 km altitude [84]. The analysis will also be focused on SSO orbits, as these are commonly employed by small satellites due to multiple reasons:

- **Consistent Lighting Conditions:** Satellites pass over the same area at the same local solar time, enabling great monitoring and remote sensing applications.
- **Global Coverage:** Over a solar day, /glsso orbits allow satellites to image a majority of the Earth, making it perfect for weather monitoring as well.

SSO orbits are also available for choosing from ride-share missions, such as the ones provided by the SpaceX transporter program [85]. The only launches available to book are for SSO orbits between 500-600 km. There are multiple goals of this section. Firstly, to support the analysis, a Python tool will be developed to simulate the spacecraft's movement in orbit and obtain a power generation profile. This tool will aid in preliminary power analysis for small satellites, where the CAD model and attitude conditions are available. The model will be used to evaluate power generation in common SSO orbits and to examine how varying β angles affect the power generation profile throughout the orbit. The model's accuracy will be validated by comparing its results to AGI STK simulations in peak conditions (noon-midnight and dusk-dawn orbits), using identical orbital parameters and attitude settings. If successful, this Python model can provide an accessible, cost-effective alternative to expensive commercial software, enabling similar analyses with lower resource requirements. Steps for developing and utilizing the model will also be outlined.

Following this, STK will be used to understand how the seasonal variations in the orbit affect the power generation onboard PocketQubes, and consequently whether these variations are different for the different configurations.

4.1.1. Preliminary Power Generation Model

As mentioned previously, a simplified power generation model was developed in python, found in Appendix A.4.1, to calculate the power generation on a tumbling satellite in orbit. The model behind the code is described in this subsection. In order to accurately model the shadows inflicted by the inactive surfaces of the spacecraft on the solar cells, ray tracing was implemented in python. However, the process of identifying the 3d mesh within python and then using the ray tracing library involved numerous steps, also outlined in this section. Primarily, this included the implementation of an incoming solar vector and two rotation matrices applied to the spacecraft, which starts at the center of it's eclipse phase in the orbit. One can visualize the model space as shown in figure 4.2.

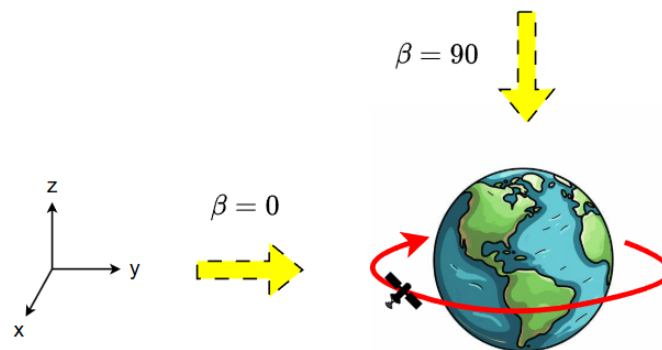


Figure 4.2: Python Model Space

Firstly, determining the eclipse duration is crucial for calculating the power generation on a satellite because it directly impacts the time the satellite spends in Earth's shadow, where it cannot receive sunlight to generate power using solar panels. In order to accurately develop the python model, this is explored in the following section. This also contributes directly to the battery sizing as well, and the discharge cycles.

Determining Eclipse Duration

Maximum eclipse time can be calculated using the following equations [86]:

$$\alpha = \sin^{-1} \left(\frac{R_0}{R_0 + h} \right) \quad (4.1)$$

$$\frac{T_e}{p} = \frac{2\alpha}{360} \quad (4.2)$$

$$T_{e\max} = \frac{p}{\pi} \sin^{-1} \left(\frac{R_0}{R_0 + h} \right) \quad (4.3)$$

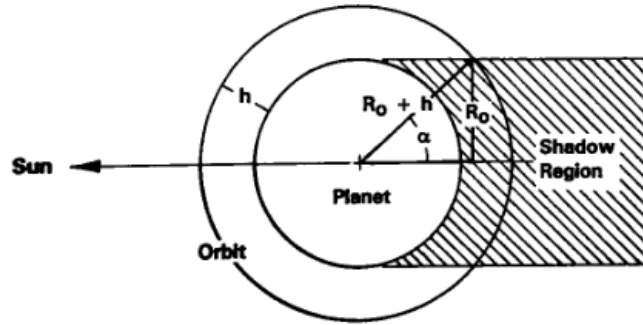


Figure 4.3: Maximum Eclipse Diagram [86]

Where h is the orbital altitude, α is the shadow region half angle, and $T_{e\max}$ is the maximum eclipse time. However, the beta angle can be varied to evaluate the impact of different orbits. For any satellite in a highly inclined polar, SSO orbit, β angle can be between -90° and 90° . Furthermore, it will vary continuously throughout the year due to the orbital perturbation and seasonal variation of solar declination and the right ascension of the sun. This solar beta angle is shown in 4.4 and can be calculated as following:

$$\beta = \sin^{-1} \left[\cos(\Gamma) \sin(\Omega) \sin(i) - \sin(\Gamma) \cos(\epsilon) \cos(\Omega) \sin(i) + \sin(\Gamma) \sin(\epsilon) \cos(i) \right] \quad (4.4)$$

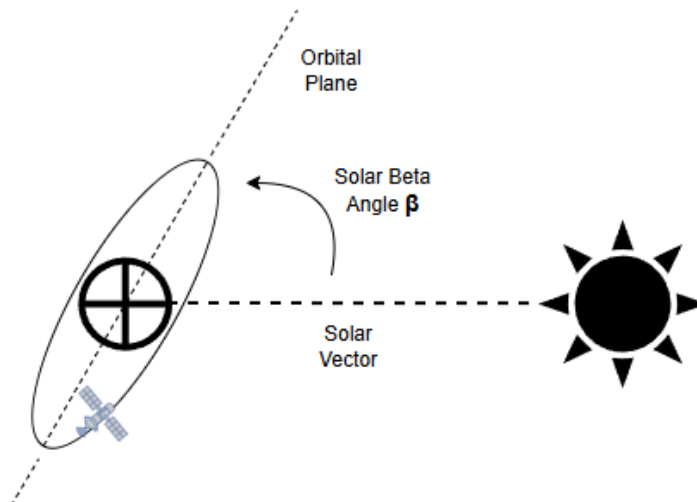


Figure 4.4: Solar Beta Angle

The eclipse time needs to be calculated based on the beta angle of the satellite's orbit. This calculation is facilitated by [87]. The fraction of the orbital time in eclipse, f_e , is given by:

$$f_e = \begin{cases} \frac{1}{180^\circ} \cos^{-1} \left(\frac{\sqrt{h^2 + 2R_e h}}{(R_e + h) \cos \beta} \right) & \text{if } |\beta| < \beta^* \\ 0 & \text{if } |\beta| \geq \beta^* \end{cases} \quad (4.5)$$

The total time period T of the orbit is given by:

$$T = 2\pi \sqrt{\frac{(R_e + h)^3}{GM}} \quad (4.6)$$

The eclipse time T_e is then calculated as:

$$T_e = T \cdot f_e \quad (4.7)$$

Where β^* , the angle at which the eclipse begins, is given by:

$$\beta^* = \sin^{-1} \left(\frac{R_e}{R_e + h} \right) \quad (4.8)$$

Model Generation Steps

In the model space described in figure 4.2, One rotation matrix represents the tumbling around the long/stable axis of the satellite. This is set to $10^\circ/s$ as that was the observed tumbling rate from Delfi-PQ. The other represents the rotation of this long axis throughout the orbit and that is set to 1 rotation per total orbit duration or $360^\circ/\text{Total Orbit Duration}$. These can be visualized in Figure 4.5. Certain fixed parameters were selected to ensure that the comparison of power generation focused solely on the impact of the configuration. These parameters are detailed in Table 4.6.

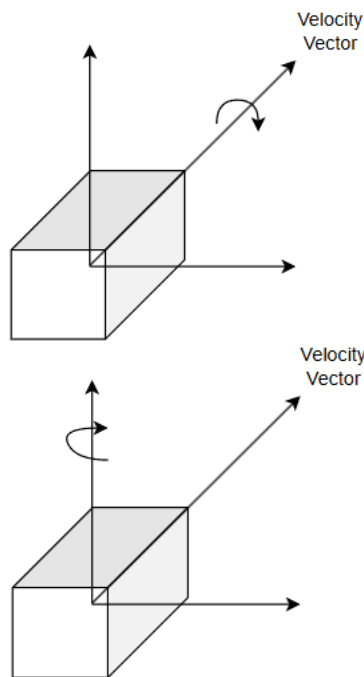


Figure 4.5: Visualising Rotation Matrices

Parameter	Value	Unit
Solar Cell Area	0.003018	m^2
No. of Cells Per Panel	2	
Rate of Spin	10	$^\circ/s$
Altitude	500	km
Solar Cell Efficiency	0.3	
Solar Flux	1361	W/m^2

Figure 4.6: Power Generation Parameters

- CAD model developed or loaded in Blender:** Initially, a CAD model of the satellite needs to be developed. This can be developed within an external software and then loaded onto Blender, or directly within Blender. The recommended approach is to utilize STL files for the export and import. Key consideration here is to model the solar cells as separate geometries/domains. The spin-stabilized axis of the spacecraft then needs to be aligned with the z-axis within Blender.
- Identification of Active and Inactive Surfaces in Blender:** Within blender, the active surfaces (solar cells) and inactive surfaces (satellite structure) are clumped into 'Vertex Groups'. These vertex groups allow for classification of the different geometries. Then, the vertex groups are assigned a color property (red [254,0,0,255] for active and blue [0,0,254,255] for inactive).
- Export from Blender and Import in Python:** The modified 3d model is exported from Blender in the Polygon File Format (PLY), ensuring that vertex color data is preserved. Then, the model is loaded within Python using the trimesh library `trimesh.load()`.
- Identifying Active and Inactive Faces within Python:** Active regions of the model were identified based on vertex colors. A specific color (e.g., [254, 0, 0, 255]) was used to isolate active vertices and faces through the `get_active_mesh()` function.
- Ray Tracing for Illumination:** The `RayMeshIntersector` from `trimesh.ray.ray_triangle` was applied to perform ray tracing. This determined the illuminated faces by checking intersections with a given solar vector.

6. **Orbital Period, Eclipse and Incoming Solar Irradiance Vector** User defined input parameters for the simulation are: `Orbital_altitude`, `beta_angle`, `panel_efficiency`. The equations defined in 4.1.1 are then used to calculate the total orbit time and eclipse time. Furthermore, the incoming solar vector defined within the model is modified based on the β angle. This modification can also be visualized in figure 4.2
7. **Power Simulation:** Firstly, the spacecraft starts at the middle of its eclipse phase, where power generated is 0. At every consequent time step, the rotation matrices are applied to the mesh based on the time elapsed and the rotational rates. The incident angle is then calculated between the specified sun vector \mathbf{S} in the previous step and the solar panel discrete surfaces' normal vectors after applying the time-dependent rotations. The mathematical setup for the calculation is described below:

Let \mathbf{S} represent the Sun vector (assumed constant in the inertial frame), and let \mathbf{P} represent the initial normal vector of the solar panel. The solar panel is rotated using two time-dependent rotation matrices.

The rotations about the x -axis and z -axis are represented as follows:

$$\mathbf{A}(\theta_x) = \begin{bmatrix} 1 & 0 & 0 \\ 0 & \cos \theta_x & -\sin \theta_x \\ 0 & \sin \theta_x & \cos \theta_x \end{bmatrix}, \quad \mathbf{B}(\theta_z) = \begin{bmatrix} \cos \theta_z & \sin \theta_z & 0 \\ -\sin \theta_z & \cos \theta_z & 0 \\ 0 & 0 & 1 \end{bmatrix}.$$

Here, $\theta_x = \omega_x t$ with $\omega_x = 10^\circ/s = \frac{\pi}{18}$ rad/s representing the rotation rate about the x -axis, and $\theta_z = \omega_z t$ with $\omega_z = \frac{360^\circ}{T_{\text{orbit}}} = \frac{2\pi}{T_{\text{orbit}}}$ rad/s representing the rotation rate about the z -axis, where T_{orbit} is the total orbital period.

After applying these rotations, the solar panel surface's normal vector becomes:

$$\mathbf{P}_{\text{rot}}(t) = \mathbf{B}(\theta_z)\mathbf{A}(\theta_x)\mathbf{P}.$$

The incident angle $\phi(t)$ between the Sun vector \mathbf{S} and the rotated surface's normal vector $\mathbf{P}_{\text{rot}}(t)$ is calculated as:

$$\cos \phi(t) = \frac{\mathbf{S} \cdot \mathbf{P}_{\text{rot}}(t)}{\|\mathbf{S}\| \|\mathbf{P}_{\text{rot}}(t)\|}.$$

Substituting the expression for $\mathbf{P}_{\text{rot}}(t)$, the equation becomes:

$$\cos \phi(t) = \frac{\mathbf{S} \cdot (\mathbf{B}(\theta_z)\mathbf{A}(\theta_x)\mathbf{P})}{\|\mathbf{S}\| \|\mathbf{B}(\theta_z)\mathbf{A}(\theta_x)\mathbf{P}\|}.$$

In this formulation:

- \mathbf{S} is the Sun vector.
 - \mathbf{P} is the initial panel surface normal vector.
 - $\theta_x = \omega_x t$ is the time-dependent angle for rotation about the x -axis, where $\omega_x = \frac{\pi}{18}$ rad/s.
 - $\theta_z = \omega_z t$ is the time-dependent angle for rotation about the z -axis, where $\omega_z = \frac{2\pi}{T_{\text{orbit}}}$ rad/s.
8. **Results** For the results, the simulation outputs the average and peak power generated throughout the orbit. Additionally, a graph is generated to show how this power generation varies over time. The results are also exported into an excel file for further data analysis.

4.1.2. Python Model Results

The results for the Python Model will be presented in this section, evaluating the difference in power generation of configurations in varying β angles to see which configurations offer the best power at different lighting conditions in orbit. Additionally, the model's accuracy will be evaluated by STK simulations featuring similar peak solar angles.

Dusk-Dawn & Noon-Midnight Orbits

The input parameters for this study are the solar panel efficiency (0.3) and the orbital altitude (500 km). The average power generated in orbit has been calculated and is provided in Table 4.1. This data contains both extremes of the β angle in dusk-dawn (no eclipse) and noon-midnight (max eclipse) orbital scenarios. The plots for individual configurations can be found in the appendix A.4.2 which show the effect of tumbling on the power generated, but Figure 4.7 shows the power generated throughout the orbit averaged over 36 second time steps for all configurations and does not show the impact of the satellite tumbling. 36 second time steps allow to account for a full rotation around its longitudinal axis with the specified tumbling rate and time-step. The averaged data is plotted to avoid clustering on the plot and clear distinction between the configurations.

ID	Power Generation Case	Average Power Generated per Orbit (W)			
		Config 1_135	Config 1_90	Config 2	Config 3
1	Non-Eclipsed, Tumbling	2.33	0.14	3.00	3.20
2	Non-Eclipsed, Sun-Pointing	7.06	9.86	3.56	9.86
3	Max Eclipse, Tumbling	1.74	2.05	1.08	1.13
4	Max Eclipse, Sun-Pointing	4.39	6.13	2.21	6.13

Table 4.1: Average Power Generated in Orbit

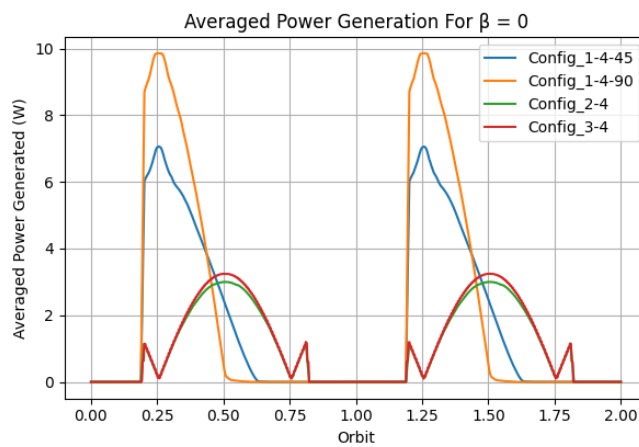


Figure 4.7: Average Power Generated for $\beta = 0$

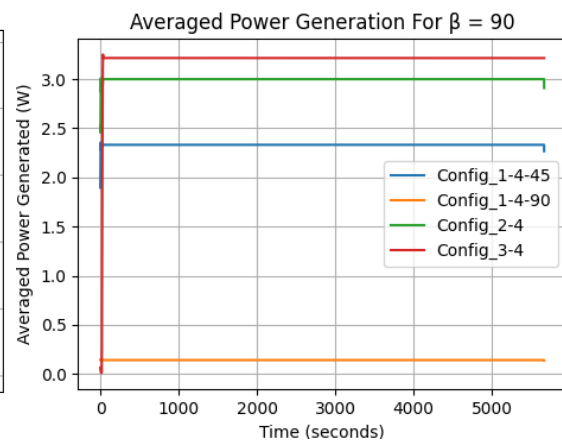


Figure 4.8: Average Power Generated for $\beta = 90$

As can be seen in figure 4.7 and figure 4.8, configurations 1-135 and 1-90 feature much higher average power generation in the maximum eclipse scenario throughout the orbit than Configurations 2 and 3. This is largely due to the fraction of time spent against the solar irradiance while tumbling. However, for the same configurations, the results are reversed when the β angle is set to 90, representing a dusk-dawn orbit. The panels on configuration 1-90, are always perpendicular to the incoming solar irradiance, resulting in near zero power generation. Configurations 2 and 3 feature the highest average power generated in this orbit. While it is beneficial to study the peak orbital scenarios, the model can be further developed to provide an estimate of how much this average power varies with changing beta angles.

Beta Angle Variance

The python model can be adjusted to account for the change in beta angle. This is done by implementing a rotation of the solar flux around the x-axis as seen in figure 4.2. This will also directly impact the eclipse times as seen earlier. The average power generated for all configurations was plotted against incremental changes in β angle of 5° and this is visualized in figure 4.9. This is an important study, as small satellites are usually secondary payloads on rideshare missions like the transporter missions, eliminating the possibility of picking precise orbits, and being subject to large variances in expected lighting conditions.

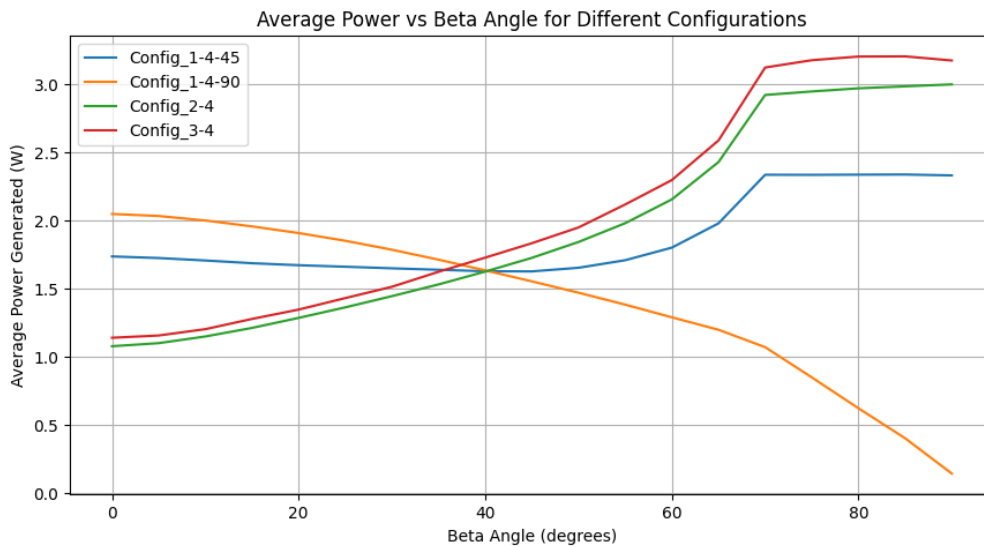


Figure 4.9: Average Power Generated While Varying β angle

For changes in the configuration, the average power generation is immensely impacted.

Configuration 1: For different deployment angles, power generation is greatly different. When deployed at 90 degrees, the solar panels are aligned perpendicular to the spacecraft's Z-axis. While this configuration may be effective in specific orientations, it becomes highly dependent on the beta angle, and for cases where $\beta = 90$ degrees, the Sun's rays are nearly parallel to the orbital plane, meaning that the arrays receive little to no direct sunlight, leading to negligible power generation during certain parts of the orbit. A 135-degree deployment angle improves average solar illumination compared to 90 degrees, as it increases exposure to a wider range of Sun incidence angles.

Configuration 2 and 3: These show a steady increase of power generation with increase in β angle, mainly due to the decrease in eclipse times. While the angle at which the solar irradiation impacts the spacecraft's orbit is changing, configurations 2 and 3 spend the same fraction of time generating power and the incident angle for this fraction is still only impacted by the tumbling, and not by the change in beta angle. Configuration 2 is expected to generate less power than 3 in all β angles due to the impact of shadows inflicted by the panels.

Another noticeable point is that around a β angle of 40° , all configurations seem to generate similar amount of power in orbit, meaning that either one can be chosen if this is the intended orbit for the mission. If there is a lack of knowledge regarding the orbit insertion, and to make the mission suitable for multiple orbits, configuration 1 with a 135° deployment angle should prove to be the best option, as the average power generated stays roughly around 2 W for 4 panels. Around $\beta = 67^\circ$, the power generation becomes fairly constant for configurations 1-135, 2 and 3, as this is the threshold for reaching zero eclipse times at the specified altitude of 500km.

4.1.3. Verification with Ansys STK

AGI STK (Systems Tool Kit) is a software platform developed by Analytical Graphics, Inc. that is widely used for modeling, simulating, and analyzing complex systems in aerospace, defense, and other industries.

In this case, STK can be used get an accurate picture of power generation and verify the results obtained with the python model. To evaluate its accuracy. for the verification case, $\beta = 0^\circ$ was chosen, representing alignment of the orbital plane with the Sun-Earth line. In STK, this was achieved by selecting the vernal equinox at an epoch date of March 20 at 03:06, with the Ω set to 0 degrees to align the orbit with the Sun.

Parameter	Value
Epoch Date	20.03.2024
h	500 km
e	0
i	97.4°
Ω	0°
ω	0°
v	0°

Figure 4.10: Orbital Parameters

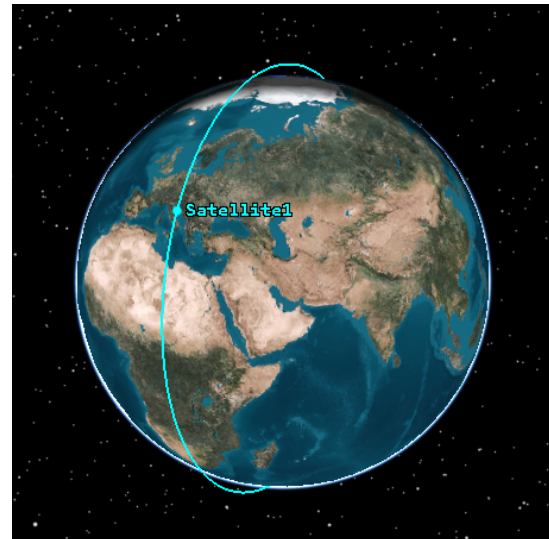


Figure 4.11: SSO Orbit Visualized in STK

In order to use and define geometry in STK, a lengthy process is needed to import the 3D geometry in the software.

1. 3D models of the PocketQubes with the different configurations are developed in SolidWorks (or other CAD software).
2. Models exported as STL files and imported into blender. Using Blender, the geometry is aligned with the correct axes and exported again into a COLLADA (dae) file format.
3. DEA file opened with NotePad++ in which the code is implemented to surfaces representing solar panels with an efficiency of 0.3 to represent the sample, Azur 3G3CA cells.

```
<extra type="attach_point">
<technique profile="AGI">
  <solar_panel group="Solar_Panels" efficiency="30.0" />
</technique>
</extra>
```

4. COLLADA file imported into STK with solar panels defined. 'Solar Panel' tool used to obtain power generation profiles.

Once the files have been imported, the orbital parameters can be added and the attitude mode can be defined. There will be two modes studied, accurately representing cases with and without dedicated active ADCS modules. One where the satellite is tumbling around its velocity vector, and one where the satellite is always sun pointing. Both these cases are shown in Figure A.13 and Figure A.13 in the appendix.

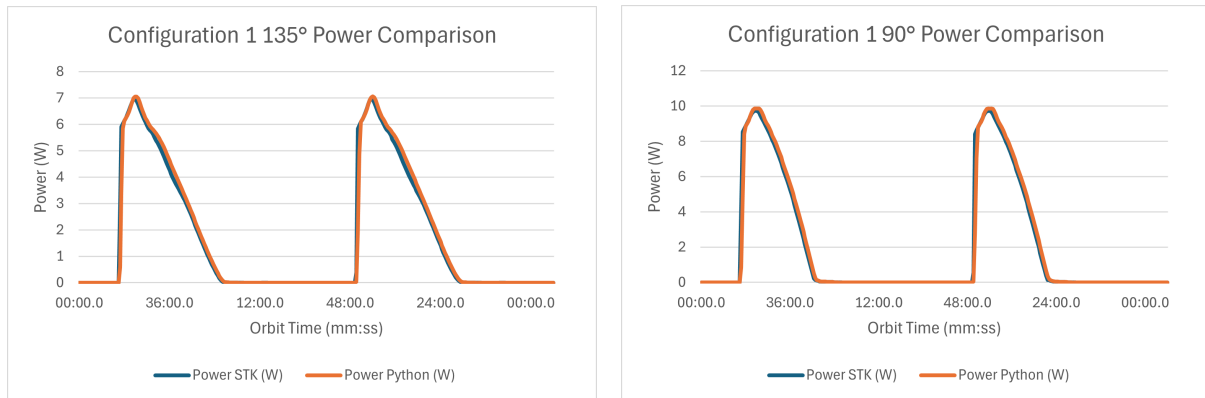
The simulation is sufficient for orbits since the verification scenario is focused on a completely spin-stabilized attitude mode, and the Beta angle for the verification case is set to 0. All 3 configurations (4 considering both angular versions of configuration 1) were simulated and the data obtained is available in appendix A.5.3.

4.1.4. Comparison of STK and Python Data

As STK was used to verify the Python model and to prove that it accurately represents the power generation in orbit for spacecraft, data from both simulations was plotted together for the different configurations and is shown in Figures 4.12a, 4.12b, 4.13a and 4.13b. The average power values and the errors are summarized in Table 4.2.

Configuration	Python Averages (W)	STK Averages (W)	Error (%)
Config 1-45	1.736	1.693	2.54
Config 1-90	2.048	2.013	1.74
Config 2	1.077	1.043	3.26
Config 3	1.139	1.107	2.89

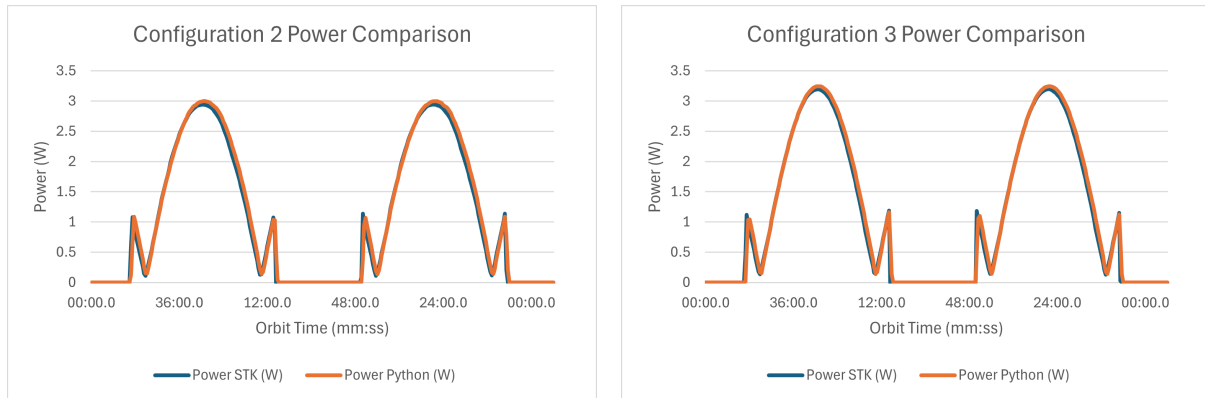
Table 4.2: Comparison of Python and STK Averages with Error



(a) Configuration 1-135 Power Verification

(b) Configuration 1-90 Power Verification

Figure 4.12: Power Verification for Configurations 1-135 and 1-90



(a) Configuration 2 Power Verification

(b) Configuration 3 Power Verification

Figure 4.13: Power Verification for Configurations 2 and 3

The power generation profiles prove to be extremely identical as the curves layered over each other are hard to distinguish. Slight differences in power generation in STK over multiple orbits are visible in 4.13a and 4.13b, where the peaks prior to entering and leaving the eclipse tend to vary and surpass the values suggested by the python model. The errors for all power generation values are also relatively minimal, proving that the python model is more than sufficient for preliminary solar array sizing in mission design. A well known resource for assessing whether this error is good enough for early phases in the design is the SMAD (Space Mission Analysis and Design), widely used amongst students in space engineering for preliminary sizing and design estimates. They note that variations in-orbit conditions can lead to a difference of 5-15% in delivered power. The error obtained between the python model and STK is small enough in comparison to this value.

4.1.5. Seasonal Variations in Power Generation

STK will be used to analyze how power generation varies seasonally in the given Dusk-Dawn and Noon-Midnight SSO orbits. As previously mentioned, SSO orbits are useful because their orbital plane precesses at the same rate as the Sun's apparent motion. This allows the satellite to pass over the same region at nearly the same solar time each day. The RAAN (Ω) precesses 360 degrees throughout the year, keeping changes in the solar beta angle relatively small and keeping relatively constant lighting conditions. However, due to the tilt of the Earth's axis (obliquity of the ecliptic), there are still seasonal changes in the solar beta angle. By simulating these variations in STK, we can understand how seasonal effects and orbital parameters influence power generated, and whether this effect is different for different configurations.

For this analysis, the starting point is the vernal equinox (March 20th, 03:06 UTCG), when the Equator aligns with Earth's orbital plane. The SSO orbit is designed using the 'Orbit Wizard' and J2 propagator to achieve the correct inclination for the chosen altitude, ensuring a daily RAAN shift of $\Omega = 0.9863^\circ$. Power generation is evaluated at 12 evenly spaced time intervals throughout the year, capturing key points such as the winter and summer solstices, as well as the autumn equinox.

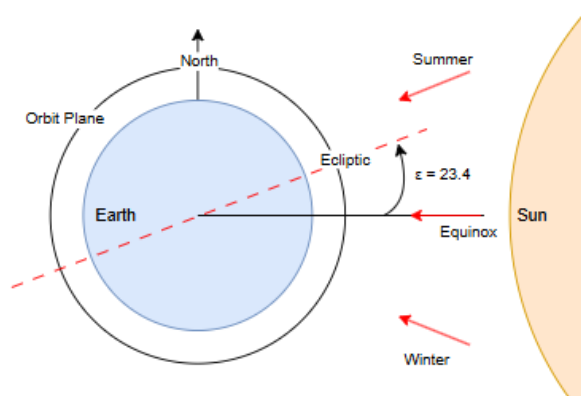


Figure 4.14: Noon-Midnight SSO

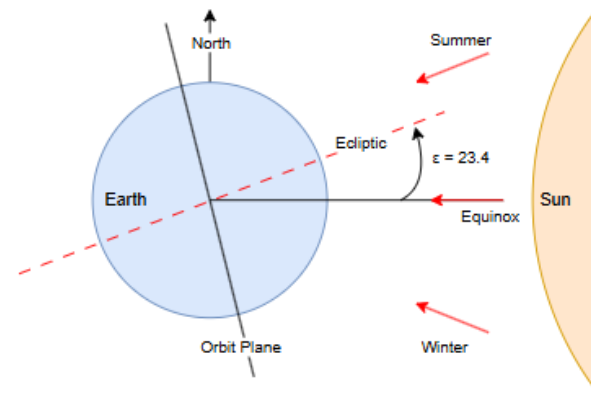


Figure 4.15: Dusk-Dawn SSO

For noon-midnight orbits, the shift in incoming solar angle due to a change in seasons can be visualized in figure 4.18. As visible, the satellite spends a maximum time in eclipse on either seasonal shift of the incoming solar vector. Due to this, the seasonal variation is expected to have minimal/negligible impact on the power generation profiles of the different configurations, and the plot obtained in figure 4.16 proves just that. The average power throughout the year have maximum variations of 5%, with configuration 1-135 showing the greatest difference.

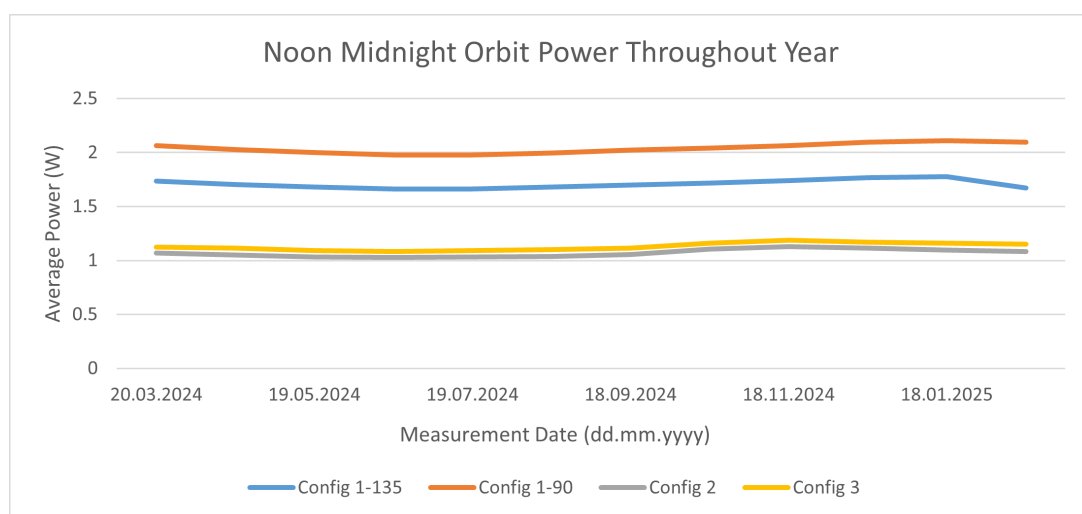


Figure 4.16: Noon-Midnight Yearly Average Power

For Dusk-dawn orbits on the other hand, change in power generation is visible in figure 4.17, possibly due to seasonal eclipses being present, and the solar β angle changing due to Earth's obliquity. These changes are quite

large, and configurations 1-135, 2 and 3 follow similar paths, with the latter two dropping nearly 30% in power around summer solstice (20 June) and having a steady increase until the maximum occurring around the vernal equinox location. Configuration 1-90 yields minimum power generation, as seen in the previous sections, but benefits from the obliquity around summer and winter solstice periods. It still proves to be an infeasible choice for power generation in this orbit.

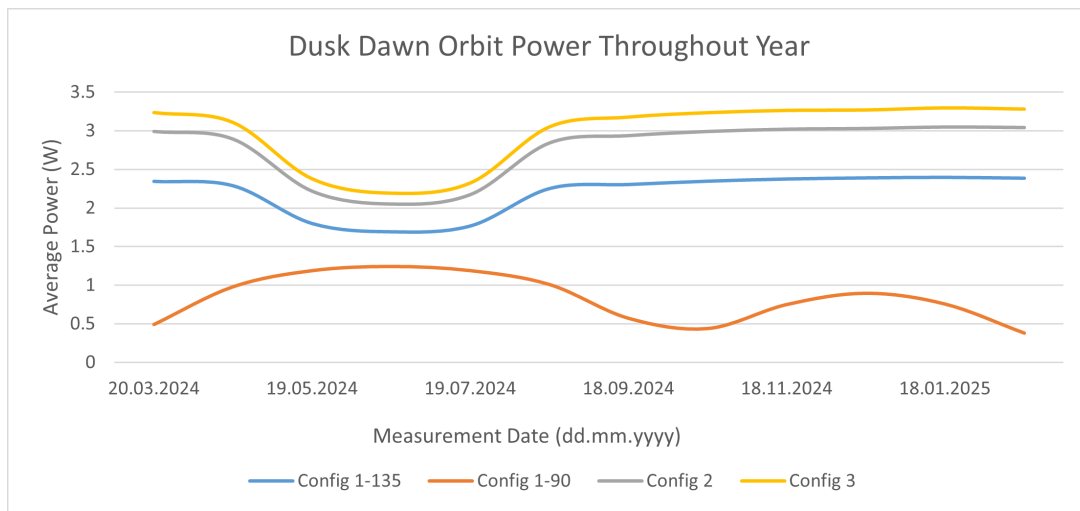


Figure 4.17: Dusk-Dawn Yearly Average Power

Impact of Orbital Decay on RAAN Evolution and Lighting Conditions

As mentioned earlier, the benefit of SSO orbits are that they provide consistent lighting conditions with minimal change in β angle due to the orbital precession matching Earth's mean motion. The change in Ω is as following:

$$\dot{\Omega} = -\frac{3}{2}J_2 \left(\frac{R_E}{a}\right)^2 \sqrt{\frac{\mu_E}{a^3}} \cos i \quad (4.9)$$

where $\dot{\Omega}$ is the RAAN precession rate (rad/s), J_2 is Earth's J_2 coefficient, R_E is Earth's mean radius (km), a is the semi-major axis of the orbit (km), μ_E is the standard gravitational parameter of Earth (km^3/s^2), and i is the inclination of the orbit (radians). The altitude and inclination are chosen specifically to provide a $\dot{\Omega}/\text{day}$ of 0.986° . The combinations of these values to support SSO orbits is provided in figure A.12, available in the appendix. While the inclination does not inherently change drastically due to the J_2 perturbation, the altitude of the orbit decreases over time due to the atmospheric drag experienced in LEO, causing a change in $\dot{\Omega}$. This means that lighting conditions can change drastically over longer missions without means of active propulsion. This effect is studied by evaluating the cumulative change in RAAN for configuration 1-90 with different drag areas and corresponding decay trajectories as computed by DRAMA in the next section.

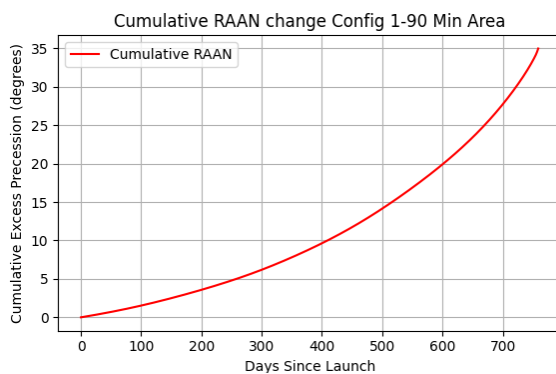


Figure 4.18: RAAN Change Config 1-90 Min Area

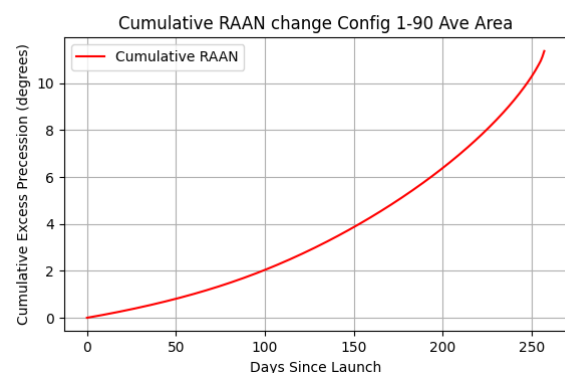


Figure 4.19: RAAN Change Config 1-90 Ave Area

As identified in the graphs above, while the change is minimal for mission durations suited for short technology demonstration missions, it could be highly impactful for longer duration missions. This was also identified as a

potential issue in Delfi-C3, as the satellite was designed for no eclipses but has experienced eclipses throughout its lifetime due to the loss of sun-synchronicity. Due to this research, and the results from section 4.2, **Configuration 1 with a 135° deployment angle** is recommended for passively tumbling satellites.

4.2. Mission Duration

In this section, the orbital life time of the different configurations will be assessed. Atmospheric drag, even at altitudes well beyond the Kármán line (100 km), plays a significant role in the orbital decay of small satellites over time. As the satellite's altitude decreases, the density increases exponentially, leading to stronger drag forces and faster altitude decay.

The orbital lifetime of satellites is regulated to protect our access to space and prevent scenarios like the 'Kessler Syndrome', a theoretical chain reaction of collisions triggered by the high density of satellites and debris in specific altitudes, LEO in this case. A guideline established by both ESA and NASA for small satellites for orbital life time in LEO was 25 years [88]. However, with the increasing number of satellites occupying this space and concurrently the increasing risk of space debris, a new guideline needed to be recommended. In fact, the Federal Communications Commission (FCC) has adopted a new rule to propose that satellites de-orbit within 5 years after completing their mission [89].

Atmospheric drag can be modeled in terms of the following equation:

$$F_d = \frac{1}{2} \rho V^2 C_d A \quad (4.10)$$

The acceleration due to drag is therefore directly affected by the area/mass ratio, which is often manipulated by engineers using sails/panels to de-orbit satellites. Due to the small scale of PocketQubes, and the limited space available for active ACS, it is necessary to evaluate how the deployed configuration of solar arrays will impact the orbital lifetime, and active strategies will be necessary to de-orbit satellites to adhere to the 5 year guideline recommended and this chapter will aim to address that.

A multitude of factors can affect the orbital life time of a small satellite and these are the following:

1. Altitude: Lower orbits experience more atmospheric drag, reducing the satellite's lifetime.
2. Satellite Mass and Size: Larger satellites with more surface area experience greater drag.
3. Solar Activity: Increases atmospheric density, causing more drag. Usually follows an 11 year solar cycle.
4. Orbital Inclination and Eccentricity: Influence the satellite's exposure to varying atmospheric densities.

The orbital lifetime could theoretically be estimated using fundamental astrodynamics equations by modeling the drag force as a retrograde thrust. However, the analysis becomes significantly more complex due to the variability in atmospheric density, which changes with decreasing altitude and fluctuates based on the phase of the solar cycle. To account for these complexities, it would be necessary to include a suitable atmospheric density model, as atmospheric drag critically depends on accurate density predictions. Therefore, in order to evaluate the orbital life time of the different configurations, ESA's Debris Risk Assessment and Mitigation Analysis (DRAMA) tool will be used. This is a comprehensive tool for the compliance analysis of a space mission with space debris mitigation standards; incorporating data from Meteoroid and Space Debris Terrestrial Environment Reference (MASTER).

Firstly, the impact of the solar cycle and solar activity will be analyzed to identify the launch dates corresponding to the maximum and minimum orbital lifetimes for a specific configuration. Subsequently, the orbital lifetimes for these peak launch dates will be evaluated for the different configurations with varying numbers of panels.

4.2.1. CROC

CROC (Cross Section of Complex Bodies) is a tool within the DRAMA module that is used to evaluate the minimum, average, and maximum cross sections for satellite bodies. Three functionalities are available within the tool:

1. User-defined aspect angle
2. User-defined aspect angle and rotation axis
3. Randomly Tumbling Satellite

To best assess the orbital life-time, minimum, maximum and average cross sections from a 'Randomly Tumbling Satellite' will all be studied. While the randomly tumbling case may overestimate the drag area in some scenarios (where the deployed panels aren't normal to the flight velocity), it is still the best estimate without delving into the aerodynamic profiles of the different configurations.

Configurations and their calculated effective cross sectional areas for our analysis are provided in Table 4.4. The solar cell and PocketQube parameters are given in Table 4.3. The panel dimensions represent the long faces of the PQ (50 mm * 178 mm) and the mass of the spacecraft is obtained from the current approximated Delfi-Twin mass.

Design Parameters	
Panel Width	44.9 mm
Panel Length	178 mm
Panel Thickness	1 mm
Panel Mass	14.7 g
PQ Mass	545 g

Table 4.3: Solar Panel Parameters

Panels	Configuration	Min (m ²)	Ave (m ²)	Max (m ²)
2	Config 1_135°	0.0090	0.0182	0.0232
	Config 1_90°	0.0085	0.0181	0.0225
	Config 2	0.0027	0.0166	0.0267
	Config 3	0.0027	0.0167	0.0264
4	Config 1_135°	0.0150	0.0252	0.0281
	Config 1_90°	0.0085	0.0249	0.0344
	Config 2	0.0028	0.0212	0.0267
	Config 3	0.0028	0.024	0.0426
6	Config 1_135°	0.0155	0.0332	0.0376
	Config 1_90°	0.0090	0.0325	0.0488
	Config 2	0.0029	0.0276	0.0426
	Config 3	0.0029	0.0316	0.0588
8	Config 1_135°	0.0185	0.0411	0.0497
	Config 1_90°	0.009	0.0404	0.0668
	Config 2	0.003	0.0336	0.0426
	Config 3	0.003	0.0395	0.075

Table 4.4: CROC Cross Section Calculations

The minimum and maximum cross sections can be visualized in figure 4.20 and 4.21 for the different configurations. The images depict the cross sections directly subjected to drag forces. They are representative of two attitude modes for the satellite. One resembles Delfi-PQ and Delfi-Twin, with the longitudinal axis velocity aligned. The other represents nadir pointing satellites, that might be equipped with earth observation payload as recommended in the AlbaPod payload user guide [90] or the fossasat shown in the image.

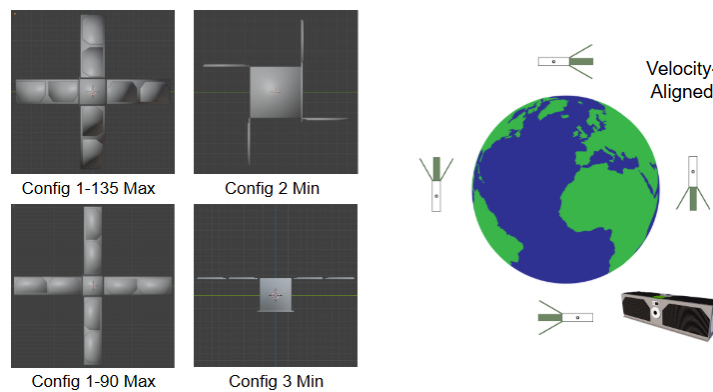


Figure 4.20: Velocity Aligned Attitude Mode Applicable Cross Sections

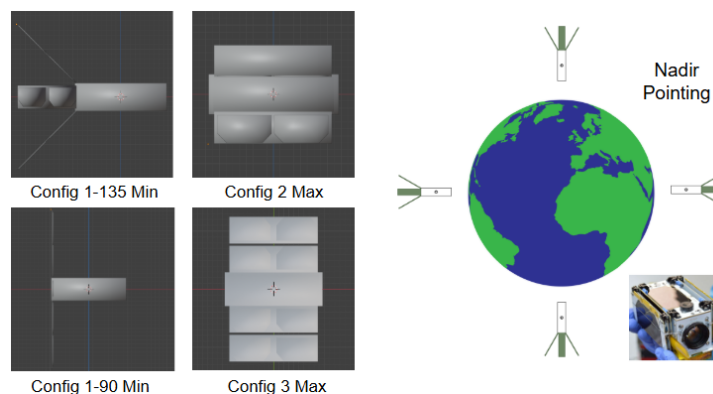


Figure 4.21: Nadir Pointing Attitude Mode Applicable Cross Sections

4.2.2. OSCAR Lifetime Evaluation

The OSCAR tool is used to understand the variance in orbital lifetime based on certain parameters. In this section, the orbital lifetime for the different configurations will be evaluated, and aspects pertaining to those lifetimes, such as the number of panels, and the launch date will also be studied.

Within the DRAMA module, Cross-Sectional Area and Mass are inputs in m^2 and kg respectively. Due to the size of PocketQubes, it is impossible to accurately assess the orbital lifetime due to the numbers of significant figures that can be inputted within the user interface. Therefore, the pyDRAMA is used for this analysis. The code for this can be found in Appendix A.3. The configuration parameters and inputs used for this analysis are provided in table 4.5.

First, the launch date corresponding to the minimum and maximum orbital lifetimes needs to be identified to conduct the analysis. These represent critical peak configurations that could jeopardize the mission by either resulting in unreasonably short mission durations or exceeding the 5-year orbital lifetime limit set by the FCC. For this purpose, a sensitivity analysis will be carried out.

Table 4.5: OSCAR: Orbital Parameters

Parameter (Symbol)	Value
Eccentricity (e)	1.0×10^{-4}
Inclination (i)	97.5°
Right Ascension of the Ascending Node (Ω)	0°
Argument of Perigee (ω)	0°
Mean Anomaly (M)	0°
Drag Coefficient (C_D)	2.2
Reflectivity Coefficient (C_R)	1.3

Sensitivity Analysis - Impact of Launch Date and Launch Altitude

The solar cycle, which lasts about 11 years, plays a significant role in affecting the atmospheric density in the thermosphere. During periods of high solar activity, known as the solar maximum, the sun emits increased levels of UV and X-ray radiation. This heats the thermosphere, causing an increase in atmospheric density at higher altitudes. Drag force is directly influenced by this atmospheric density, which in turn impacts the orbital lifetime of satellites.

Understanding the impact of the solar cycle can have a great influence on the mission design and planning for LEO satellites. That is why it is empirical to do a sensitivity analysis to see how drastically the orbital time will change. For this sensitivity analysis, the configuration 1-135° with 4 panels and a mass of 610.9 g (mass of satellite + mass of 4 panels) will be used. The orbital lifetime is evaluated annually for 12 years from the start of the most recent solar cycle which is approximated to be in December 2019. The results are plotted in Figure 4.22. Additionally, launch altitudes will also be varied to understand if there is a difference in the launch dates corresponding to the minimum and maximum orbit times.

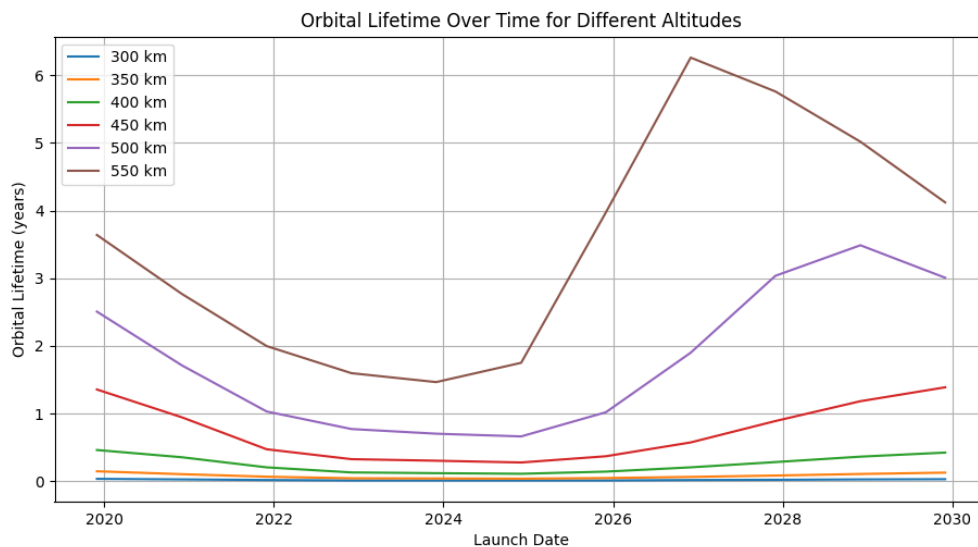


Figure 4.22: Sensitivity analysis with launch date

The differences in orbital lifetimes is drastically different for different launch dates. For example, for an altitude of 500km, the orbital lifetime is nearly 3.5 years with a launch date of Dec 2028 in comparison to 0.7 years with a launch

date of Dec 2024. This difference could be largely influential in mission design, and consequently choosing the type of deployment configuration for solar arrays. Another noticeable aspect is that the launch dates corresponding to minimum and maximum orbital lifetimes change with different launch altitudes.

Since the desired altitude for launching PocketQubes is at 500km, launch dates of Dec, 2024 and 2028 will be considered to study the orbital lifetime across different configurations and number of panels.

OSCAR Lifetimes for Different Configurations

In this section, the results of OSCAR simulations will be looked at for the different deployment configurations with different number of panels. The key evaluation here is whether any of the options exceed the 5 year orbital lifetime limit set by the FCC, and what type of mission design lifetimes are these configurations suited for. These options will need to incorporate active de orbit measures in order to meet the guidelines. The plots below contain the data obtained from the simulations, with the number of panels being represented on the x-axis, and the different curves corresponding to the minimum, average (random tumbling), and maximum cross sectional values obtained from CROC in figure 4.21 and figure 4.20. The red colored curves correspond to a launch date of Dec, 2024, while the blue curves correspond to the launch date of Dec, 2028. This is also pointed out in figure 4.23.



Figure 4.23: Orbital Lifetime Chart Legend

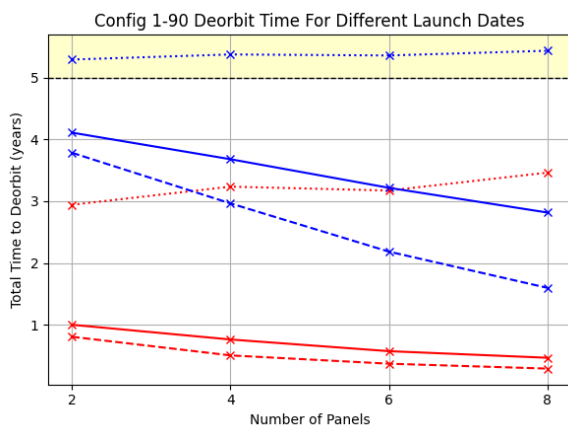


Figure 4.24: Configuration 1-90 OSCAR Results

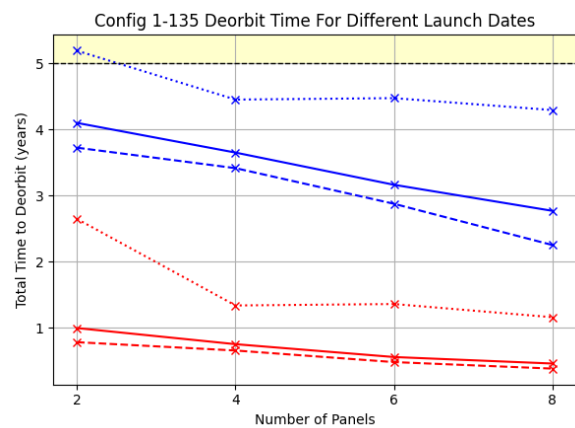


Figure 4.25: Configuration 1-135 OSCAR Results

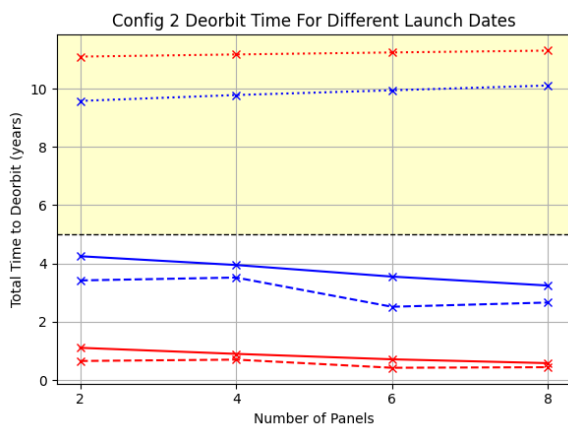


Figure 4.26: Configuration 2 OSCAR Results

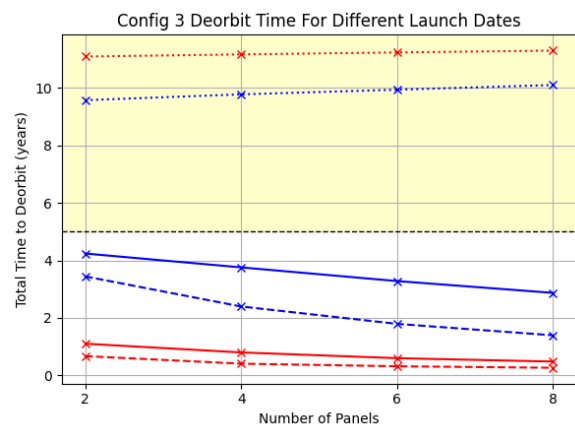


Figure 4.27: Configuration 3 OSCAR Results

For configuration 1, in both deployment angles, the expected cross sectional area should be between the average and maximum cross sectional areas calculated in CROC. Therefore, even though the orbital lifetimes corresponding to

the minimum area are slightly above the 5 year mark as seen in figure 4.24 and figure 4.25, configuration 1 should not be expected to violate this requirement with any given number of panels or launch date as this will include the operational mission time. This makes this type of deployment feasible for numerous missions and an easy choice to comply with the requirement, as even satellites with failed solar array deployment will be expected to decay within the de orbit time limit. However, with the expected drag area and a launch date of Dec 2024, mission lifetimes can be expected to be below 1 year, limiting the time available for operations. Such short durations may suffice for technology demonstration missions or academic projects like Delfi-Twin, ArduSat 1 [91], and AAUSat-3 [92], with design lifetimes of upto 6 months. They may also support thermospheric research missions such as AeroCube and Pegasus (QB50) [93].

For configurations 2 and 3, the expected cross-sectional area is likely to fall between the minimum and average values calculated in CROC, as the panel surfaces remain parallel to the flight angle in a spin-stabilized or longitudinal spin scenario. Both show a large range of lifetime values, with the minimum cross sections reaching beyond 10 years in orbital lifetime for either launch date as seen in figure 4.26 and figure 4.27. This is concerning as, to meet the de-orbit requirement for end-of-life de-orbiting passively, the mission lifetimes for these PocketQubes would need to be planned to be really long—on the order of 5-7 years. If this isn't possible using propulsive methods, the satellites will require active ACS to orient the spacecraft to apply the maximum drag area possible. This won't be feasible for satellites that fail to activate or whose attitude control system becomes inoperative due to incomplete solar panel deployment, leaving them without sufficient power.

Therefore, these configurations are feasible for longer SAR or Earth imaging missions, such as the Dove constellation [94] and the ICEYE constellations [95], which have intended lifetimes of 2-5 years.

Limitations of DRAMA

It is important to note that lifetimes obtained using DRAMA can be inaccurate, particularly for cases where minimum cross-sectional areas contribute to perfect velocity alignment of the satellite. Several factors contribute to this discrepancy. First, the satellite's angle of attack is expected to oscillate, leading to significant deviations in the actual drag area. Second, the drag coefficient is approximated as 2.2, whereas in reality, it can vary between 2 and 3 for CubeSats. Additionally, the drag model used in DRAMA, NRLMSISE-00, introduces further errors into the calculation.

This inaccuracy is evident in a comparison with a known case: Delfi-PQ. When initialized with launch conditions and TLE values, DRAMA predicts a decay date of 2024-03-15 using a randomly tumbling drag area approximation. However, in reality, the satellite decayed on 2024-01-06, highlighting the model's limitations.

4.3. Results

As seen throughout this chapter, the deployed configuration of solar arrays has a huge impact on the power generation and orbital lifetime of the satellite, therefore it is necessary to identify which configuration is best for your chosen mission based on the studies conducted. The results of the studies are summarized in this section.

1. Power Generation

Initially, a tool was developed to show the power generation at different β angles and dusk-dawn and noon-midnight conditions. Since Sun-synchronous orbits (SSO) are widely used for current and upcoming missions, as highlighted in [5], they are evaluated for this analysis. Given the nature of SSO orbits, it is reasonable to assume that the β angles will experience only slight variations throughout the year. The table below summarizes the results for this analysis, showing the most suitable configurations for the planned/expected SSO orbit. The results from the python model were verified by using the solar panel tool in STK, the steps to which were outlined in 4.1.3.

Condition	Most Average Power
Peak Power (Pointing)	1-90, 3
Average Power (Tumbling) - Uncertain Orbit Insertion	1-135
Average Power (Tumbling) - $\beta < 40^\circ$	1-90
Average Power (Tumbling) - $\beta > 40^\circ$	2, 3

Table 4.6: Configurations for Different Orbit Conditions

It is important to analyze the power generation for different dates over the course of the year, as both the β angle, and consequently eclipse durations, vary due to the Earth's tilt. This analysis was done by evaluating

power generation at different points throughout the year, starting from the vernal equinox on March 20, 2024. This observed effect was especially pronounced near 'dusk-dawn' orbits, with config 2, 3 and 1-135 featuring nearly 30% declines in power generation around summer solstice in comparison to vernal equinox, but was negligible near 'noon-midnight' orbits, with power staying constant throughout the year.

Over time, the satellite's altitude decreases due to drag, causing a stronger J2 effect and thus a faster RAAN shift. Because inclination remains fairly constant, the change in RAAN is tied directly to altitude, so the β angle also varies more throughout the year. Due to this, and the unpredictability of rideshare mission's orbit insertion, **Configuration 1 with 135° deployment** is recommended as the choice of deployment configuration for passive, velocity aligned PocketQubes. Alternatively, for missions with pointing capabilities, Configuration 1-90 and 3 both feature peak power generation, essential for missions requiring high data-rates for Earth Observation (EO). However, **Configuration 3** is preferable as it not only benefits from a lower moment of inertia, enabling smaller and more efficient reaction wheels, but also allows multiple mounting locations for the hinges, providing greater flexibility in structural design. Additionally, it improves torsional stability, reducing deformations and enhancing overall pointing accuracy.

2. Mission Duration

Mission durations were evaluated by using European Space Agency (ESA)'s DRAMA software, designed to study orbital decay of space debris. As realized in section 4.2.2, deployed configurations of solar arrays has a huge impact on the de-orbit time of satellites.

Initially a sensitivity analysis was done to see where these orbital lifetimes would be at their minimum and maximum due to the solar cycle. For an orbit insertion altitude of 500 km, the shortest orbital lifetime was predicted for a launch date occurring 5 years into the solar cycle, while the longest lifetime was predicted at 9 years into the solar cycle. For passively tumbling satellites, Table 4.7 summarizes the expected mission duration and possible mission types for the configurations chosen in this study, taking into account these minimum and maximum launch dates.

	Configuration 1 90° & 135°	Configuration 2 & 3
Expected Orbital Lifetime (Launch Date 12/2028)	1.5 - 4 Years	10 - 11 Years
Expected Orbital Lifetime (Launch Date 12/2024)	3-12 Months	9 - 10 Years
Suitable Mission Type	Technology Demonstration Thermospheric Research	Earth Imaging SAR

Table 4.7: Expected Orbital Lifetimes For Velocity Aligned PocketQubes with Suitable Mission Types

These are results for passively tumbling satellites, expecting to be spin stabilized. However, in reality, the angle of attack defers and changes due to the aerodynamic stability of the chosen configuration, and can largely affect the expected orbital lifetime, especially for configurations 2 and 3 where the range in values is quite large, as visualized in figures 4.26 and 4.27. This range is particularly large because a small change in angle of attack in these configurations translates to a large change in the drag area. Therefore, while OSCAR results suggest 10-11 years in expected orbital lifetime, realistically the lifetime should be much shorter. Another realization during the OSCAR simulations was that orbital lifetimes for configurations with higher ballistic coefficients were expected to be largely influenced by the launch date, while ones with small ballistic coefficients were barely impacted.

5

Conclusion and Recommendations

This chapter details the conclusions arrived at throughout the research conducted on deployable solar arrays for PocketQubes. It contains key observations and results obtained from the chapters and breaks them down with respect to the research questions provided at the start of the thesis. Possible enhancements and recommendations for future work are also provided, including possible additions to the design and testing considerations to aid throughout the design process.

5.1. Conclusion

How does the deployment configuration impact the mission design of 3P PocketQubes with deployable solar panels?

This research question aimed to study the impact of deployed configurations on the mission design of 3P PocketQubes, focusing purely on the power generation capabilities and orbital lifetime. A Python model was developed to assess power generation profiles and average orbital power for various β angles on velocity-aligned, spinning spacecraft, as found in section 4.9. First, for peak power generation using pointing capabilities, which may be used for high resolution cameras or high data rate transmissions, configuration 1 with 90° deployment angle and configuration 3 are favorable and able to generate 6.1 W - 9.86 W average orbital power based on the eclipse durations. Configuration 1 with a 135° deployment angle achieved the highest average orbit power under uncertain β angles. These are largely applicable in rideshare missions, where only the altitude and sun-synchronous nature of the orbit may be guaranteed with unexpected lighting conditions. Configurations 2 and 3 were optimal for β angles above 40° , while Configuration 1 with a 90° deployment angle was best for angles below 40° . All configurations converged to similar average power around $\beta = 40^\circ$. Since β angles remain relatively stable throughout the year due to the precessing RAAN, these findings are extremely useful for researchers. These simulations were validated using AGI STK's solar panel tool, with detailed steps provided for researchers in section 4.1.3. Verification proved that the python tool was accurate enough for preliminary EPS sizing in section 4.1.4

Due to Earth's obliquity, β angles vary even for precessing sun-synchronous orbits. This effect was investigated in section 4.1.5 by simulating average orbital power throughout the year in STK, beginning at the vernal equinox. For dusk-dawn orbits, there was a 30% reduction in power generation near summer solstice for configurations 1- 135° , 2 and 3, proving to have a major impact in EPS sizing for satellites. This effect was negligible for noon-midnight orbits, as it had no impact on the eclipse times or the incident angles. These observations were consistent with the hypothesis. Lastly, it was important to study how the orbital decay could potentially impact the sun-synchronicity of satellites in LEO. Orbital decay was found to have little effect on the cumulative RAAN change in short-duration LEO missions. However, for longer missions, it can significantly impact sun-synchronicity, largely affecting the expected power generation. In conclusion, **Configuration 1- 90°** is recommended for passively tumbling PocketQubes due to the unpredictability of orbit insertion and changing lighting conditions throughout orbital lifetime. **Configuration 3** is recommended for PocketQubes with pointing capabilities and high peak power requirements.

Orbital lifetimes were evaluated using ESA's DRAMA software, showing they are heavily influenced by the attitude mode, launch dates, and launch altitudes, in addition to the deployed panel configurations. The CROC module was used for min, max and randomly tumbling average cross sections of the bodies. These are outlined in section 4.4, with an indication of which attitude mode they represent. A sensitivity analysis was initially performed in section 4.22 to evaluate how launch dates influence the expected orbital lifetimes, considering variations in atmospheric density caused by the point within the 11-year solar cycle. This study was conducted from Dec 2019 - Dec 2030, as this is the current solar cycle we are in. The study yielded that orbital lifetimes vary drastically for different launch dates, and also that the maximum and minimum orbital lifetimes corresponding to these launch dates also vary

for different altitudes. For example, launching at an altitude of 550km, a launch date of Dec 2026 corresponds to the maximum lifetime, while launching at an altitude of 500km, Dec 2028 corresponds to the maximum lifetime attainable.

Since the expected launch altitude is 500km for PocketQubes from ride-share programs, the rest of the analysis was conducted for this altitude, and the minimum and maximum orbital lifetimes were obtained from launch dates of Dec 2024, and Dec 2028 respectively in section 4.2.2. For the expected velocity-aligned attitude mode, Configuration 1 (for both deployment angles) yielded the smallest expected orbital lifetime, ranging from 1.5 - 4 years starting Dec 2028, and 3 - 12 months starting Dec 2024. This makes this configuration suitable for technology demonstration, or thermosphere research missions with limited, short design lifetimes. Configuration 2 and 3 on the other hand yielded large orbital lifetimes ranging from 10-11 years for both launch dates, proving to be better suited for longer design lifetimes in Earth Imaging or SAR missions. It is important to note that the orbital lifetime calculations using DRAMA prove to be inaccurate in comparison to decay times seen for past missions (Delfi-PQ, Unicorn 2). This is due to the inaccuracy of the drag model NRLMSISE-00, the unrealistic attitude alignment expected, and the approximations regarding drag coefficient and reflectivity coefficient. While 10-11 years is highly unlikely for configurations 2 and 3, one can still expect these configurations to have larger mission lifetimes than configuration 1 in the velocity aligned attitude mode.

How can proven deployable solar array designs for CubeSats and other small satellites be adapted to develop a reliable design of deployable arrays for PocketQubes?

This research aimed to evaluate existing mechanisms for deployable structures on small satellites, and consequently design deployable solar arrays for PocketQubes capable of achieving a configuration similar to those used on FossaSat-2 and Unicorn-2. After an extensive qualitative assessment of industry options through a thorough literature review, a spring-loaded deployment mechanism was selected in section 3.3.1. This mechanism features a torsion spring hinge and a resistor-based burn wire hold-down system, best suiting the constraints and requirements posed by the small, compact size of PocketQubes. Due to the compact nature of a z-folded wing PCB assembly, it was necessary to determine an optimal combination of material, thickness, and spacing to prevent damaging the PV cells and avoid contact with the deployer walls. Vibrational analysis suggested that a thickness of 1.0 mm with a spacing of 1.4 mm yielded a structurally sound assembly, which then informed the sizing and development of the torsion spring hinge. Additionally, COTS spacers were obtained to help minimize deformation of the panels.

Knowing the complexities of in-house manufacturing of springs, the design constraints from the PCB assembly yielded in a COTS **LTR012A 05 SS** from the LEE Springs catalog to be the deployment guide, storing and providing the spring energy to deploy the panels from their z-folded configuration. This was consequently used to model the supporting hinge structure that would interface between the panels and the PocketQube. In total, 3 assemblies were necessary to complete the final assembly, renders of which are visible in figures 5.1 and 5.2. Additionally, the angular impact velocities for the hinge at the end of deployment were calculated and these exceeded 20 rad/s, requiring explicit analysis to simulate the impact on the hinge structure. LS-Dyna simulations yielded acceptable equivalent stresses observed for the hinges made of Al7075 alloy, with an added fillet to reduce the localized stresses near a 90 degree corner. Finally vibrational analysis was done on the entire stowed array assembly, representing the launch conditions experienced with a conservative PSD profile obtained from the GEVS qualification standard. While the equivalent stresses observed in the hinges and PCB were acceptable, the deformation observed yielded that the outer hinges have a large probability of colliding with the inner deployer wall. This calls for additional tie-down cables, or additional damping within the PCB substrates through the use of viscoelastic tapes.

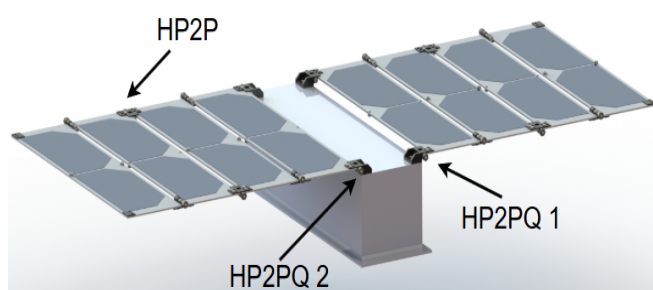


Figure 5.1: Render of Deployable Arrays - Deployed

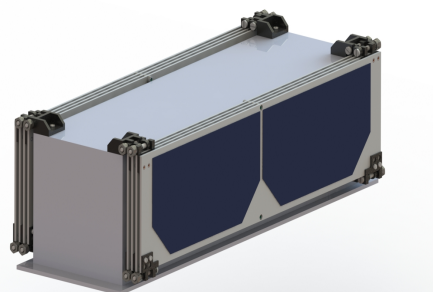


Figure 5.2: Render of Deployable Arrays - Stowed

Mass and cost budgets were developed for the final assembly to compare it to industry solutions for the larger CubeSat format. The mass budget yielded a total mass of 204.8g for two 4-panel assemblies, and a specific power of **96.2 W/kg**, which places it right around the two best deployable rigid arrays for CubeSats found in NASA's Power State of The Art report from 2021, Blue Canyon Technologies' 3U Quadruple Array (108 W/kg) and Ecuadorian Space Agency's 1U DSA/1A (107 W/kg). The total estimated procurement cost of **1480 Euro** was also obtained,

which is relatively high excluding man hours. However, this could be greatly reduced with larger order quantities for formation flying missions accommodating multiple PocketQubes.

5.2. Recommendation for Future Work

1. Reducing Assembly Mass with Thinner PCBs and Viscoelastic Stiffeners:

Throughout the design process, it became evident that multi-panels assemblies consisting of 3-4 panels are subject to large deformations and bending due to the vibrational loads experienced during launch. These PCBs that support the solar cells are the largest contributing masses to the deployable arrays. For the design presented in chapter 3, they are approximately 84% of the mass of the final assembly, and 15.9% of the maximum 3P PocketQube launch mass of 750g. Application of viscoelastic tapes or stiffener material on PCBs to reduce the dynamic board deflection is a way to incorporate thinner PCBs and reduce the overall system mass. This is pursued in [36], where they incorporate 3M 966 acrylic tape that are subjected to shear deformation such that the constrained viscoelastic layers dissipate vibration energy. These tapes are also visible on Unicorn 2 satellites.

2. Thermal Analysis of Deployed Configurations:

Deployable solar panels often face dramatic temperature swings as they move between sunlight and shadow. These shifts can cause the panels, hinges, and springs to expand and contract, leading to stress, bending, or even vibrations. A thermal analysis is important to find out which materials, coatings, or active controls can help lessen these temperature swings and mitigate structural concerns. It's also useful to examine the temperature differences across the panels to decide on the best way to implement Maximum Power Point Tracking (MPPT). MPPT helps optimize power output by taking into account the temperature and irradiance on the panels. If there are large temperature differences, individual MPPT units might be needed; if temperatures are similar, a single MPPT per array could simplify the setup.

3. Improvement in DRAMA Model:

In orbital lifetime analysis in chapter 4, the spacecraft were featured as velocity aligned, spin-stabilized bodies. However, in reality, the aspect angle in flight varies due to instability, and the limitations imposed by passive magnetic stabilization attribute to these instabilities. Due to this, the satellite bodies are subject to varying cross-sections, changing the expected orbital lifetimes calculated within DRAMA. The type of configuration directly attributes to the change in angle of attack, as studied in [96]. As mentioned previously, this can have quite large impact on configurations 2 and 3, as a small change in angle of attack results in a large change in cross sectional area. Additionally, the simulation needs to be improved to match observed lifetimes of past missions. This can be done by adding a multiplier to the expected ballistic coefficient for different attitude modes and matching the simulation results to real life missions.

4. Incorporation of additional systems within Design:

- (a) The release mechanism selected within the trade-off requires an additional information circuit involving a deployment switch. Incorporation of a deployment switch had not been assessed within the thesis, but serves as a critical point in the electrical setup of the solar arrays as the power supplied to the burn resistors needs to be turned off after deployment to prevent overheating.
- (b) Addition of IMUs, gyroscopes and radio antennas can also be assessed, getting rid of the need of additional deployable assemblies to support these systems. Typically, one or more subsystems are provided as options in COTS solar arrays provided by suppliers such as NanoAvionics and Endurosat [97] [98].

5. Development Testing: Development tests are performed to support the design feasibility and to assist in the evolution of design. A few development tests can assist in design of deployable solar arrays

- (a) **Hinge Screws Pullout Tests:** The hinges used to separate the 1mm stacked PCBs are limited to a thickness of 0.7mm, significantly halting thread engagement. By simulating the tensile forces experienced at the impact moment in deployment, one can conduct pullout tests for the screws, and see at what loads they are subject to fail.
- (b) **Release Function Tests:** [32] describes a test setup used to assess the functionality of release mechanisms, focusing on both the release times and the deployment speed of the panels. These tests are crucial for validating burn-wires and can be conducted with varying thicknesses and numbers of windings on the tie-down cable to determine how they affect release times. Typically, such tests can be performed under ambient conditions because the temperature needed to sever the tie-down cable is well above the expected operational environment. However, it is advisable to conduct the test in a thermal chamber at temperatures ranging from -40°C to $+80^{\circ}\text{C}$ (or other extremes based on thermal analysis), as demonstrated with the double-deployed panel prototypes by AAC Clyde Space [64].

A dedicated release circuit on the PocketQube is not strictly necessary; an external power supply can be connected to the burn wires at the expected current and voltage. In addition to verifying release times, these tests help confirm that the hinges are designed with adequate clearance between the shaft and the hinge holes—since any misalignment from manufacturing or assembly could result in deployment failures. Release testing also indicates whether stronger torsion springs or lubricants might be needed.

Although a 1g environment introduces friction forces that are absent in microgravity, successful 1g tests still provide confidence in the system's feasibility for space applications.

Bibliography

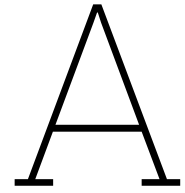
- [1] Statista. *Number of small satellites launched worldwide from 2010 to 2022*. Accessed: 2024-05-16. 2024. URL: <https://www.statista.com/statistics/1267439/small-satellites-launched-worldwide/>.
- [2] Stefan M. Spremo, Alan R. Crocker, and Thomas L. Panontin. *Small Spacecraft Overview*. Tech. rep. 20190031730. Accessed: 2024-11-27. NASA, 2017. URL: <https://ntrs.nasa.gov/citations/20190031730>.
- [3] Balaji Shankar Kumar, Alfred Ng, and Keisuke Yoshihara. "Differential Drag as a Means of Spacecraft Formation Control". en. In: 47.2 (2011).
- [4] NASA. *NASA Space Mechanisms Handbook*. Tech. rep. Accessed: 2024-05-16. NASA, 2005. URL: <https://ntrs.nasa.gov/citations/20050203793>.
- [5] *Nanosats Database*. <https://www.nanosats.eu/database>. Accessed: 2024-05-10.
- [6] Wikipedia contributors. *PocketQube*. <https://en.wikipedia.org/wiki/PocketQube>. Last updated 2024-05-10, Accessed: 2024-05-10. 2024.
- [7] S. Radu et al. *The PocketQube Standard*. 2018.
- [8] Alba Orbital. *PocketQube Standard*. <https://www.albaorbital.com/pocketqube-standard>. Accessed: 21 December 2024.
- [9] Alba Orbital. *PocketQube Interface Control Document (ICD) v0.1*. <https://static1.squarespace.com/static/53d7dcdce4b07a1cdbc08a4/t/5abbec4d1ae6cf78146594a3/1522265166258/ICD+v0.1.pdf>. Accessed: 21 December 2024.
- [10] European Space Agency (ESA). *AlbaPod: The Most Advanced, Space-Proven PocketQube Deployer*. <https://connectivity.esa.int/news/albapod-most-advanced-spaceproven-pocketqube-deployer>. Accessed: 21 December 2024.
- [11] Delft University of Technology (TU Delft). *Delfi-C3*. <https://www.tudelft.nl/lr/delfi-space/delfi-c3>. Accessed: 21 December 2024.
- [12] Delft University of Technology (TU Delft). *Delfi-N3XT*. <https://www.tudelft.nl/lr/delfi-space/delfi-n3xt>. Accessed: 21 December 2024.
- [13] Delft University of Technology (TU Delft). *Delfi-PQ*. <https://www.tudelft.nl/lr/delfi-space/delfi-pq>. Accessed: 21 December 2024.
- [14] S. Radu et al. "Delfi-PQ: The first pocketqube of Delft University of Technology". en. In: *Proceedings of 69th International Astronautical Congress* (2018). Publisher: International Astronautical Federation, IAF. URL: <https://repository.tudelft.nl/islandora/object/uuid%3Ae9129c1d-273f-4f93-be93-05d5f7cc4ce8> (visited on 04/17/2024).
- [15] NASA Small Spacecraft Systems Virtual Institute. *State-of-the-Art of Small Spacecraft Technology*. Tech. rep. Accessed: 2024-11-02. National Aeronautics and Space Administration (NASA), 2023. URL: <https://www.nasa.gov/wp-content/uploads/2024/03/soa-2023.pdf?emrc=8ad1a1>.
- [16] Sunware Solar. *Power Incidence Angle*. 2020. URL: https://en.sunware.solar/v2020/static/items_img/Skizze_Kruemmung_EN.pdf.
- [17] National Aeronautics and Space Administration. *Power State of the Art*. Tech. rep. Accessed: December 17, 2024. NASA, 2021. URL: https://www.nasa.gov/wp-content/uploads/2021/10/3_soa_power_2021.pdf.
- [18] Wikipedia contributors. *Solar constant*. Accessed: 2024-05-16. 2024. URL: https://en.wikipedia.org/wiki/Solar_constant.
- [19] AZUR SPACE Solar Power GmbH. *3G30C Advanced - Triple Junction Space Solar Cell*. Accessed: 2024-05-17. 2024. URL: https://www.azurspace.com/images/products/0003805-01-01_DB_3G30A.pdf.
- [20] Stratonautica. *StratoSat TK-1-C Spacecraft*. <https://www.nanosats.eu/sat/stratosat-tk1-c.html>. Accessed: 2025-02-03.
- [21] Francesco Cocco. "Chapter 8 - Mechanisms for CubeSats and SmallSats". In: *Next Generation CubeSats and SmallSat*. Academic Press, 2023, pp. 431–468. ISBN: 978-0-12-824541-5. DOI: 10.1016/B978-0-12-824541-5.00016-9. URL: <https://www.sciencedirect.com/science/article/pii/B9780128245415000169>.
- [22] Adam Thurn et al. "A Nichrome Burn Wire Release Mechanism for CubeSats". en. In: ().

- [23] NASA. *Deployable Composite Booms (DCB)*. Accessed: 2024-06-25. 2020. URL: <https://www.nasa.gov/centers-and-facilities/langley/deployable-composite-booms-dcb/>.
- [24] Mark Schenk et al. "Review of Inflatable Booms for Deployable Space Structures: Packing and Rigidization". In: *Journal of Spacecraft and Rockets* 51.3 (2014), pp. 762–778. DOI: 10.2514/1.A32598. URL: <https://arc.aiaa.org/doi/10.2514/1.A32598>.
- [25] Dhv Technology. *SADA*. <https://dhvtechnology.com/products/sada/>. n.d.
- [26] Fabio Santoni et al. "An innovative deployable solar panel system for Cubesats". In: *Acta Astronautica* 95 (Feb. 2014), pp. 210–217. ISSN: 0094-5765. DOI: 10.1016/j.actaastro.2013.11.011. URL: <https://www.sciencedirect.com/science/article/pii/S0094576513004037> (visited on 04/09/2024).
- [27] Fabio Santoni et al. "An orientable solar panel system for nanospacecraft". In: *Acta Astronautica* 101 (Aug. 2014), pp. 120–128. ISSN: 0094-5765. DOI: 10.1016/j.actaastro.2014.04.020. URL: <https://www.sciencedirect.com/science/article/pii/S0094576514001453> (visited on 04/09/2024).
- [28] W. Keith Belvin et al. "Advanced Deployable Structural Systems for Small Satellites". In: *NATO CSO STO Specialist Meeting AVT-257 /RSM-041 on Best Practices for Risk Reduction for Overall Space Systems*. NASA Langley Research Center. Zaragoza, Spain, 2016. URL: <https://ntrs.nasa.gov/api/citations/20170003919/downloads/20170003919.pdf>.
- [29] Chandler Dye. *A systematic study into the design and utilization of burn wire as a means of tensioning and releasing spacecraft mechanisms through applied Joule heating*. URL: <https://scholarworks.uark.edu/meeguht/120/>.
- [30] Knowles Capacitors. "The Important Role of a Bypass Capacitor". In: *Knowles Capacitors Blog* (2023). Accessed: 2024-07-24. URL: <https://blog.knowlescapacitors.com/blog/the-important-role-of-a-bypass-capacitor#:~:text=The%20bypass%20capacitor%20acts%20as,Circuit%20diagram%20and%20resulting%20trace>.
- [31] Anirudh P. Kailaje et al. "Implementation of Wire Burn Deployment Mechanism Using COTS Resistors and Related Investigations". en. In: *2019 IEEE Aerospace Conference*. Big Sky, MT, USA: IEEE, Mar. 2019, pp. 1–9. ISBN: 978-1-5386-6854-2. DOI: 10.1109/AERO.2019.8741776. URL: <https://ieeexplore.ieee.org/document/8741776/> (visited on 05/08/2024).
- [32] Tae-Yong Park, Bong-Geon Chae, and Hyun-Ung Oh. "Development of 6 U CubeSat's Deployable Solar Panel with Burn Wire Triggering Holding and Release Mechanism". In: *International Journal of Aerospace Engineering* 2019 (Apr. 2019), pp. 1–13. DOI: 10.1155/2019/7346436.
- [33] Mouser Electronics. *Preci-Dip 0900CLIP Spring-Loaded Contacts*. <https://eu.mouser.com/new/preci-dip/preci-dip-0900clip-spring-loaded-contacts/>. n.d.
- [34] Tae-Yong Park et al. "Experimental Investigation on the Feasibility of Using Spring-Loaded Pogo Pin as a Holding and Release Mechanism for CubeSat's Deployable Solar Panels". In: *International Journal of Aerospace Engineering* 2018 (Sept. 2018), pp. 1–10. DOI: 10.1155/2018/4854656.
- [35] Hyun-Ung Oh, Su-Hyeon Jeon, and seong-cheol Kwon. "Structural Design and Analysis of 1U Standardized STEP Cube Lab for On-Orbit Verification of Fundamental Space Technologies". In: *International Journal of Materials, Mechanics and Manufacturing* 2 (Aug. 2014), pp. 239–244. DOI: 10.7763/IJMMM.2014.V2.135.
- [36] Shankar Bhattarai, Hongrae Kim, and Hyun-Ung Oh. "CubeSat's Deployable Solar Panel with Viscoelastic Multilayered Stiffener for Launch Vibration Attenuation". In: *International Journal of Aerospace Engineering* 2020 (Aug. 2020), pp. 1–10. DOI: 10.1155/2020/8820619.
- [37] CubeSat Shop. *Nano Release Nut (ND3RN)*. Accessed: 2024-07-09. 2024. URL: <https://www.cubesatshop.com/product/nano-release-nut-nd3rn/>.
- [38] NASA. "A Huge Development for Tiny Satellites". In: *NASA Spinoff* (2024). Accessed: 2024-11-08. URL: https://spinoff.nasa.gov/A_Huge_Development_for_Tiny_Satellites.
- [39] Ecuadorian Space Agency. *HDRM Nano Nanosat-Sized Nano-Morphodynamic HDRM - Datasheet*. Accessed: 2024-11-15. 2024. URL: https://satcatalog.s3.amazonaws.com/components/1467/SatCatalog_-_Ecuadorian_Space_Agency_-_HDRM_Nano_Nanosat_Sized_Nano-Morphodynamic_HDRM_-_Datasheet.pdf?lastmod=20240404210634.
- [40] Elbara Ziade, Calvin S. Patmont, and T. Fritz. "Design and Characterization of a Spring Steel Hinge for Deployable CubeSat Structures". In: 2016. URL: <https://www.semanticscholar.org/paper/Design-and-Characterization-of-a-Spring-Steel-Hinge-Ziade-Patmont/7d06b6ec5e3ba112955d647feebd205fd272fe29> (visited on 04/15/2024).
- [41] Thanh Dao et al. "Design, fabrication, and bending test of shape memory polymer composite hinges for space deployable structures". In: *Journal of Intelligent Material Systems and Structures* 29 (Nov. 2017), p. 1045389X1774272. DOI: 10.1177/1045389X17742728.

- [42] Satsearch. *EXA Hinges Nano*. <https://satsearch.co/products/exa-hinges-nano>. n.d.
- [43] C. Śliwiński. "Kinetic energy recovery systems in motor vehicles". In: *IOP Conference Series: Materials Science and Engineering*. Vol. 148. 1. 2016, p. 012056. doi: 10.1088/1757-899X/148/1/012056. URL: https://www.researchgate.net/publication/308709935_Kinetic_energy_recovery_systems_in_motor_vehicles.
- [44] Megha Thaker et al. "Tape spring for deployable space structures: A review". en. In: *Advances in Space Research* 73.10 (May 2024), pp. 5188–5219. ISSN: 02731177. doi: 10.1016/j.asr.2024.02.027. URL: <https://linkinghub.elsevier.com/retrieve/pii/S0273117724001704> (visited on 05/06/2024).
- [45] Xin Lan et al. "Smart Solar Array Consisting of Shape-Memory Releasing Mechanisms and Deployable Hinges". In: *AIAA Journal* 59.6 (June 2021). Publisher: American Institute of Aeronautics and Astronautics (AIAA), pp. 2200–2213. ISSN: 0001-1452. doi: 10.2514/1.J059281.
- [46] NASA Glenn Research Center. *Shape Memory Alloy (SMA) Hinges for Small Satellite Deployment Mechanisms*. Accessed: 2024-11-14. 2020. URL: <https://ntrs-prod.s3.amazonaws.com/t2p/prod/t2media/tops/pdf/LEW-TOPS-135.pdf>.
- [47] H. Heidt et al. "CubeSat: A New Generation of Picosatellite for Education and Industry Low-Cost Space Experimentation". In: *14th Annual AIAA/USU Conference on Small Satellites*. 2000. URL: <https://digitalcommons.usu.edu/cgi/viewcontent.cgi?article=2069&context=smallsat>.
- [48] Japan Aerospace Exploration Agency (JAXA). *IKAROS Overview*. https://global.jaxa.jp/countdown/f17/overview/ikaros_e.html. n.d.
- [49] ASR Engineering. "How Spacecraft Survive Launch | Dynamic Analysis". In: (2018). Accessed: 2024-12-09. URL: <https://asrengineering.com/2018/12/18/how-spacecraft-survive-launch/>.
- [50] Alphonzo Stewart. *Design and Testing of Redundant Release Mechanisms for Spacecraft Solar Arrays*. Tech. rep. 20210020397. NASA, 2021. URL: <https://ntrs.nasa.gov/api/citations/20210020397/downloads/Alphonzo%20Stewart-%20Final%20Paper.pdf>.
- [51] ExoTerra Corporation. *Power Products*. <https://exoterracorp.com/products/power/>. Accessed: 2024-12-31. 2024.
- [52] Max Hillebrandt. "Design and Verification of a Modular Attitude Control System for a CubeSat Platform". Accessed: 2024-11-14. Bachelor's Thesis. Technische Universität Berlin, 2020. URL: https://elib.dlr.de/134661/1/Thesis_Hillebrandt_A5_final.pdf.
- [53] CubeSat Market. *Nano Release Nut (ND3RN) Datasheet*. Accessed: 2024-07-19. 2024. URL: https://www.cubesat.market/_files/ugd/696de6_7919556f6c61428a9427f92bcb150ddf.pdf.
- [54] Hyun-Ung Oh and Myoung-Jae Lee. "Development of a Non-explosive Segmented Nut-type Holding and Release Mechanism for Cube Satellite Applications". In: *TRANSACTIONS OF THE JAPAN SOCIETY FOR AERONAUTICAL AND SPACE SCIENCES* 58 (Jan. 2015), pp. 1–6. doi: 10.2322/tjsass.58.1.
- [55] Sangwon Kwon et al. "Development of 6 U CubeSat's Deployable Solar Panel with Burn Wire Triggering, Holding and Release Mechanism". In: *ResearchGate* (2019). Accessed: 2024-09-09. URL: https://www.researchgate.net/publication/332769184_Development_of_6_U_CubeSat%27s_Deployable_Solar_Panel_with_Burn_Wire_Triggering_Holding_and_Release_Mechanism.
- [56] *MatWeb Material Property Data: Dyneema® SK75 (Ultra High Molecular Weight Polyethylene)*. Accessed: 2024-05-15. 2024. URL: <https://www.matweb.com/search/DataSheet.aspx?MatGUID=8552ae3f68e8401483d0641b8244792e&ckck=1>.
- [57] *Nylon Properties and Applications*. Accessed: 2024-05-15. 2024. URL: <https://laminatedplastics.com/nylon.pdf>.
- [58] *Vectran® Product Brochure*. Accessed: 2024-05-15. 2017. URL: https://www.kuraray.eu/fileadmin/product_ranges/vectran/downloads/2017_VECTRAN_Product_Brochure.pdf.
- [59] *MatWeb Material Property Data: Polycarbonate, Lexan 9034*. Accessed: 2024-05-15. 2024. URL: <https://www.matweb.com/search/datasheet.aspx?MatGUID=77b5205f0dcc43bb8cbe6fee7d36cbb5>.
- [60] Jianing Wu and Shaoze Yan. "Reliability analysis of the solar array based on Fault Tree Analysis". In: *Journal of Physics: Conference Series*. Vol. 305. 1. IOP Publishing. 2011, p. 012006. doi: 10.1088/1742-6596/305/1/012006. URL: https://s3vi.ndc.nasa.gov/ssri-kb/static/resources/Reliability_analysis_of_the_solar_array_based_on_F.pdf.
- [61] CubeSatShop. *Solar Panels*. <https://www.cubesatshop.com/product/solar-panels/>. Accessed: 2024-12-31. 2024.
- [62] DHV Technology. *Solar Panels for CubeSats*. <https://dhvtechnology.com/products/solar-panels-cubesats/>. Accessed: 2024-12-31. 2024.

- [63] ISISpace. *ISIS CubeSat Solar Panels*. <https://www.isispace.nl/product/isis-cubesat-solar-panels/>. Accessed: 2024-12-31. 2024.
- [64] AAC Clyde Space. *Photon Solar Arrays*. <https://www.aac-clyde.space/what-we-do/space-products-components/photon-solar-arrays>. Accessed: 2024-12-31. 2024.
- [65] Omer Safak. "Structural Design and Analysis of a Solar Array Substrate for a GEO Satellite". Director: José Ignacio Velasco Perero. Master's thesis. Barcelona, Spain: Universitat Politècnica de Catalunya, June 2013. URL: <https://upcommons.upc.edu/handle/2099.1/20260>.
- [66] Proto-Electronics. "Space-Grade PCBs: Challenges in Designing Electronics for Extreme Environments". In: *Proto-Electronics Blog* (2024). Accessed: 2024-08-07. URL: <https://www.proto-electronics.com/blog/space-grade-pcb-challenges-in-designing-electronics-for-extreme-environments>.
- [67] H. S. Rauschenbach. *Solar Cell Array Design Handbook, Volume 1*. Tech. rep. NASA-CR-149364, JPL-SP-43-38-VOL-1. Accessed: 2024-11-08. Jet Propulsion Laboratory, California Institute of Technology, 1976. URL: <https://ntrs.nasa.gov/api/citations/19770007250/downloads/19770007250.pdf>.
- [68] Eurocircuits. *Eurocircuits: PCB & PCBA Prototypes and Small Series*. Accessed: 2024-12-30. 2024. URL: <https://www.eurocircuits.com/>.
- [69] Isola Group. *PCB Materials Quality for Aerospace and Defense*. <https://www.isola-group.com/pcb-materials-quality/markets/aerospace-and-defense/>. Accessed: 2024-04-27. Accessed: 2024-04-27.
- [70] Dlubal Software GmbH. *Natural Vibrations of Rectangular Plate*. <https://www.dlubal.com/pl/webfile/000113/2200172/0110-natural-vibrations-of-rectangular-plate.pdf>. Accessed: 2024-04-27. 2022.
- [71] M. J. L. van der Linden, M. J. Bentum, and C. J. M. Verhoeven. "A framework for small satellite deployable structures and how to deploy them reliably". In: *Communications Engineering* 3 (2024), Article 210. DOI: 10.1038/s44172-024-00210-7. URL: <https://www.nature.com/articles/s44172-024-00210-7>.
- [72] SMSI. *SMSI SMT Steel Spacer M1 6 Internal Thread*. https://www.we-online.com/en/components/products/SMSI_SMT_STEEL_SPACER_M1_6_INTERNAL_THREAD. Accessed: 2024-12-31. 2024.
- [73] ASBG Insights. *Engineering Guide*. Accessed: 2025-01-02. n.d. URL: <https://insights.asbg.com/engineering-guide/>.
- [74] Lee Spring. *Spring Materials*. Accessed: 2024-12-30. URL: <https://www.leespring.com/spring-materials#part-453021>.
- [75] EngineerExcel. *Torsion Spring Formulas: A Complete Guide*. Accessed: 2024-05-15. 2023. URL: <https://engineerexcel.com/torsion-spring-formula/>.
- [76] Daizong Li, Patrick Harkness, and Tom Walkinshaw. "Design of a solar panel deployment and tracking system for Pocketcube pico-satellite". In: *2017 IEEE Aerospace Conference* (Mar. 2017). Conference Name: 2017 IEEE Aerospace Conference ISBN: 9781509016136 Place: Big Sky, MT, USA Publisher: IEEE, pp. 1–19. DOI: 10.1109/AERO.2017.7943910. URL: <http://ieeexplore.ieee.org/document/7943910/> (visited on 04/10/2024).
- [77] National Aeronautics and Space Administration. *Process Specification for Installation of Threaded Fasteners (PRC-9007C)*. <https://www.nasa.gov/wp-content/uploads/2023/03/prc-9007-current.pdf>. Accessed: 2025-01-21. 2023.
- [78] Andrew Strain. *It's All About the Power*. Accessed: 2024-12-18. Apr. 2020. URL: <https://www.aac-clyde.space/articles/its-all-about-the-power>.
- [79] ASM International. *Aluminum 7075-T6; 7075-T651*. Accessed: 2024-12-31. 2024. URL: <https://asm.matweb.com/search/specifmaterial.asp?bassnum=ma7075t6>.
- [80] Ayman A Farid and Steve Hranilovic. "Capacity analysis of free-space optical communication channels with multiple receivers". In: *2011 Proceedings of the International Conference on Space Optical Systems and Applications (ICSOS)*. IEEE, 2011, pp. 164–170. DOI: 10.1109/ICSOS.2011.5979419. URL: <https://ieeexplore.ieee.org/document/5979419>.
- [81] Michael J. Dube and Wayne R. Gamwell. *Performance Characterization of Loctite® 242 and 271 Liquid Locking Compounds (LLCs) as a Secondary Locking Feature for International Space Station (ISS) Fasteners*. Technical Memorandum NASA/TM-2011-217068. NASA Langley Research Center, 2011. URL: <https://ntrs.nasa.gov/api/citations/20110011064/downloads/20110011064.pdf>.
- [82] Wikipedia contributors. *Space Tribology — Wikipedia, The Free Encyclopedia*. Accessed: 2024-02-02. 2024. URL: https://en.wikipedia.org/wiki/Space_tribology.

- [83] Andreas Merstallinger, E. Semerad, and B.D. Dunn. "Influence of coatings and alloying on cold welding due to impact and fretting". In: *Proceedings of the 10th European Space Mechanisms and Tribology Symposium (ESMATs)*. ESA. 2003, pp. 37–44. URL: <https://esmat.s.eu/esmatpapers/pastpapers/pdfs/2003/merstallinger.pdf>.
- [84] Unknown (Author not specified). "Aerodynamic Stability for CubeSats at ISS Orbit". In: *Journal of Small Satellites (JOSS)* 3 (1 2014). Accessed: 2024-12-19, pp. 201–212. URL: https://www.jossonline.com/storage/2014/12/0201-Aerodynamic-Stability-for-CubeSats-at-ISS-Orbit.pdf?utm_source=chatgpt.com.
- [85] SpaceX. *SpaceX Rideshare Program*. Accessed: 2025-01-14. 2025. URL: <https://www.spacex.com/rideshare/>.
- [86] Ömer Şafak. "Structural Design and Analysis of a Solar Array Substrate for a GEO Satellite". Supervised by José Ignacio Velasco and Gürbüz Gülersoy. Master Thesis. Barcelona, Spain: Universitat Politècnica de Catalunya, May 2013. URL: <https://core.ac.uk/download/pdf/41808415.pdf>.
- [87] Sumanth R M. "Computation of Eclipse Time for Low-Earth Orbiting Small Satellites". In: *International Journal of Aviation, Aeronautics, and Aerospace* 6.5 (2019). DOI: 10.15394/ijaaa.2019.1412. URL: <https://commons.erau.edu/ijaaa/vol6/iss5/15/>.
- [88] NASA Small Satellite Coordination Group. *Deorbit Systems*. Accessed: 2024-09-07. NASA, 2024. URL: [https://www.nasa.gov/smallsat-institute/sst-soa/deorbit-systems/#:~:text=The%20general%20guideline%20is%20that,of%20their%20mission%20\(3\)](https://www.nasa.gov/smallsat-institute/sst-soa/deorbit-systems/#:~:text=The%20general%20guideline%20is%20that,of%20their%20mission%20(3)).
- [89] Federal Communications Commission (FCC). *FCC Adopts New 5-Year Rule for Deorbiting Satellites*. Accessed: 2024-09-07. Federal Communications Commission, 2022. URL: <https://www.fcc.gov/document/fcc-adopts-new-5-year-rule-deorbiting-satellites-0>.
- [90] Alba Orbital. *Unicorn-2 Interface Control Document (V1.1)*. Accessed: 2025-01-18. 2020. URL: <https://static1.squarespace.com/static/53d7dcdce4b07a1cdbbc08a4/t/5f64819c21f96b78c4f54820/1600422408593/Unicorn-2+ICD+%28V1.1%29.pdf>.
- [91] *ArduSat-1*. Accessed: 2025-01-07. URL: https://space.skyrocket.de/doc_sdat/ardusat-1.htm.
- [92] *AAUSat-3*. Accessed: 2025-01-07. URL: <https://en.wikipedia.org/wiki/AAUSat-3>.
- [93] *Pegasus QB50*. Accessed: 2025-01-07. URL: https://space.skyrocket.de/doc_sdat/pegasus_qb50.htm.
- [94] *PlanetScope Mission Description*. Accessed: 2025-01-07. URL: <https://earth.esa.int/eogateway/missions/planetscope/description>.
- [95] *ICEYE Satellite Programme*. Accessed: 2025-01-07. URL: <https://space.oscar.wmo.int/satelliteprogrammes/view/iceye>.
- [96] David Mostaza-Prieto and Peter Roberts. "Methodology to Analyze Attitude Stability of Satellites Subjected to Aerodynamic Torques". In: *Journal of Guidance, Control, and Dynamics* 39.3 (2016), pp. 437–449. DOI: 10.2514/1.G001481. URL: <https://doi.org/10.2514/1.G001481>.
- [97] NanoAvionics. *12U Cubesat Nanosatellite M12P*. <https://nanoavionics.com/small-satellite-buses/12u-cubesat-nanosatellite-m12p/>. Accessed: 2025-01-09.
- [98] EnduroSat. *3U Deployable Solar Array*. <https://www.endurosat.com/products/3u-deployable-solar-array/>. Accessed: 2025-01-09.
- [99] Hemant Arora et al. "Investigation of tape flexures for space borne deployable structures". en. In: *International Journal of Space Structures* 37.1 (Mar. 2022). Publisher: SAGE Publications Ltd STM, pp. 37–48. ISSN: 0956-0599. DOI: 10.1177/09560599211064096. URL: <https://doi.org/10.1177/09560599211064096> (visited on 05/08/2024).



Appendix

A.1. Azur 3G3CA Assembly

30% Triple Junction GaAs Solar Cell
Type: TJ Solar Cell 3G30C - Advanced

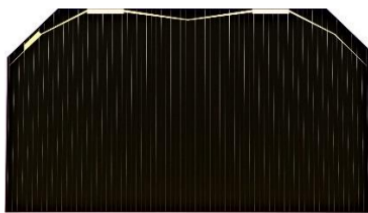


Figure A.1: Azur Space 3G30C

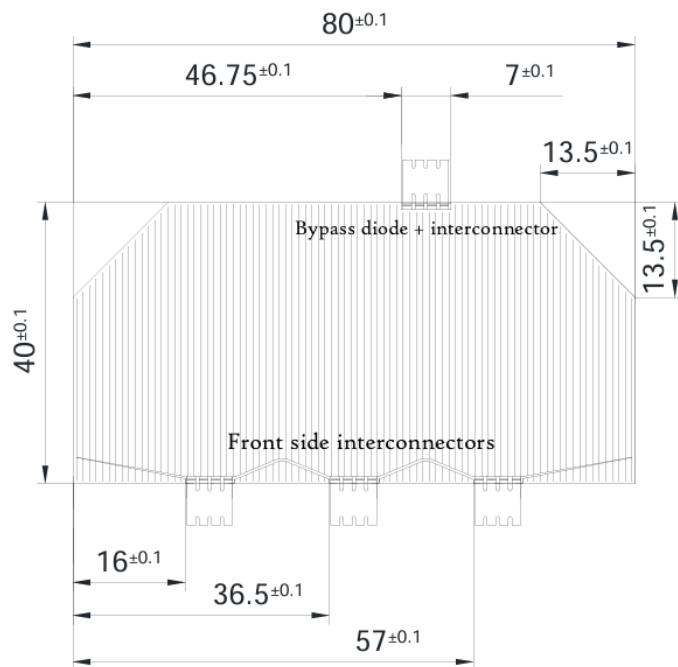


Figure A.2: Cell Dimensions

A.2. PCB Design

Material	TC (W/m·K)	CTE (ppm/°C)	Tg (°C)
Al2O3 96%	25	6.4	350
AlN	170	5.6	1726
BeO 99.5%	150-285	9	N/A
VT-5a2	Z: 2.2, X/Y: 3.4	45	190
IS400	0.36	Z: 50, X/Y: 13/14	150
370HR	0.4	Z: 45, X/Y: 13/14	180
FR406N	0.3-0.4	Z: 60, X/Y: 13/14	170
RO4003C	0.5	Z: 46, X/Y: 11/14	280
RO4835	0.66	35	N/A
Kapton HN	0.2	20	N/A
Isola P95	0.4	Z: 55, X/Y: 13/14	260

Table A.1: Thermal Conductivity and Coefficient of Thermal Expansion of Substrate Materials

Table A.2: Elastic Properties

Category	Material	Density (g/cm ³)	Young's Modulus (GPa)	Poisson's Ratio (Length Direction)
Ceramic	Al2O3 96%	3.80	300	0.22
	AlN	3.20	320	0.27
	BeO 99.5%	2.85	345	0.26
	VT-5a2	2.20	20	0.17
Mid-Tg Fr-4	IS400	1.85	25.3	0.183
High-Tg Fr-4	370HR	1.86	25.8	0.177
	FR406N	1.85	25.4	0.191
PTFE (Teflon)	RO4003C	1.79	19.65	0.46
	RO4835	1.92	7.78	0.46
Polyimide	Kapton HN	1.42	2.5	0.34
	Isola P95	1.43	27.2	0.187

Substrate	Mass	Flexural Rigidity	Mode 1 (Hz)
Al2O3 96%	38.02	51.312	232.18
AlN	32.02	56.179	264.74
BeO 99.5%	28.51	60.223	290.45
VT-5a2	18.51	3.352	85.05
IS400	18.51	4.261	95.89
370HR	18.61	4.335	96.46
FR406N	18.51	4.291	96.22
RO4003C	17.91	4.057	95.12
RO4835	19.21	1.606	57.79
Kapton HN	14.21	0.460	35.97
Isola P95	14.31	4.588	113.17

Table A.3: Natural Frequency of Simply Supported Rectangular Plate

A.2.1. PCB Thickness and Spacing Analysis Mode Shapes

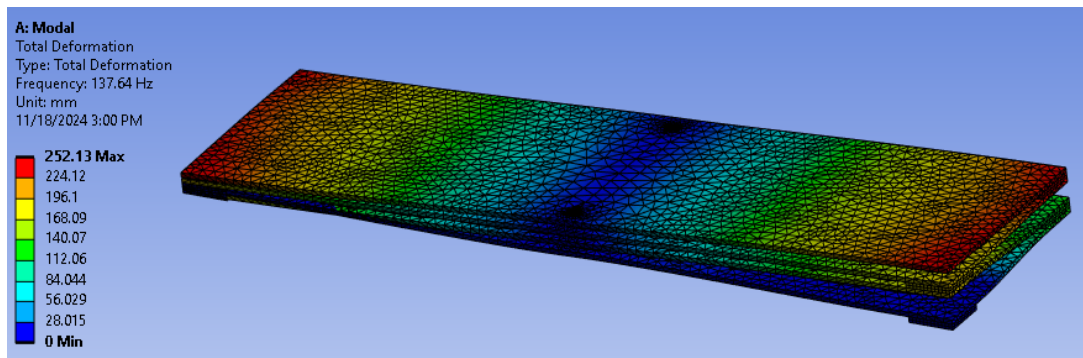


Figure A.3: Mode Shape 1

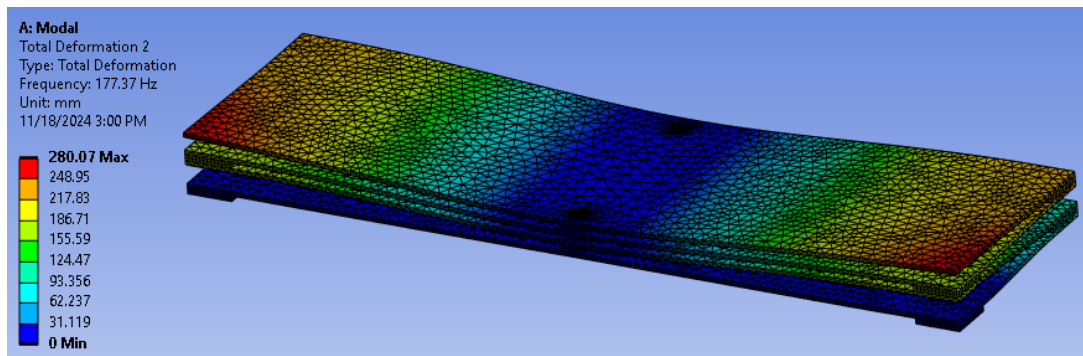


Figure A.4: Mode Shape 2

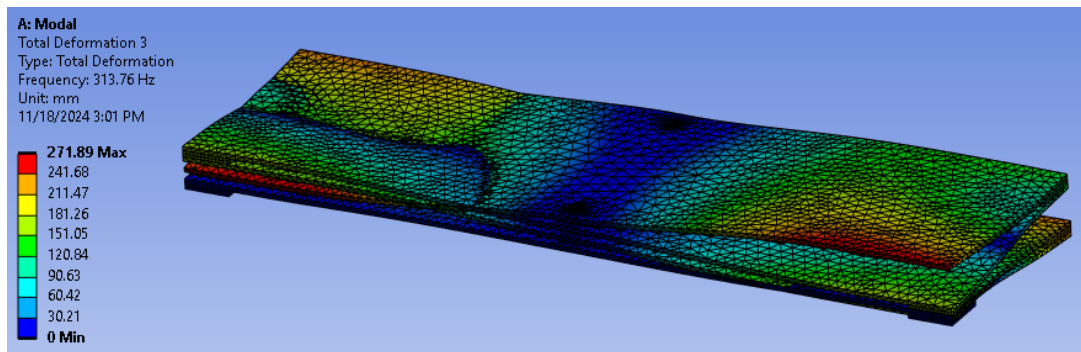


Figure A.5: Mode Shape 3

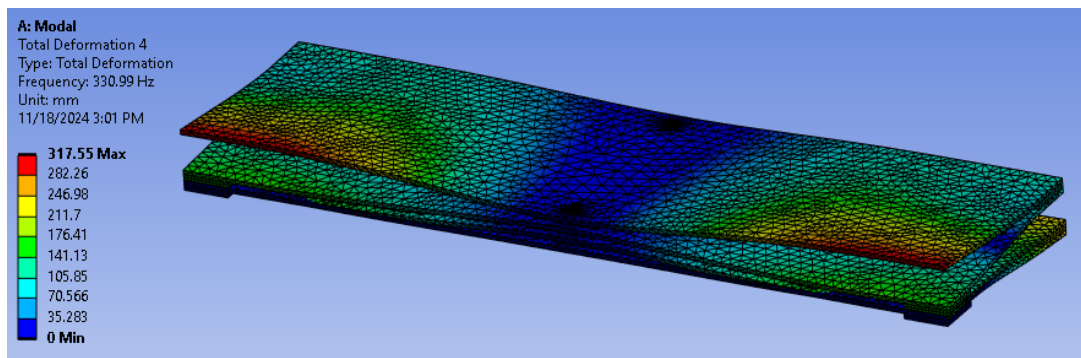


Figure A.6: Mode Shape 4

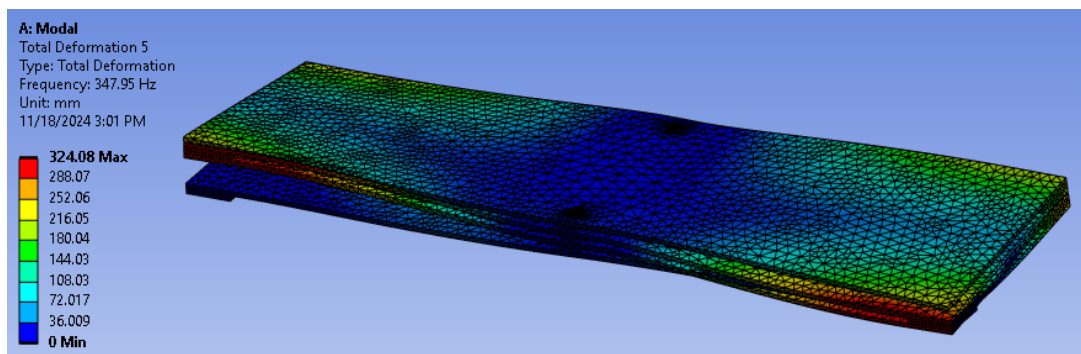


Figure A.7: Mode Shape 5

A.3. DRAMA Code

```
import drama
from drama import oscar
import datetime
import pandas as pd
import matplotlib.pyplot as plt

mass_to_panels = {
    0.5744: 2,
    0.6038: 4,
    0.6332: 6,
    0.6626: 8
}
```

```

results_by_date = {
    datetime.datetime(2024, 12, 1): {"min": [], "ave": [], "max": []},
    datetime.datetime(2028, 12, 1): {"min": [], "ave": [], "max": []}
}

year_color_map = {
    2024: "red",
    2028: "blue"
}

line_style_map = {
    "min": ":",
    "ave": "-",
    "max": "--"
}

if __name__ == '__main__':
    configs = [
        {'mass': 0.5744, 'cross_section': 0.0027},
        {'mass': 0.5744, 'cross_section': 0.0167},
        {'mass': 0.5744, 'cross_section': 0.0264},
        {'mass': 0.6038, 'cross_section': 0.0028},
        {'mass': 0.6038, 'cross_section': 0.024},
        {'mass': 0.6038, 'cross_section': 0.0426},
        {'mass': 0.6332, 'cross_section': 0.0029},
        {'mass': 0.6332, 'cross_section': 0.0316},
        {'mass': 0.6332, 'cross_section': 0.0588},
        {'mass': 0.6626, 'cross_section': 0.003},
        {'mass': 0.6626, 'cross_section': 0.0395},
        {'mass': 0.6626, 'cross_section': 0.075}
    ]

    base_config = {
        'ecc': 1.0E-4,
        'inc': 97.5,
        'raan': 0,
        'aop': 0,
        'ma': 0,
        'drag_coefficient': 2.2,
        'reflectivity_coefficient': 1.3,
        'disposal_option': 4,
        'lifetime_limit': 25,
        'generate_oad_plot': 0
    }

    for launch_date in results_by_date.keys():
        for idx, config in enumerate(configs):
            specific_config = base_config.copy()
            specific_config.update(config)
            specific_config['sma'] = 6878
            specific_config['epoch'] = launch_date

            result = oscar.run(
                config=specific_config,
                project=r"C:\\Users\\divya\\Desktop\\Master_Thesis\\Drana\\NEW\\NEW",
                save_output_dirs=None,
                parallel=True,
                ncpus=8,
                timeout=None,
                keep_output_files='summary',
                trajectory=True,
                spell_check=True,

```

```

        geo_cross=False
    )

    trajectory_data = result['results'][0]['trajectory']
    time_list = [
        datetime.datetime.strptime(entry['epoch'], '%Y-%m-%d %H:%M:%S')
        for entry in trajectory_data
    ]
    total_deorbit_time_years = (time_list[-1] - time_list[0]).days / 365
    current_label = ["min", "ave", "max"][idx % 3]
    current_panels = mass_to_panels[config['mass']]
    results_by_date[launch_date][current_label].append((current_panels,
        ↪ total_deorbit_time_years))

plt.figure(figsize=(6, 4.5))
for launch_date, times_data in results_by_date.items():
    year = launch_date.year
    color = year_color_map[year]
    for label in ["min", "ave", "max"]:
        x_vals = [item[0] for item in times_data[label]]
        y_vals = [item[1] for item in times_data[label]]
        style = line_style_map[label]
        plt.plot(x_vals, y_vals, marker='x', color=color, linestyle=style,
            ↪ label=f"{year}-{label}")

low, high = plt.ylim()
if high < 5:
    high = 6
plt.ylim(low, high)
plt.axhspan(5, high, facecolor='yellow', alpha=0.2)
plt.axhline(y=5, color='black', linestyle='--', linewidth=1)
plt.xlabel("Number of Panels")
plt.ylabel("Total Time to Deorbit (years)")
plt.title("Config 3 Deorbit Time For Different Launch Dates")
plt.xticks([2, 4, 6, 8])
plt.grid(True)
plt.tight_layout()
plt.show()

```

A.4. Power Generation Model

A.4.1. Power Generation Spin Stabilized

```

import numpy as np
import math
import trimesh
from trimesh.ray.ray_triangle import RayMeshIntersector
import matplotlib.pyplot as plt
import pandas as pd

# Load the mesh from a PLY file
mesh = trimesh.load('C:/Users/divya/Documents/Thesis_Blend/Python_Model/Config_1-4-90.ply')

# Alignment matrix to rotate the mesh (+Z to [0, -1, 0], 90 degrees around X-axis)
alignment_matrix = np.array([
    [1, 0, 0, 0],
    [0, 0, -1, 0],
    [0, 1, 0, 0],
    [0, 0, 0, 1]
])
aligned_mesh = mesh.copy()

```

```

aligned_mesh.apply_transform(alignment_matrix)

# Verify mesh
print(f"Loaded mesh with {len(mesh.vertices)} vertices and {len(mesh.faces)} faces.")

# Define active and inactive surfaces
active_color = np.array([254, 0, 0, 255], dtype=np.uint8) # Red
inactive_color = np.array([0, 0, 254, 255], dtype=np.uint8) # Blue
is_active_vertex = np.all(mesh.visual.vertex_colors == active_color, axis=1)
is_inactive_vertex = np.all(mesh.visual.vertex_colors == inactive_color, axis=1)
active_vertex_indices = np.where(is_active_vertex)[0]
inactive_vertex_indices = np.where(is_inactive_vertex)[0]

# Print the count of active and inactive vertices
print(f"Number of active vertices: {len(active_vertex_indices)}")
print(f"Number of inactive vertices: {len(inactive_vertex_indices)}")

# Map vertices to faces for active and inactive surfaces
active_face_mask = np.all(np.isin(mesh.faces, active_vertex_indices), axis=1)
inactive_face_mask = np.all(np.isin(mesh.faces, inactive_vertex_indices), axis=1)

# Extract active and inactive faces
active_face_indices = np.where(active_face_mask)[0]
inactive_face_indices = np.where(inactive_face_mask)[0]

# Create submeshes for active and inactive parts
active_mesh = mesh.submesh([active_face_indices], append=True)
inactive_mesh = mesh.submesh([inactive_face_indices], append=True)

# Print the count of active and inactive faces
print(f"Number of active faces: {len(active_face_indices)}")
print(f"Number of inactive faces: {len(inactive_face_indices)}")

# Function for rotation around the X-axis
def rotation_matrix_x(theta):
    return np.array([
        [1, 0, 0],
        [0, np.cos(theta), -np.sin(theta)],
        [0, np.sin(theta), np.cos(theta)]
    ])

# Function for rotation around the Z-axis
def rotation_matrix_z(theta):
    return np.array([
        [np.cos(theta), np.sin(theta), 0],
        [-np.sin(theta), np.cos(theta), 0],
        [0, 0, 1]
    ])

# Apply rotations to the mesh based on given angles
def apply_rotations(mesh, theta_L, theta_S):
    R = rotation_matrix_z(theta_S) @ rotation_matrix_x(theta_L)
    T = np.eye(4)
    T[:3, :3] = R
    rotated_mesh = mesh.copy()
    rotated_mesh.apply_transform(T)
    return rotated_mesh

# Calculate power
def calculate_power(rotated_full_mesh, rotated_active_mesh, sun_direction, panel_efficiency,
    ↪ irradiance=1361):
    intersector = RayMeshIntersector(rotated_full_mesh)
    face_centers = rotated_active_mesh.triangles_center

```

```

normals = rotated_active_mesh.face_normals
origins = face_centers + normals * 1e-6
directions = np.tile(sun_direction, (origins.shape[0], 1))

locations, index_ray, index_tri = intersector.intersects_location(
    ray_origins=origins,
    ray_directions=directions,
    multiple_hits=False
)

is_hit = np.zeros(len(origins), dtype=bool)
is_hit[index_ray] = True
illuminated_faces = np.logical_not(is_hit)

cos_theta = np.dot(normals, sun_direction)
cos_theta = np.clip(cos_theta, 0, 1)
face_areas = rotated_active_mesh.area_faces
power = np.sum(panel_efficiency * irradiance * face_areas * cos_theta * illuminated_faces)

return power

# Define Orbital Parameters and Constants
G = 6.674 * 10**-11 # (m^3 kg^-1 s^-2)
M_E = 5.972 * 10**24 # (kg)
earth_radius = 6371 * 10**3 # m
orbital_altitude = 500 * 10**3 # m
beta_angle = 0 # Angle in degrees
panel_efficiency = 0.3

# Calculate total orbital time
semi_major_axis = earth_radius + orbital_altitude # a = R_E + h
total_orbit_time = 2 * math.pi * math.sqrt(semi_major_axis**3 / (G * M_E)) # T = 2(a^3/GM)
num_orbits = 1

# Calculate beta_star
beta_star = math.degrees(math.asin(earth_radius / semi_major_axis)) # * = sin^1(Re / (Re + h))

# Calculate f_e (fraction of orbit in eclipse) with degrees
if abs(beta_angle) < beta_star:
    f_e = (1 / 180) * math.degrees(math.acos(
        math.sqrt(orbital_altitude**2 + 2 * earth_radius * orbital_altitude) /
        (semi_major_axis * math.cos(math.radians(beta_angle))) # Ensure beta_angle is treated
        ↪ in degrees
    ))
else:
    f_e = 0 # No eclipse if || *

# Calculate eclipse time
eclipse_time = total_orbit_time * f_e

sunlit_phase = set(range(int(eclipse_time/2), int((eclipse_time/2) +
    ↪ (total_orbit_time-eclipse_time))))
# Time steps for the simulation
time_steps = np.arange(0, num_orbits*total_orbit_time, 1)

# Rotation rates
rotation_rate_long_axis = np.radians(10)
rotation_rate_short_axis = np.radians(360 / total_orbit_time)

# Track power over time
power_over_time = []

# Sun direction

```

```

beta_angle_rad = np.radians(beta_angle)
sun_direction = np.array([0, 1, 0])
sun_direction = rotation_matrix_x(beta_angle_rad) @ sun_direction

# Simulate power generation over one orbit
for t in time_steps:
    #Map the current time to a single orbit
    t_mod= int(t % total_orbit_time)
    if t_mod in sunlit_phase:
        theta_L = rotation_rate_long_axis * t
        theta_S = rotation_rate_short_axis * t

        rotated_full_mesh = apply_rotations(mesh, theta_L, theta_S)
        rotated_active_mesh = apply_rotations(active_mesh, theta_L, theta_S)

        power = calculate_power(rotated_full_mesh, rotated_active_mesh, sun_direction,
                                ↪ panel_efficiency)
        power_over_time.append(power)
    else:
        power_over_time.append(0)

# Plot power generation over time
plt.figure(figsize=(12, 6))
plt.plot(time_steps, power_over_time, label='Power Generation with Shadows')
plt.xlabel('Time (seconds)')
plt.ylabel('Power Generated (W)')
plt.title('Power Generation Over One Orbital Period Config 1-90-4')
plt.legend()
plt.grid(True)
plt.show()

# Calculate and display average and peak power
average_power = np.mean(power_over_time)
peak_power = np.max(power_over_time)
print(f"Average Power Generation: {average_power:.2f} W")
print(f"Peak Power Generation: {peak_power:.2f} W")

# Save power data to an Excel file
# power_data = pd.DataFrame({'Time (s)': time_steps, 'Power (W)': power_over_time})
#
↪ power_data.to_excel('C:/Users/divya/Desktop/Master_Thesis/Configuration_Trade-Off/power_generation_over_tim
↪ index=False)

```

A.4.2. Power Generation Plots, Single Orbit

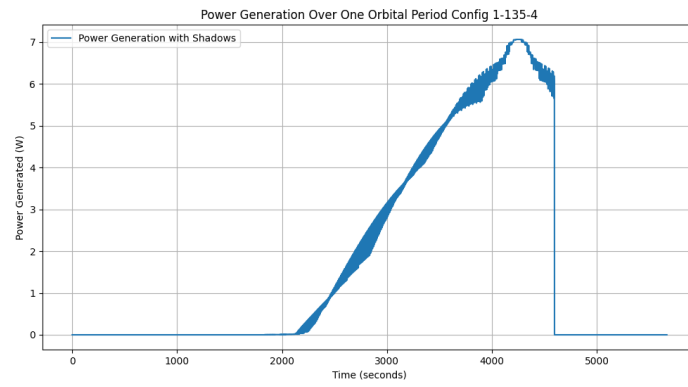


Figure A.8: Config 1 135 Power Generation Python, Single Orbit

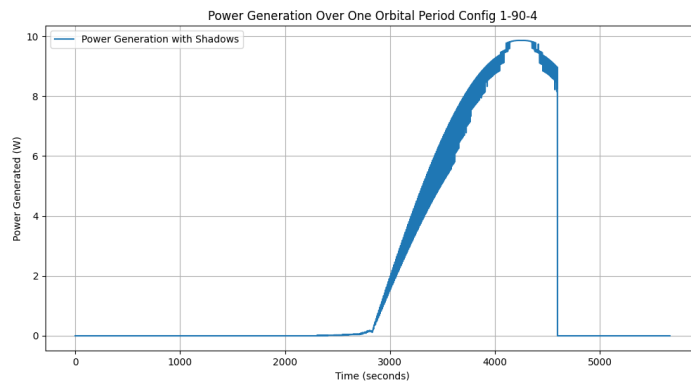


Figure A.9: Config 1 90 Power Generation Python, Single Orbit

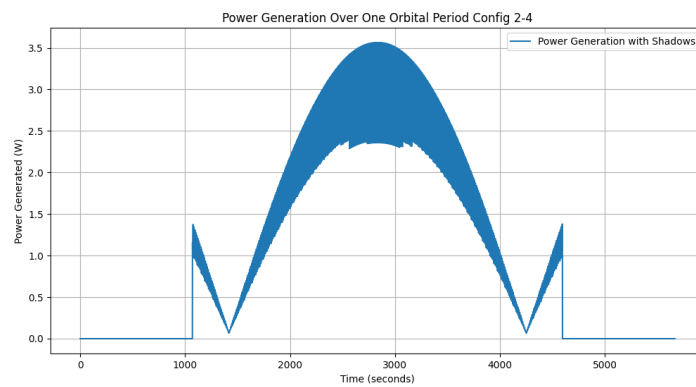


Figure A.10: Config 2 Power Generation Python, Single Orbit

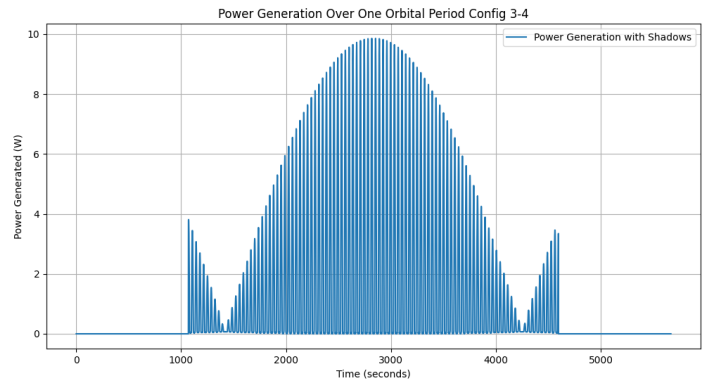


Figure A.11: Config 3 Power Generation Python, Single Orbit

A.4.3. RAAN Precession Rate Inclination & Altitude Combination

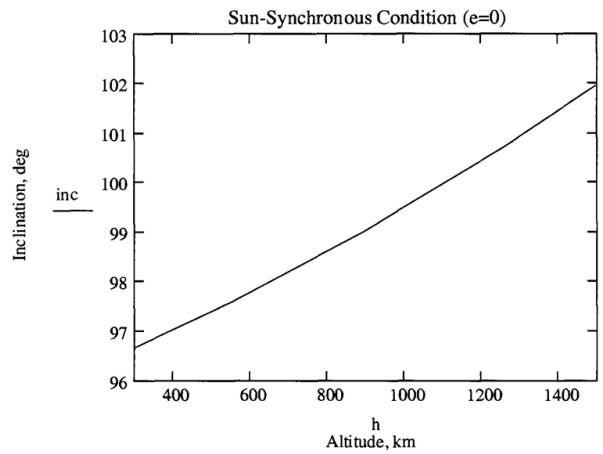
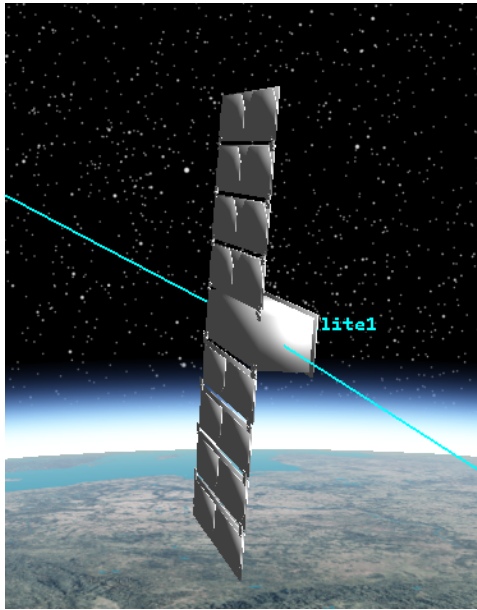


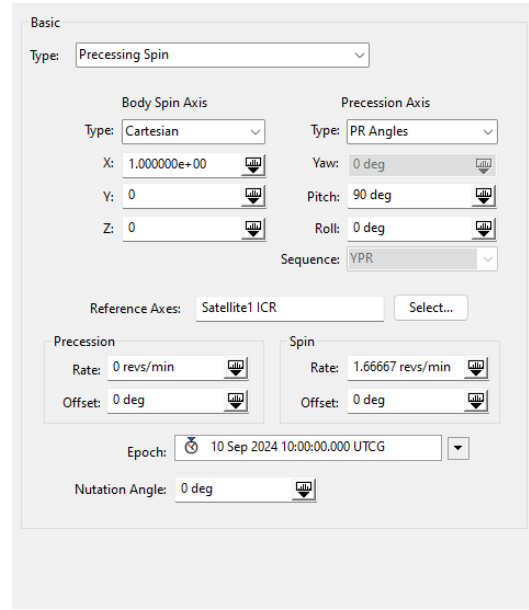
Figure A.12: Altitude & Inclination for advised RAAN Precession

A.5. STK Power Generation

A.5.1. Tumbling and Sun-Pointing Settings in STK

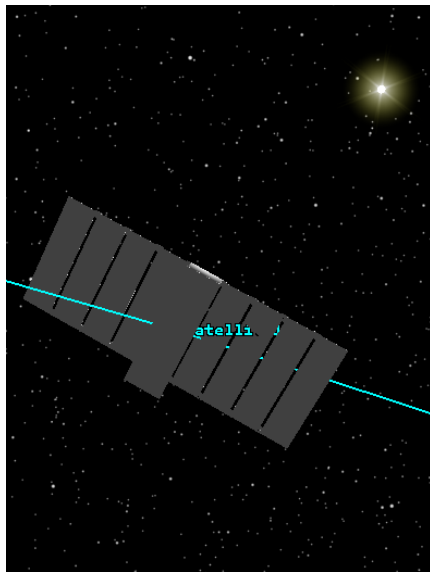


(a) PocketQube Tumbling Around Velocity Vector

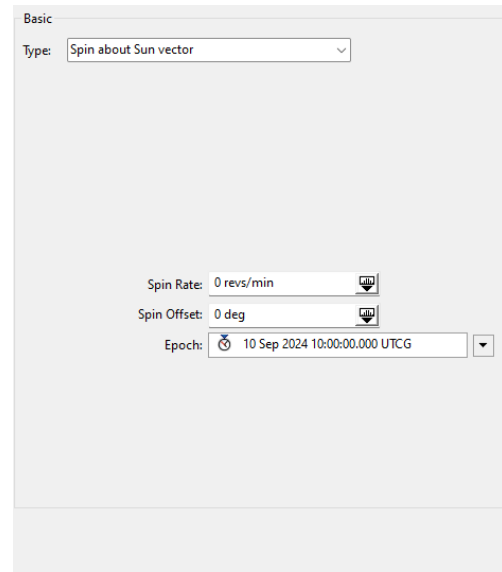


(b) STK Settings for Tumbling

Figure A.13: STK Environment for Tumbling



(a) PocketQube Sun Pointing



(b) STK Setting for Sun-Pointing

Figure A.14: STK Environment for Sun-Pointing

A.5.2. Settings for Spin Stabilized Tumbling and Sun-pointing

A.5.3. STK Power Plots

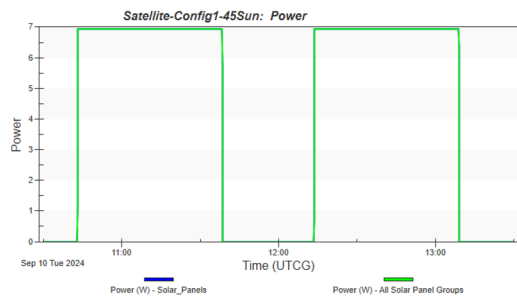


Figure A.15: Config1 (45°) Sun-Pointing

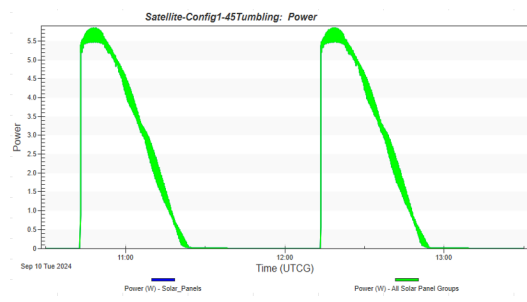


Figure A.16: Config1 (45°) Tumbling

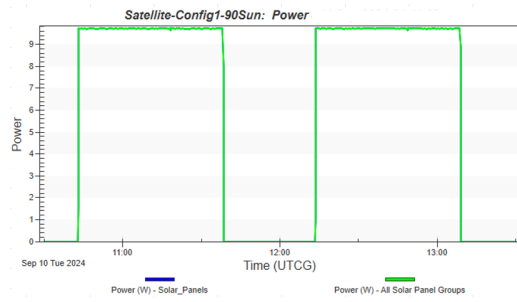


Figure A.17: Config1 (90°) Sun-Pointing

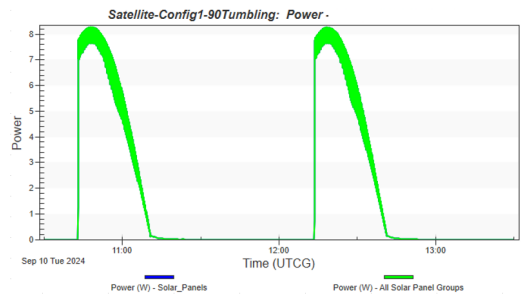


Figure A.18: Config1 (90°) Tumbling

Figure A.19: Configuration 1 (45°) & Configuration 1 (90°)

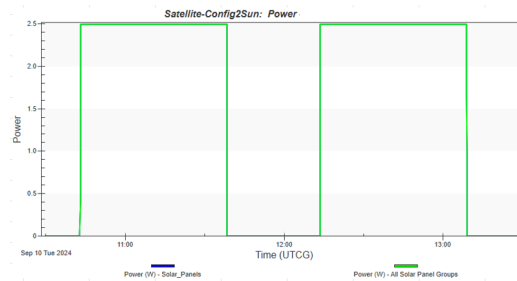


Figure A.20: Config2 Sun-Pointing

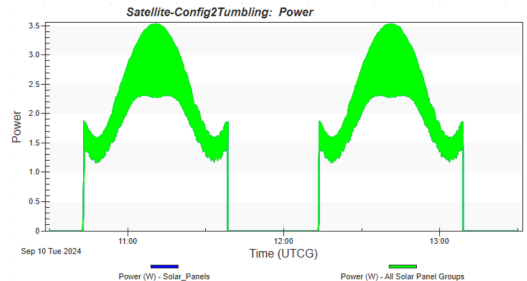


Figure A.21: Config2 Tumbling

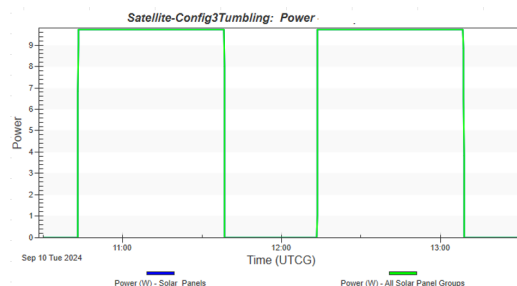


Figure A.22: Config3 Sun-Pointing

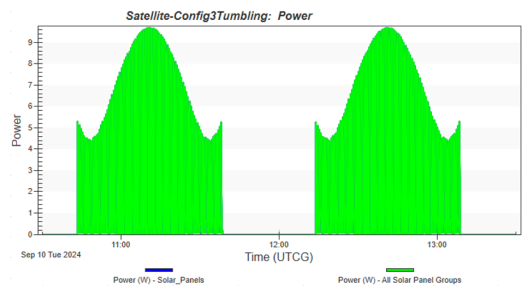


Figure A.23: Config3 Tumbling

Figure A.24: Configurations 2 & 3

A.6. Tape Spring Calculation

Storage of Strain Energy

The stored strain energy during the folding and bending of tape springs is a crucial parameter for their design and implementation in deployable appendages. The strain energy per unit surface area can be related to changes in curvature, with the assumption that torsion is neglected:

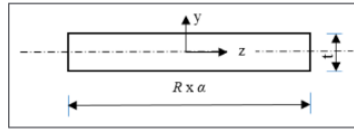


Figure A.25: Tape Spring Bend Length

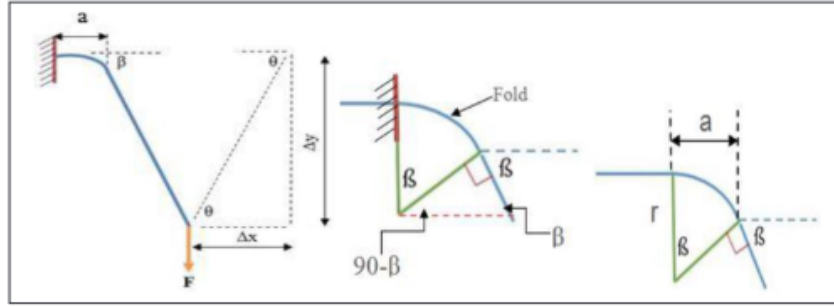


Figure A.26: Tape Spring Bend Parameters

$$e = \frac{D}{2} \left(k_l^2 + \nu k_t^2 \pm 2\nu k_l k_t \right) \quad (\text{A.1})$$

where:

- k_l and k_t are the changes in longitudinal and transverse curvatures, respectively,
- ν is Poisson's ratio,
- D is the flexural rigidity.

The signs in the equation indicate:

- + for equal sense bending,
- - for opposite sense bending.

To determine the strain energy, it is necessary to calculate the changes in curvature. The changes in longitudinal and transverse curvatures are given by:

$$k_l = \frac{1}{r} \quad (\text{A.2})$$

$$k_t = \pm \frac{1}{R} \quad (\text{A.3})$$

where:

- r is the final longitudinal radius of curvature,
- R is the initial transverse radius of curvature,
- + corresponds to equal sense loading,
- - corresponds to opposite sense loading.

From the generalized Hooke's law for shell elements, the moment-curvature relationship is described as:

$$M = \left(R - \frac{1}{r} \right) \left(\frac{Et^3}{12(1-\nu^2)} \right) \left(\frac{1}{r} \mp \frac{\nu}{R} \right) \quad (\text{A.4})$$

where:

- E is Young's modulus,

- t is the thickness of the tape spring,
- $-$ sign corresponds to equal sense, and $+$ sign corresponds to opposite sense.

The analytical solution for the strain energy is shown to be a pretty accurate representation of experimental data as presented by [99] up until the point of snapback. The snapback is a non-linear phenomena that can be studied further with an experiment driven design approach.

A.7. GEVS Profile

Frequency [Hz]	G Acceleration [G^2/Hz]
20	2.6e-002
50	0.16
800	0.16
2000	2.6e-002

Table A.4: Random Vibration Profile

A.8. Hinge

A.8.1. Hinge Material

	Aluminum Al- loys (7075)	BeCu (17200)	Titanium Al- loys (Ti-6Al)	Stainless Steel (302/304)
Yield Strength (MPa)	462	532.5	880	215
Modulus of Elasticity (GPa)	71.7	127	113.8	193
Density (kg/m³)	2810	8250	4430	8000
Strength-to-weight (Nm/kg)	164413	64545	198646	26875
Machinability	Fair	Good	Poor Generally	Good
Corrosion Resistance	Good	Excellent	Good	Fair
Cost	Low	Fair	High	Low

Table A.5: Comparison of Material Properties

A.9. Final COTS Parts

Item	Dimensions	Material	Supplier	Part No.
M1 Screws	Thread Diameter: M1 Thread Step: 0.25mm Length: 2.0mm	AISI 302	McMasterCarr	91800A050
M1.2 Screws	Thread Diameter: M1.2 Thread Step: 0.25mm Length: 3.0mm	AISI 303	McMasterCarr	91800A077
M1.6 Shoulder Screw	Shoulder Length: 12mm Thread Diameter: 1.6mm Shoulder Diameter: 2.0mm	AISI 304	McMasterCarr	90270A223
M1.6 Hexagon LockNut	Thread Diameter: 1.6mm Total Diameter: 2.7mm Thickness: 1.7mm	AISI 304	Accu	HNN-M1.6-A2
M1 Threaded Insert	Diameter: 2.1mm Length: 1.0mm	6061-T6	PEM	MSIA-M1-100

Table A.6: COTS Parts and Suppliers